UNIVERSITETET I BERGEN

Master Thesis

Disko Bay sea-ice variability: Oceanic and Atmospheric drivers

Dana Margareta King

dana.king@student.uib.no
M.Sc. Physical Oceanography

Supervisor: Professor Dr. Lars H. Smedsrud (UiB)
Co-Supervisor: Professor Dr. Johnny A. Johannessen (NERSC)

Deadline: 20.11.2023

Acknowledgements

I am extremely grateful to my supervisor, Lars, for all the long discussion, your invaluable feedback, your input on my writing, and for providing me with the opportunity to learn so much in a single year. I am also very grateful to Johnny for his invaluable feedback in discussions. Thank you so much.

Thank you to the Climate Narratives Project for allowing me to be part of this great project and fulfilling a lifelong dream of mine to go to Greenland and research sea ice. IT WAS UNBELIEVABLE! These two weeks in Greenland were an absolute dream come true, and I got to spend it with the kindest people (Iliana, Lars, Linda, Martin, Per, Torkel, Øystein, etc.). Huge thanks to our hunters, Abel Brandt and Johannes Mølgaard, for your kind company and for ensuring we stayed safe. A special thanks to Linda. We were both committed to gathering as much information as possible and did not fear anything. It was a lot of fun and absolutely worth it, and we are now both baptised by the Arctic. Many thanks to Martin for providing the statistical models, which were incredibly interesting and fun tow work with. Additionally, thank you for answering all my questions and discussing the results. A special thanks to Lars, Linda, and Martin, who walked with me to the (sea-ice) edge during what felt like the worst weather conditions possible to try our luck and find open water - and it was worth it. Warm waters at 120 dbar!

My beloved fellow birds, I am quite certain that life at uni would have been incredibly dull without the three of you. You took me in when I grumpily sat in the classroom during coffee breaks. One Lunch turned into (endless more lunches), coffee breaks, strolls through the park, a medal support system, games nights and an admirable aggregation of bird sounds. Sofie, the absolutely best boulder partner, not so long ago, we were wondering how the hell we were supposed to finish this. But here we are - WE DID IT! I cannot wait to go bouldering again and smash those pull-ups. Ingrid, you were an absolutely glorious neighbour, and I hope I can invite you to my flat sometime soon-ish, and we can cook and continue to try our best in HP. Thorbjørn, somehow, we always end up discussing oceanography, and I absolutely love it. I am excited to explore ALL the caves and find all mini kits!

A special thank you to Julia and Vivi for your emotional support throughout my studies, even though you still have no idea what I do. I could not have done this without the help of my Mum and Dad. I am eternally grateful for your support (financially and emotionally). I love you. Finley, your endless support, listening to all my explanations of the different but nevertheless cool sea ice types, and all the cool sea ice plots I created, and just being there for me (even from a distance). I love you so much.

From the bottom of my heart, thank you all so much.

Dana Margareta King
Bergen, 17 November 2023

Abstract

Climate change impacts the Arctic sea-ice cover and thickness with a related Arctic Amplification and an increased ocean heat transport towards the Arctic. There has been a profound decline of Arctic winter sea-ice extent, exemplified by a gradual reduction in maximum sea-ice extent during March. Disko Bay on the west coast of Greenland is an excellent case study to investigate atmosphere, ocean, and sea-ice variability. The inflowing West Greenland Current influences Disko Bay, and the variability of the inflow appears to be related to the North Atlantic Oscillation. In this thesis, I have investigated the variability of the winter sea-ice concentration in January, February, and March (JFM) from 2003 to 2023 in connection with atmospheric and oceanic forcing. Atmospheric forcing is provided by ERA 5, while hydrographic observations are available for nine years. Two Sea-Ice Concentration (SIC) products of different spatial resolutions are evaluated and used to create a mean SIC time series for Disko Bay. This revealed a pronounced year-to-year variability and a small positive trend in SIC. A random forest model is used to relate daily atmospheric variables to SIC variability. I consider the variables which increase the mean square error of the model performance the most if they were to be removed (%IncMSE). In addition, a correlation of atmospheric and oceanic parameters to SIC was applied. Correlations between SIC and oceanic forcing were related to determining the presence of cold and fresh Polar Water (PW) (θ < 1 °C and S $\leq$ 33.7), its thickness and the temperature of the top 50 dbar, $T_{50\ \mathrm{dbar}}$, in the water column. For atmospheric forcing, the three most important variables are Sea Surface Temperature (SST), the 2 m Temperature (T2M), and Surface net Latent Heat Flux (SLHF) with an %IncMSE of $\geq$ 40% each. Events of high SIC (> 75%, 2008 and 2012) and low (< 30%, 2010 and 2011) years were selected, and their variability was further investigated. This revealed that SST, T2M, the length of the sea-ice growth season determined by SST and T2M, the NAO of the previous year, $T_{50\ \mathrm{dbar}}$, and the thickness of the PW are important. The presence of a thicker PW layer insulates the sea ice against the warmer West Greenland Irminger Water layer below. In conclusion, both atmospheric and oceanic forcing contribute to Disko Bay winter sea-ice variability expressed through the SST, T2M, winter length, SLHF, and $T_{50\ \mathrm{dbar}}$.

Contents

List of Figures

List of Tables

Chapter 1

Introduction

The consequences of climate change are observed in every level of the climate system in the Arctic and are also evident at the interface between the atmosphere, the sea ice and the ocean (air-ice-ocean interaction) (Pörtner et al., 2019; IPCC, 2022). The atmosphere in the Arctic has been experiencing increasing temperatures over the last two decades as a response to increased atmospheric emissions of greenhouse gases. This warming occurs faster in the Arctic than anywhere else (Arctic Amplification) (Serreze et al., 2009; Notz & Stroeve, 2016; Pörtner et al., 2019; IPCC, 2022; Rantanen et al., 2022). Additionally, more heat is transported to the Arctic due to large volumes of warm water inflow, contributing to sea-ice loss and further changes in the sea ice. Consequently, the Arctic is experiencing warming through the atmosphere and from below the ocean surface.

The most apparent effect of a warming climate in the Arctic is a decreasing trend in maximum and minimum sea-ice extent, reached in March and September, respectively (Figure 1.1, Carmack et al., 2015; Notz & Stroeve, 2016; Stroeve & Notz, 2018)

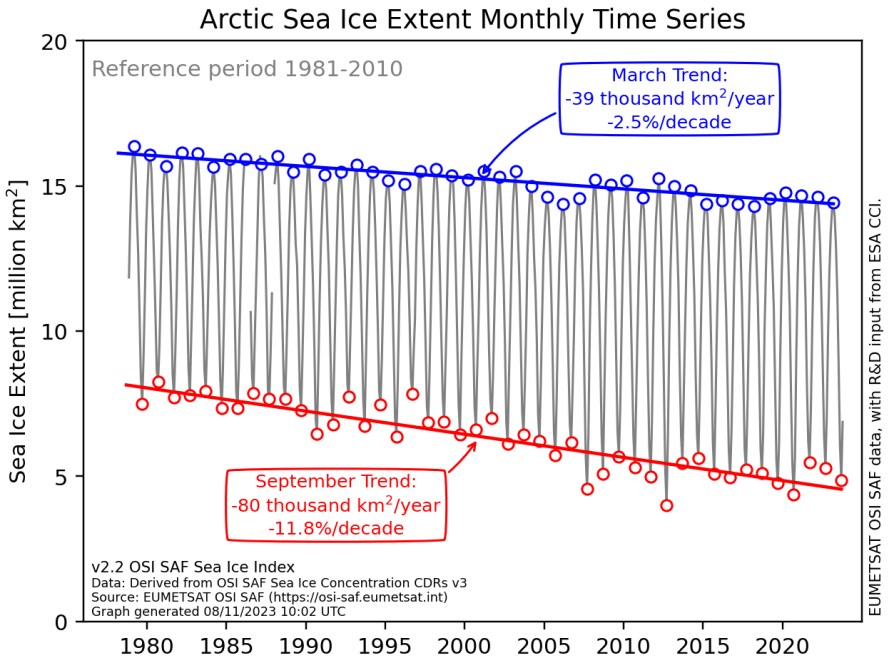

Figure 1.1: *Monthly Arctic sea-ice extent and the September and March trends from 1979 to 2023. Taken from Met-Norway, Cyro (2023).*

The more pronounced trend is visible during the September sea-ice minimum with a loss of 80.000 km^2 per year, equivalent to a loss of 11.8% per decade (Figure 1.1). Moreover, the past 17 years had the lowest sea-ice minimum extents since satellite records started in October 1978 (NSDIC, 2023a). Satellite-derived measurements of Arctic sea ice have been a great tool to consistently observe the state of the sea ice and large-scale changes on short and long timescales (e.g. Stroeve & Notz, 2018).

To potentially predict the future development of sea ice in the Arctic, it is essential to understand the causes of the ongoing decline in sea ice. Atmospheric temperatures in the Arctic are projected to continue to increase due to continued global emissions and burning of fossil fuels, but rates vary under different emission scenarios (Pörtner et al., 2019; IPCC, 2022). Through increased atmospheric temperatures in the Arctic (Arctic Amplification), the Arctic sea-ice cover faces prolonged summer seasons, with earlier melt onsets and delays in the freeze-up reducing the time sea ice can grow, resulting in thinner sea ice (Pörtner et al., 2019; IPCC, 2022). Thinner sea ice is more prone to melting, deformation and/or export out of the Arctic by wind-induced forcing (Zhang et al., 2012; Rampal et al., 2019; Pörtner et al., 2019; IPCC, 2022).

In addition, the Arctic Ocean has absorbed more heat in recent years due to an increased inflow of relatively warm (above 0 °C) and saline water, also known as Atlantic Water due to its origin in the Atlantic Ocean (Carmack et al., 2015; Smedsrud et al., 2022). This inflow is associated with sea-ice loss in the Arctic and more open water (Carmack et al., 2015; Smedsrud et al., 2022). More open water stretches in the Arctic, allowing for an increase in the absorption of solar radiation as the ocean has a lower albedo than the sea ice. This is a positive feedback mechanism known as the ice-albedo feedback, as the absorption of more heat further increases the heat contact in the ocean and can inhibit sea ice growth (Serreze et al., 2009; Thomas, 2017). Increased heat from a warmer atmosphere and ocean affects the Arctic sea ice on many levels.

Greenland (Kalaallit Nunaat) (Figure 1.2) is an important part of the Arctic, which is sensitive to climate change, particularly through the accelerated loss of mass from the Greenland ice sheet and increased glacial discharge (Masson-Delmotte et al., 2012; Beaird et al., 2017; Pörtner et al., 2019). The effects climate change has on Greenland impact the whole world. If the Greenland ice sheet were to melt completely, the resulting sea level rise would be equivalent to approximately 7.2 m (Dahl-Jensen et al., 2009; Masson-Delmotte et al., 2012; Pörtner et al., 2019; IPCC, 2022).

Moreover, Greenland is home to numerous marine-terminating glaciers. Increasing atmospheric temperatures and warming of the ocean water have been associated with the fast retreat of marine-terminating glaciers like Jakobshavn Isbræ (Sermeq Kujalleq), located in Disko Bay (Figure 1.2, Masson-Delmotte et al., 2012; Straneo & Cenedese, 2015; Gladish et al., 2015a,b; Beaird et al., 2017). It is not only the mass loss of the Greenland ice sheet that is important but also the sea ice cover around Greenland, especially on the coasts. Reduced sea-ice cover affects the biology, e.g. Arctic copepods (Møller & Nielsen, 2019; Møller et al., 2023). Disko Bay (Figure 1.2, red box) is a marine biodiversity and fisheries hot spot most likely influenced by the, e.g. sea-ice cover (Møller et al., 2023). Moreover, inhabitants on the west coast of Greenland depend on the stability of the sea ice as it provides fishing and hunting grounds, which are a vital part of the economy. Furthermore, the sea ice is used for travels between villages (Madsen et al., 2001).

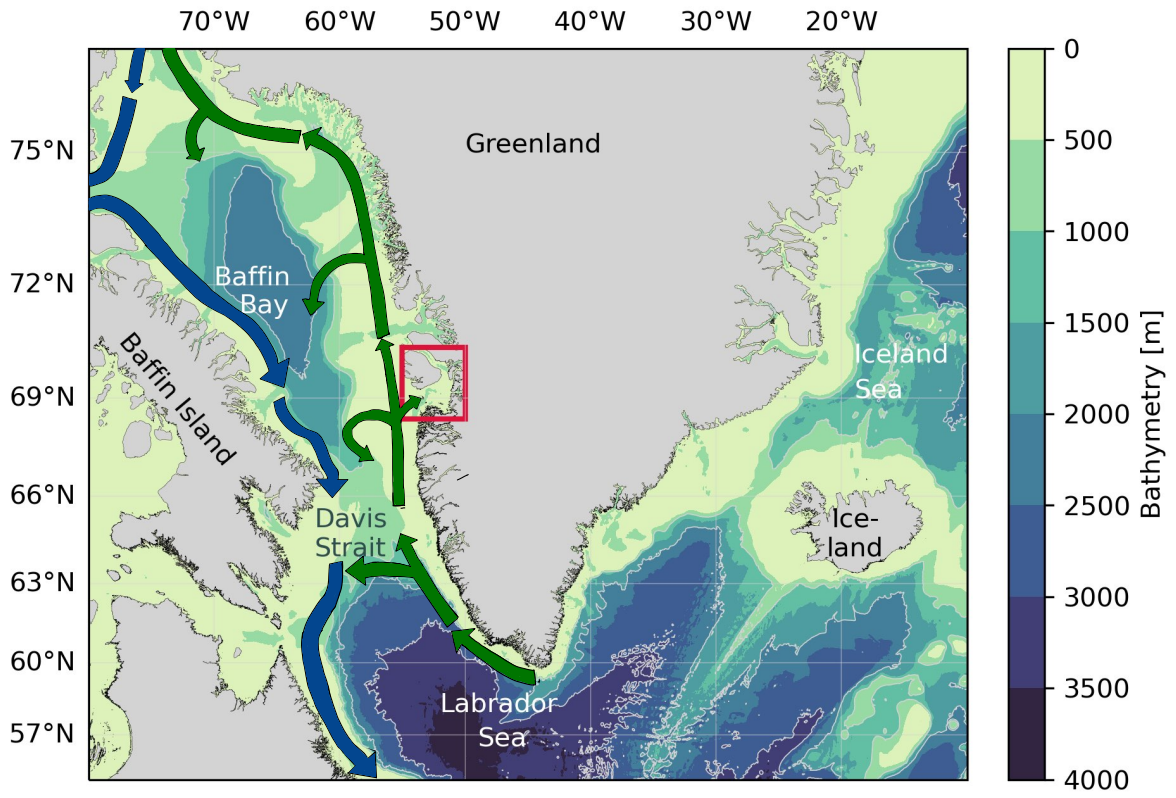

Figure 1.2: *Map of Greenland from 54 °N to 78 °N, Baffin Island, and the circulation on the west side of Greenland. The red box marks the location of Disko Bay. Blue arrows indicate the pathway of the Baffin Island Current, and in dark green, the pathway of the West Greenland Current. The width of the arrows does not indicate the strength or the volume of the transported water masses. Isobaths in 1000 m steps are marked in light grey. The high-resolution coastline is from NOAA (Wessel & Smith, 1996), and the Bathymetry shading is from ETOPO 2022 (NOAA, 2022a).*

The sea ice on the western side of Greenland is partly restricted in its drift by the surrounding currents, the West Greenland Current and the Baffin Island Current. In South Greenland, the influence of wind speed and direction at the surface is particularly dominant (Figure 1.2, Mosbech et al., 2007). The sea ice formed on Greenland's west coast is drift ice, often referred to as "The West Ice" (Mosbech et al., 2007). Most sea ice inside Baffin Bay and Davis Strait (Figure 1.2) is first-year ice (Mosbech et al., 2007). The sea ice in Baffin Bay can be divided into two categories: fast ice and drift ice. The former, often called land-fast ice, is relatively stable and connected to the coast, while the latter is highly variable and seasonally changing. During summer, the sea ice in Baffin Bay is almost entirely absent and forms late in autumn and continues to grow until February or March (Stern & Heide-Jørgensen, 2003; Heide-Jørgensen et al., 2007b).

Disko Bay (Qeqertarsuup Tunua) (Figure 1.2, red box), south of Disko Island (Qeqertarsuaq), Greenland's largest island on the west coast (69.5 °N, 53 °W), is subject to a unique combination of influencing factors as it lies between 60 °N and 72 °N, a region known to be influenced by the inflow of warm water from the West Greenland Current and the southward flow of the Baffin Island Current, affecting sea-ice formation (Figure 1.2, Mosbech et al., 2007; Gladish et al., 2015a,b; Møller et al., 2023). Moreover, in the east of Disko Bay lies the marine-terminating glaciers Jakobshavn Isbræ (Myers & Ribergaard, 2013; Gladish et al., 2015a,b;

Khazendar et al., 2019). Icebergs calved off from Glaciers are frequent in west Greenland and Disko Bay and are highly influential to the area (Mosbech et al., 2007). This makes Disko Bay an excellent area to study the interaction between the atmosphere, the ocean, and the sea ice (air-ice-ocean interaction).

Objectives

The present work is part of the Climate Narrative Project, aiming to improve the understanding of the ocean-glacier system of Disko Bay and the impact on seasonal fjord climate. The main objective of this thesis is to expand the knowledge of winter conditions in Disko Bay. I aim to investigate the variability of the winter sea-ice concentration, the ocean conditions, and sea-ice concentration variability and its correlation to oceanic and atmospheric forcing. Herein, I will focus on the winter months of January, February, and March from 2003 to 2023. Twenty-one years should allow me to differentiate between seasonal, annual and internal variability. Satellite-derived sea-ice concentration from two different products are used. Atmospheric forcing is from ERA5, and hydrographic data are in situ measurements from various sources for 2008 to 2012, 2018, 2020, 2022, and 2023. In March 2023, I was part of a two-week fieldwork at the Arctic Station in Qeqertarsuaq, Disko Bay.

In my thesis, I aim to investigate the sea-ice variability in Disko Bay and its correlation to oceanic and atmospheric forcing from 2003 to 2023. To reach this objective, I aim to answer the following research questions:

1. How did sea-ice concentration in January, February, and March change between 2003 and 2023 in Disko Bay?
2. Which varying ocean conditions can be documented during January, February, and March in Disko Bay?
3. Is the ocean or the atmosphere the main driver for Disko Bay's winter sea-ice variability?

Whenever I use the term "we", this is to clarify that this work was carried out in a group and is related to fieldwork. Otherwise, I will use the "I" form to clarify that I conducted the work.

The thesis structure is as follows: Chapter 2 provides an overview of sea ice formation and sea-ice conditions in the Arctic, Baffin Bay, and Disko Bay, the circulation and transport of water masses around Greenland, the hydrography of Disko Bay, and the North Atlantic Oscillation. Chapter 3 follows with a detailed description of the fieldwork, the data I used, and the methods I applied. Throughout this thesis, I distinguish between sea ice, ocean and atmosphere to better understand their interrelationship and influence on each other. Chapter 4 will present the result which are discussed in Chapter 5. Concluding remarks and future work are presented in Chapter 6.

Chapter 2

Background

In this chapter, I present an overview of the theory behind sea-ice growth, the relation between the freezing point, temperature and salinity and the sea-ice conditions in the Arctic, Baffin Bay and Disko Bay (Section 2.1). Then, I illustrate the large-scale ocean circulation around Greenland and its connection to the transport of cold and warm water masses (Section 2.2). Followed by an introduction of Disko Bay, its circulation on a regional scale, and its hydrography (Section 2.3). Lastly, I present the North Atlantic Oscillation (NAO) and its connection to atmospheric conditions on the west coast of Greenland and Disko Bay (Section 2.4).

2.1 Sea Ice Formation and Sea Ice in Disko Bay

Properties of Seawater

Sea ice formation heavily depends on the water's salinity since it determines the freezing temperature at which sea ice starts to grow (Figure 2.1). With increasing salinity, the freezing point decreases further (Figure 2.1). A reference point for this is a salinity of 24, which yields a freezing point of -1.33 °C (Figure 2.1). After this, the temperature of maximum density and the freezing point are the same, and seawater increases in density as temperature decreases towards the freezing point (Figure 2.1). The Arctic is salinity-stratified, implying that density depends on the salinity of the water; density lines are always vertical because density does not vary significantly with temperature (Figure 2.1).

In general, sea-ice growth can either be thermodynamic or dynamic. For thermodynamic sea-ice growth, low air temperatures are needed to cool the temperature of the seawater at the surface and increase the density at the surface. This leads to convection, where the colder and denser waters sink and are replaced by lighter and warmer waters at the surface. This process continues until the seawater at the surface reaches the freezing point (Thomas, 2017). Sea ice starts to form after the surface water is at freezing point. During the sea-ice growth process, part of the salt content of the freezing water is lost to the water underneath. This process is known as brine release (Weeks, 2010).

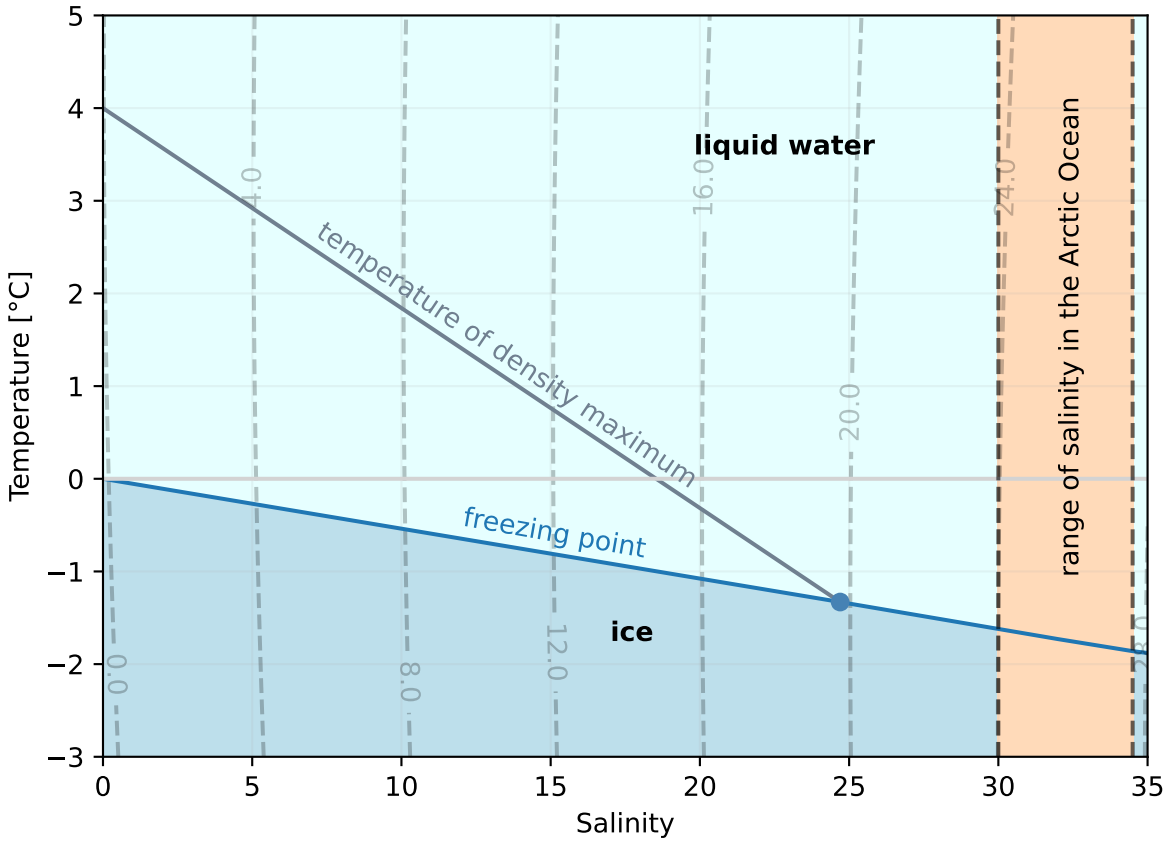

Figure 2.1: *Schematic illustration of the relation between salinity, temperature and the freezing point (blue line) and the relation between the temperature density maximum (dark grey line) and the freezing point. The orange-shaded area indicates the range of salinity found in the Arctic Ocean. The dot marks a reference point with a salinity of 24.7 and a freezing point of -1.33 °C, after which the temperature of maximum density and the freezing point are the same. Dashed lines in light grey represent density contours. Adapted from an Illustration of Markus Ritschel.*

In addition, there are two conditions under which thermodynamic sea-ice growth occurs: calm or aggregated conditions. The different conditions lead to distinct patterns of sea-ice growth. During calm conditions, in a sea without swell or waves, sea ice forms into a continuous thin layer called Nilas. If it is less than 5 cm thick, it is called dark Nilas, as the layer appears quite dark due to the visibility of the water underneath. At this stage, sea-ice growth occurs through bottom-freezing. As the sea ice thickens, the surface appears white, and it reflects more light. When the thickness is between 5 and 10 cm, it is called light Nilas. If these calm conditions persist and sea-ice thickness increases, sea ice grows into young ice. Young ice is separated into grey ice (10 to 15 cm) and grey-white ice (15 to 30 cm). If sea-ice growth continues, sea ice grows into first-year white ice and then old ice, which entails second-year and multiyear ice (Thomas, 2017).

In contrast, sea-ice growth under agitated conditions, a sea state with wind and waves, sea ice starts to grow in an accumulation of frazil ice. In this state, sea ice is called Grease ice. Grease ice forms into a surface layer if the growth process continues. Continued sea-ice growth leads to aggregations of Grease ice into larger groups, named pancake ice. If winds and waves persist, these ice aggregations are rafted on top of each other and freeze, forming larger units until they form a solid ice sheet (Thomas, 2017).

Thermodynamic growth is limited by the thickness of the sea ice and levels off at 1 to 2 m for the first winter; after that, dynamic processes take over. Dynamic processes are separated into convergent and divergent regimes. I am interested in the formation of sea ice; therefore, I only describe convergent regimes. Converging regimes of sea ice are rafting and ridging. The former is largely limited to thin sea ice and describes the process of two sea ice floes overlapping and gliding over and under each other. The latter process describes a regime where ice fragments are pushed towards each other due to external pressure forces (Thomas, 2017).

Sea Ice in the Arctic, Baffin Bay and Disko Bay

Sea ice in the Arctic has a periodic character as it grows in winter and melts in summer (Thomas, 2017). Arctic sea ice reaches its maximum sea-ice extent in March and its minimum in September (Figure 2.2b). Based on satellite records, the ten lowest maxima of sea-ice extent occurred between 2006 and 2023, with the majority (7 out of 10) after 2014 (Figure 2.2, NSDIC, 2023b). Moreover, the last 16 sea-ice extent maximums were the lowest measured since satellite records started in 1978 (Figure 2.2, NSDIC, 2022). This year's sea-ice maximum extent, reached on the 6^{th} of March, is the fifth lowest on record (Figure 2.2a, NSDIC, 2023c).

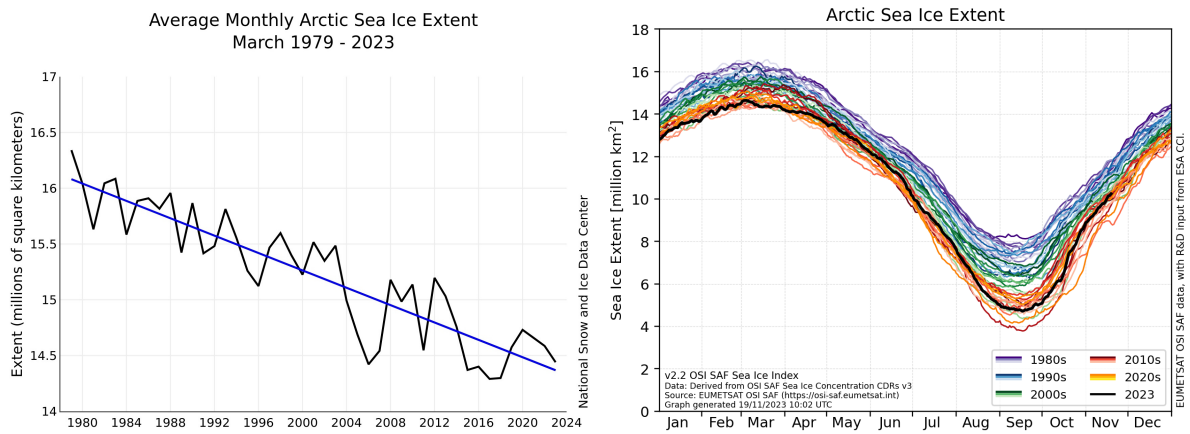

(a) **(b)**

Figure 2.2: *Average monthly Arctic sea-ice extent in March from 1979 to 2023 (a) taken from NSDIC (2023c) and Arctic sea-ice extent from the 1980's to 2023 (b) taken from Met-Norway, Cyro (2023). The blue line in (a) indicates a decrease of 2.5 % per decade, representing a loss of 39 thousand km^2 per year.*

To understand sea-ice variability in the Arctic, it is necessary to examine regions with a substantial influence on seasonality and trends. Onarheim et al. (2018) distinguish between northern regions with the greatest variability in sea-ice extent and trend during either summer (summer mode) or winter (winter mode). My focus lies in the winter months of January, February and March (JFM); hence, I only consider winter modes. Regions identified as winter modes, e.g. the Bering Sea, Sea of Okhotsk, and Baffin Bay/Gulf of St.Lawrence. These show considerable variability in winter months and are generally ice-free in summer. These also have the greatest influence on March sea-ice extent in the Northern Hemisphere (Onarheim et al., 2018).

Baffin Bay has the most significant sea-ice loss in January and February with a loss of $50{\cdot}10^4$ km^2 per decade (Onarheim et al., 2018). Moreover, there is a decadal cycle in winter sea-ice

area of 8.2 years in (Stern & Heide-Jørgensen, 2003). Baffin Bay stretches along the west coast of Greenland down to 45°N, including Disko Bay.

Both Baffin Bay and Disko Bay are generally ice-free during summer. The sea-ice cover in Disko Bay starts to form in late December (Møller & Nielsen, 2019; Møller et al., 2023), and in the inner fjord parts in November and December (Mosbech et al., 2007). Maximum sea-ice extent is reached in March (Stern & Heide-Jørgensen, 2003; Møller et al., 2023) and starts to break up in April and May (Hansen et al., 2006; Møller et al., 2023).

The last 35 years in Disko Bay showed a decrease in sea-ice cover, and the previous 15 years were characterised by considerable interannual variability (Møller et al., 2023). In some years, there is no sea ice, while in other years, Disko Bay experiences a sea-ice cover like in the 1990s (Møller et al., 2023). From 1991 to 2004, the period of a sea-ice covered Disko Bay reduced by 50%. The average winter between 1994 and 2004 had 131 days of 100% sea-ice cover (Hansen et al., 2006). The loss of sea-ice cover days occurred at the start of the winter in January and at the end of the season in May (Hansen et al., 2006).

2.2 Circulation around Greenland

One of the influencing factors for sea-ice variability in Disko Bay is the water underneath the ice, which is, after all, frozen seawater. The incoming current influencing the stratification, salinity and temperature in Disko Bay is part of a combination of five currents dominating the circulation around Greenland (Figure 2.3).

On the western side of Greenland, relatively warm (above 0 °C) and saline waters originate from the North Atlantic. They are transported by the North Atlantic Current (NAC). A branch of the NAC enters the Nordic Seas as the Norwegian Atlantic Current (NwAC). The NwAC transports water masses that reach the Arctic Ocean through the Fram Strait and the Barents Sea (Figure 2.3, Carmack et al., 2015). The Irminger Current (IC) splits from the NAC near Iceland and transports warm and saline waters south of Iceland towards the east coast of Greenland. The IC continues to flow south and alongside the East Greenland Current (EGC) toward Cape Farewell. The EGC transports cold waters originating from the Arctic Ocean. After the EGC and IC pass Cape Farewell, they merge and form the West Greenland Current (WGC) as they flow west of Greenland (Figure 2.3, Madsen et al., 2001; Fried & de Jong, 2022).

The WGC bifurcates south of Davis Strait and can recirculate southwards towards Canada at Fylla Bank (64 °N) to join the Labrador Current and ultimately flow into the Labrador Sea. Or the WGC flows along the west coast of Greenland and minxes in the Davis Strait with the BIC (Figure 2.3, Buch, 1990; Madsen et al., 2001). Due to the bifurcation, the WGC decreases in strength when it passes Davis Strait, flowing northward through Baffin Bay. Along its way north, the waters are diluted by the runoff of fjords along the west coast of Greenland (Mosbech et al., 2007). Nevertheless, the WGC transports relatively warm and saline waters. Within this thesis, I will refer to the relatively warm and saline water masses inside the WGC as West Greenland Irminger Water (WGIW) (Tang et al., 2004). WGIW represents waters originating from the IC but being mixed with colder and fresher water on its way north by the EGC (Figure 2.3, Myers & Ribergaard, 2013). At the same time, Baffin Bay experiences a southward flow of cold water originating from the Arctic Ocean, the Baffin Island Current (BIC) (Figure 2.3). The BIC flows southward, and after passing Davis Strait is the Labrador Current (Figure 2.3, Buch & Institut, 2002; Mosbech et al., 2007).

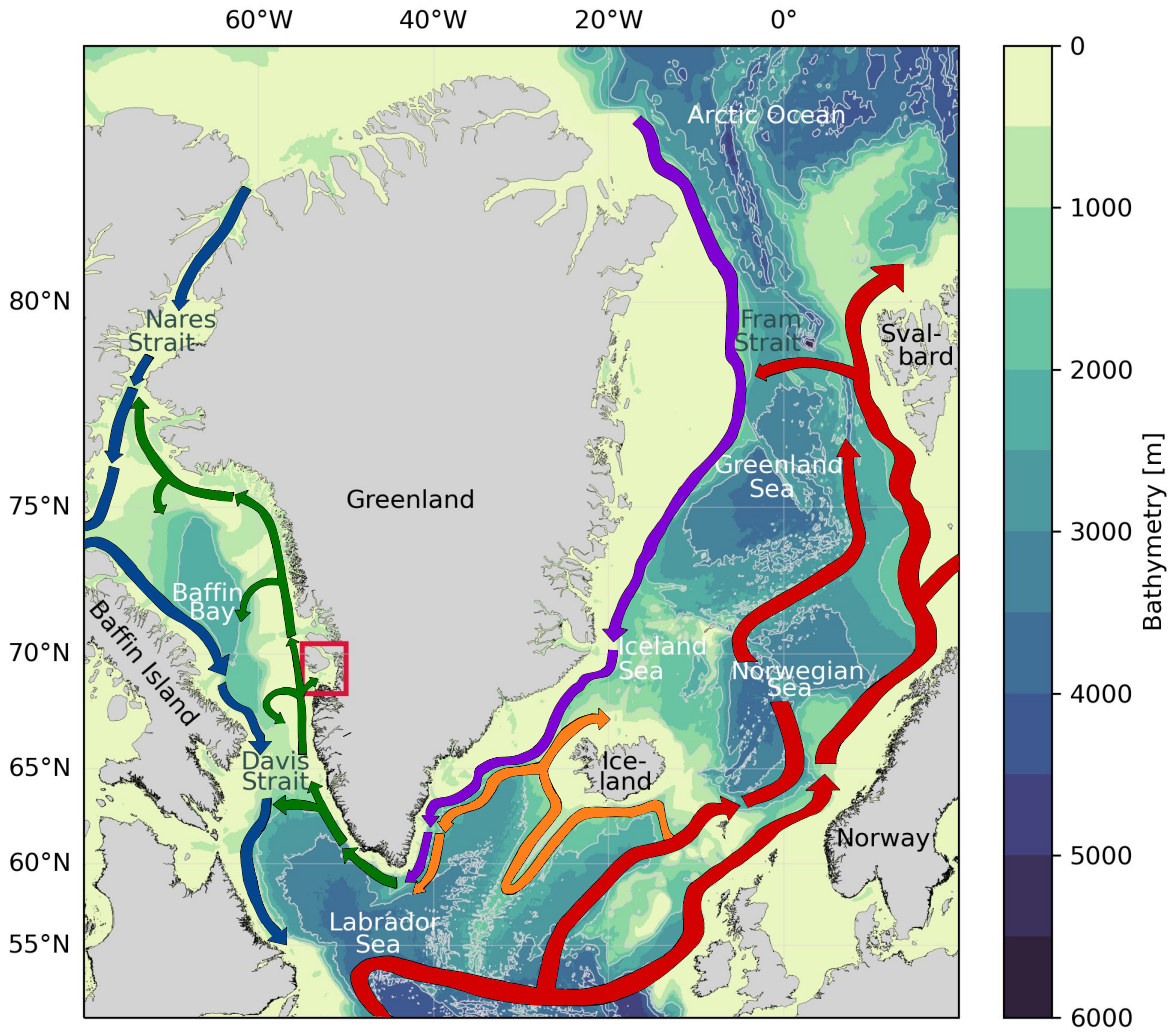

Figure 2.3: *Circulation around Greenland, in the North Atlantic, and Baffin Bay. Orange arrows indicate the pathway of the Irminger Current (IC), and red arrows indicate the pathway of the North Atlantic Current (NAC) and the Norwegian Atlantic Current (NwAC). Purple arrows indicate the East Greenland Current (EGC) and, in dark green, the pathway of the West Greenland Current (WGC). The Baffin Island Current (BIC) pathway is marked in dark blue. Warm colours indicate warmer water properties, while cooler colours indicate the transport of colder properties. The width of the arrows does not indicate the strength or the volume of the transported water masses. The width of the arrows does not indicate the strength or the volume of the transported water masses. The red box marks the location of Disko Bay. Isobaths in 1000 dm steps are marked in light grey. The high-resolution coastline is from NOAA (Wessel & Smith, 1996), and the Bathymetry shading is from ETOPO 2022 (NOAA, 2022b). Adapted from Curry et al. (2011); Straneo & Cenedese (2015); Brakstad et al. (2023).*

The inflow waters into Disko Bay are relatively warm and saline waters transported by the WGC (Figure 2.3, Madsen et al., 2001). These warm and saline waters have the potential to influence the sea-ice cover in Disko Bay, as higher temperatures relate to a higher heat content inside the water column. Suggesting that more heat must be extracted from the ocean for sea ice to form. However, not only the inflow temperature is influential, but the strength of the inflow and other local factors are crucial to identifying reasons for the sea-ice variability in Disko Bay. Runoff and melted ice from Jakobshavn Isbræ from the east further influence Disko Bay, especially on an interannual scale, as it introduces sources of fresher surface water

influencing the stratification (Kiilerich, 1939; Andersen, 1981; Nielsen & Hansen, 1995, 1999; Madsen et al., 2001; Gladish et al., 2015a,b). The strength of warm and saline water inflow is seasonally varying and strongest during autumn and winter (Mosbech et al., 2007). Moreover, a long-term study of 50 years in west Greenland showed that hydrographic measurements of temperature and salinity show a substantial variability on an interannual scale (Mosbech et al., 2007).

2.3 Hydrography of Disko Bay

To investigate local factors influencing the waters inside Disko Bay, I consider the circulation at the entrance and inside Disko Bay and the stratification of the water column. The waters of the WGC enter Disko Bay through the Egedesminde Deep, with a depth $\geq$ 900 m between Disko Island and Aasiaat (Figure 2.4, Krawczyk et al., 2022). The outflow occurs through the Vaigat strait in the north and recirculation in the bay south of Disko Island (Figure 2.4, Andersen, 1981; Heide-Jørgensen et al., 2007b; Hansen et al., 2012; Krawczyk et al., 2022).

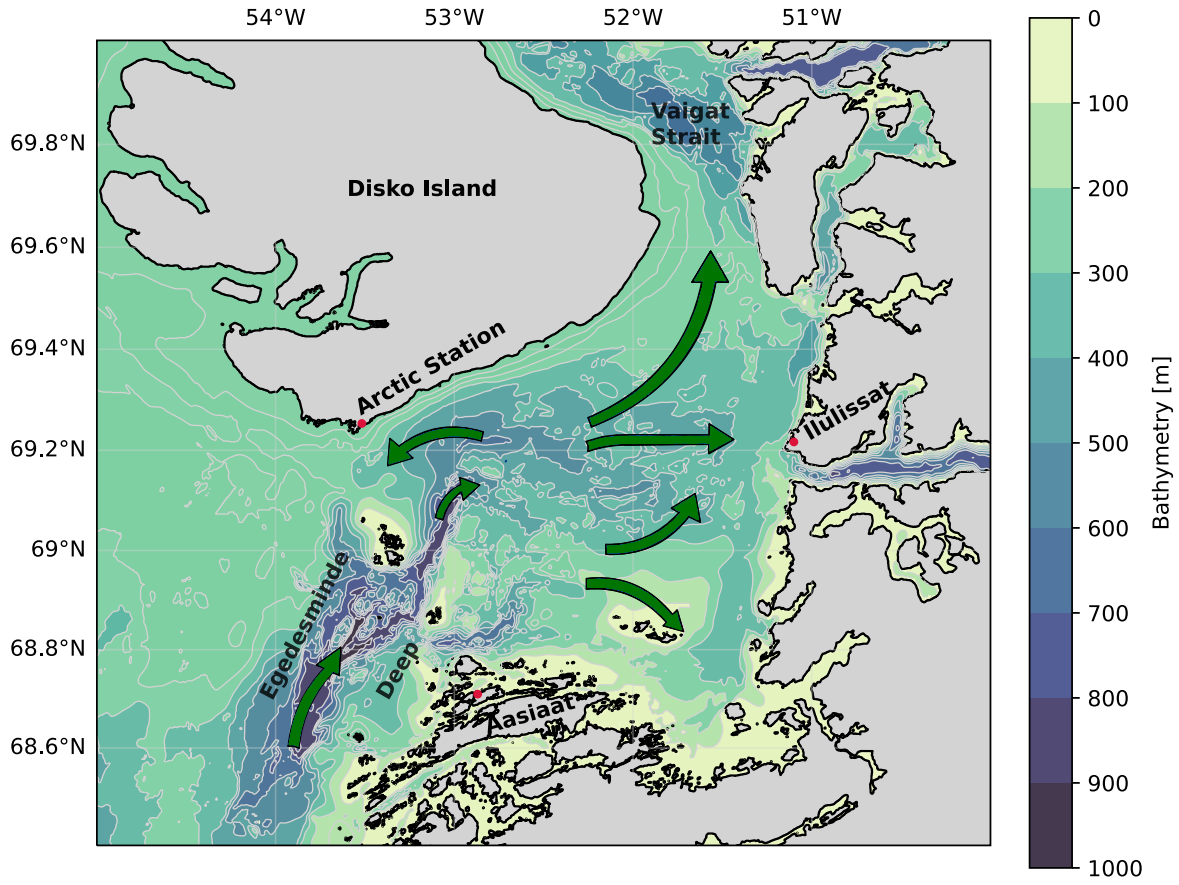

Figure 2.4: *Dark green arrows indicate the pathway of the West Greenland Current (WGC) at the entrance and inside of Disko Bay. The width of the arrows does not indicate the strength or the volume of the transported water masses. Isobaths in 100 m steps are marked in light grey. The high-resolution coastline is from NOAA (Wessel & Smith, 1996), and the Bathymetry shading is from ETOPO 2022 (NOAA, 2022a). Adapted from Khazendar et al. (2019); Krawczyk et al. (2022). ETOPO 2022 estimates the bathymetry around Disko Island to be deeper than it is.*

The hydrography of Disko Bay is heavily influenced by the WGC, its sea-ice coverage and the

freshwater runoff originating from the Greenland ice sheet (Krawczyk et al., 2022). The stratification inside Disko Bay is as follows: the surface layer is very fresh and varies by season (Myers & Ribergaard, 2013; Krawczyk et al., 2022). Underneath the surface layer lies a layer of cold and fresh Polar Water (PW) to a depth of around 200 m. Below PW lies a layer of WGIW (Tang et al., 2004). The interface between the PW and the WGIW has been changing over the last decades (Holland et al., 2008; Myers & Ribergaard, 2013; Khazendar et al., 2019).

The surface layer varies by season, as in summer, but also generally, the fresh layer originates from melt from glaciers, sea ice and river runoff (Hansen et al., 2012). The freshwater input from Jakobshavn Isbræ (JI) is also visible in the salinity close to the glacier (Buch, 1990). There also seems to be a connection between the inflow of warm waters from the WGC and Icebergs that calved off JI (Figure 2.4, Holland et al., 2008; Hansen et al., 2012; Krawczyk et al., 2022). In contrast, The hydrographic conditions in winter represent a well-mixed water column (Andersen, 1981; Heide-Jørgensen et al., 2007b).

PW is defined by (θ < 1 °C and S $\leq$ 33.7) (Tang et al., 2004). In this thesis, I use the definition of WGIW with characteristics of (θ > 2 °C and S > 34.1) (Tang et al., 2004). Cold PW enters Disko Bay at a depth of 30 to 200 m and started to warm in the mid-1990s by 1 to 2 °C, increasing the heat content in west Greenland compared to before 1990 by a "factor of 3.6" (Myers & Ribergaard, 2013). Higher water temperatures in Disko Bay resulted from a considerable inflow of warm and saline water from the IC in 1997. These waters travelled east and reached Ilulissat Icefjord, located east of Disko Bay. As a result of the warm water masses, JI began to rapidly thin and retreat in 1997 (Myers & Ribergaard, 2013; Wood et al., 2021). In 1997, WGIW became saltier, warmer and shallowed (Holland et al., 2008; Myers & Ribergaard, 2013). Before and during the mid-1990s, PW had an average temperature below 0 °C, and its interface to the warm layer below lay at 200 m.

However, between 2014 and 2016, the ocean temperature in the top 250 m in Disko Bay had cooled to values that had not been detected since the 1980s, resulting from irregular heat loss during winter in the Western Boundary Current in south Greenland (Khazendar et al., 2019). This cooling lowered the ocean temperature by almost 2 °C at below a depth of 150 m.

2.4 North Atlantic Oscillation and its connection to west Greenland

Sea ice only forms when enough heat is extracted by the atmosphere, and seasonal varying atmospheric conditions strongly affect the top 150 m of the water (Hansen et al., 2012). Hence, it is essential to understand the large-scale variability of the atmospheric conditions on the west coast of Greenland and Baffin Bay. An understanding of the large-scale variability contributes to understanding the influencing factors of Disko Bay. Variations in the North Atlantic Oscillation (NAO) affect the sea-ice edge between the Davis Strait and the Labrador Sea (Heide-Jørgensen et al., 2007a).

The NAO expresses an internal atmospheric variability, a pattern of climate variability at mid and high latitudes. The NAO also indicates a relationship between the Greenlandic climate, the EGC and the intensity of the westerlies over the North Atlantic (Figure 2.5, Wanner et al., 2001; Buch & Institut, 2002). The NAO is the difference in atmospheric pressure between the Icelandic Low in the high latitudes of the North Atlantic Ocean (Subpolar low) and the Azores High in the central North Atlantic (Subtropical high). The NAO can be in a positive or negative phase (Figure 2.5, Wanner et al., 2001)

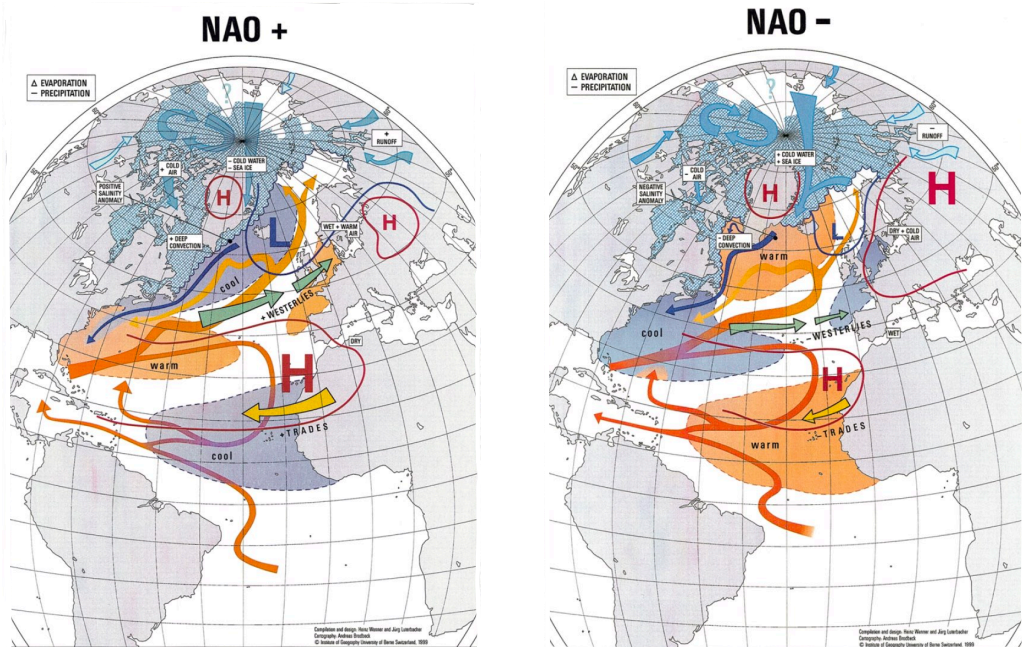

(a) **(b)**

Figure 2.5: *Schematic illustration of the NAO in positive (a) and negative (b) phase, taken from Wanner et al. (2001).*

Positive or negative NAO phases express atmospheric conditions and wind-forced ocean circulation changes (Figure 2.5, Wanner et al., 2001). NAO in a positive phase translates to a stronger pressure anomaly than normal between the subpolar low and the subtropical high (Figure 2.5a, Wanner et al., 2001). This increases the pressure gradient, resulting in stronger winds, as these follow the strong pressure gradient and cooler sea surface temperatures in the North Atlantic (Figure 2.5a, Wanner et al., 2001).

In contrast, in years with a negative NAO phase, the IC transporting warm and saline waters intensifies and travels further towards the eastern coast of Greenland and mixes with the cooler waters from the Arctic Ocean (Figure 2.5b, Wanner et al., 2001). At the same time, the EGC intensifies towards the south of Greenland/Cape Farewell, and the North Atlantic and lower parts of west Greenland experience higher sea surface temperatures (Figure 2.5b, Wanner et al., 2001). During the 1990s, Disko Bay went through an atmospheric shift, leading to more warm waters reaching further into the west coast of Greenland and towards Disko Bay (Buch et al., 2004; Myers et al., 2007; Holland et al., 2008; Hansen et al., 2012). Similar is known to occur in the Barents Sea, resulting in Arctic Atlantification as warm waters move further into the Arctic, limiting sea-ice growth and decreasing sea-ice coverage (Årthun et al., 2012).

The connection between the NAO and atmospheric conditions in Baffin Bay and Davis Strait is well-documented (Figure 2.5, Rigor et al., 2000; Hanna & Cappelen, 2003; Heide-Jørgensen et al., 2007a). Changes in the NAO during the late 1990s were responsible for warming at the subsurface level along western Greenland (Holland et al., 2008), and the NAO influences atmospheric conditions in Disko Bay (Gladish et al., 2015a). However, there is a difference in their response time. Davis Strait is most likely to respond faster to changes in the NAO, while further north in Baffin Bay, changes occur with a lag of approximately one year (Heide-Jørgensen et al., 2007a). Stern & Heide-Jørgensen (2003) found a distinct correlation between sea-ice concentration in March in Baffin Bay as a reaction to the 1-year delay of the winter NAO index.

Chapter 3

Data and Methods

In the following chapter, I present our fieldwork from Arctic Station in March of this year (Section 3.1). Then, I describe the products used to investigate sea-ice concentration (Section 3.2). Further, an overview of the hydrographic observations and all auxiliary data sets are presented (Section 3.3). Followed by an overview of the atmospheric data (Section 3.4). Lastly, I introduce two statistical approaches correlating atmospheric and oceanic variables to sea-ice concentration (Section 3.5).

3.1 Fieldwork

From the 6^{th} to the 20^{th} of March 2023, we stayed at the Arctic Station in Qeqertarsuaq, Disko Island, Greenland. Arctic Station is located around 300 m from the coast, allowing easy access to the fast ice growing in Qeqertarsuup Tuna (QT), the bay ahead. A smaller, adjacent bay, Lyngmarkt Bugt (LB), is west of Arctic Station (Figure 3.1). The aim of this fieldwork was to acquire as many winter profiles as possible and attempt to understand the sea-ice conditions and the hydrography underneath the sea ice. Hydrographic properties like temperature and salinity provide insight into important processes in the ocean, like ocean transport, water mass transformation and pre-conditioning of sea-ice growth.

Hydrographic properties are measured by a CTD (**C**onductivity, **T**emperature, and **D**epth), which measures temperature, conductivity and pressure. With these, it is possible to derive further hydrographic properties like density and salinity. Salinity is an important parameter calculated as a function of conductivity and temperature, $S = f(C, T)$. The CTD we brought for the fieldwork was a Sea & Sun CTD Standard Memory Probe C48 M equipped with a pressure sensor ([dbar]), a conductivity sensor ([mS cm^{-1}]) and a temperature sensor Pt100 ([°C]) (Sea & Sun Technology, 2020).

During our fieldwork, we planned a multitude of CTD and ICE stations in QT and LB (Figure 3.1). Every CTD station includes an ICE station. At an ICE station, we measured sea-ice and snow thickness, and the bottom depth of the water column. In the case of a CTD station, we additionally conducted a CTD cast.

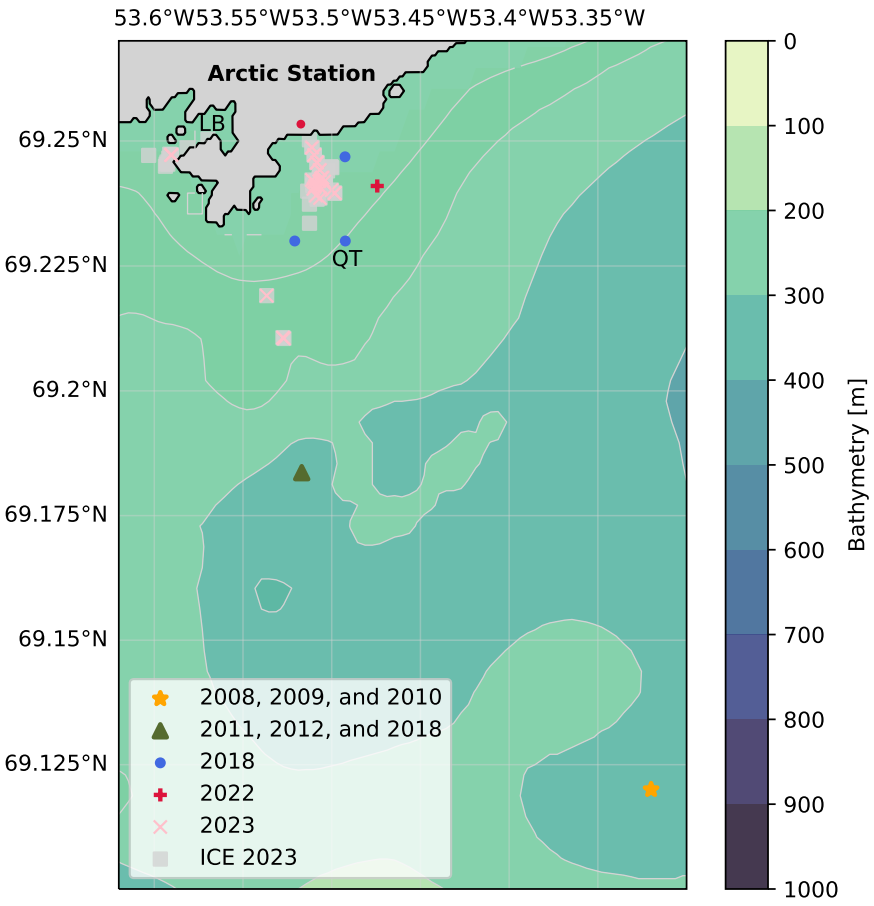

Figure 3.1: *Locations of all CTD and ICE stations of the hydrographic available data in proximity to Arctic Station. Measurements from 2023 were taken between the 6th of March and the 20th of March 2023. Grey squares mark the locations of sea-ice thickness measurements (ICE stations), and crosses represent CTD stations. The measurements for 2008 to 2010 were taken at the same spot and are marked with a yellow star. The measurements for 2011, 2012, and three of 2018 were also taken at the same location; therefore, they are marked with a green triangle. The remaining measurements of 2018 are marked by a blue dot. The red dot marks the location of Arctic Station. QT represents Qeqertarsuup Tuna and LB Lynngmarkt Bugt. The high-resolution coastline is from NOAA (Wessel & Smith, 1996), and the Bathymetry shading is from ETOPO 2022 (NOAA, 2022a) with isobaths in 100 m intervals in light grey. ETOPO 2022 estimates the bathymetry around Disko Island to be deeper than it is.*

The procedure at each CTD station was as follows: we drilled a hole and measured sea-ice thickness with an ice thickness gauge. We measured a positive or negative freeboard with a folding ruler. Then, we would measure snow thickness by drawing a 1 x 1 m square in the snow with our folding ruler, measured in each corner and, once, in the middle. The average of these five measurements was the stations's snow thickness. We tried to use a patch of snow that seemed relatively homogeneous and avoided small hills or snow slabs. Afterwards, we would measure the bottom depth of the water column with a handheld sonar and conduct a CTD cast.

After lowering the CTD into the water, we waited for the sensors to display constantly stable values. This process could take up to a few minutes, and at other times, we flushed the sensors by lowering and heaving the CTD a few meters so the sensor could adjust to the

waters'temperature and salinity. Flushing the CTD sensors was sometimes necessary as the temperature sensor range has a minimum of -2 °C, and the air temperature was substantially lower. After temperature and salinity values stabilised, we lowered the CTD by hand with an approximated speed of 1 m s^{-1} around 5 to 8 dbar above the bottom. This was possible as the CTD was connected to the computer, where we could read off pressure values.

In total, we obtained 84 sea-ice thickness measurements (ICE stations) and 37 CTD casts. Thirty were taken under the fast ice in and one in open water in QT. Four CTD casts were conducted in LB. The furthest CTD cast under the sea ice was taken 1.5 km from the coast. The furthest three CTDs were taken approximately 4 km from Arctic Station during an expedition with a boat. Two of those were taken on an ice floe, and one was taken in open water from the boat. The depth for those three CTD casts ranged between 150 and 200 dbar, the deepest profiles during the fieldwork. The CTD casts taken on the fast ice in QT ranged between 12 and 120 dbar, and sea-ice thickness varied between 10 and 75 cm. The CTD casts in LB were down to around 80 dbar, and sea-ice thickness varied between 20 to 30 cm.

3.2 Sea Ice

One of my main objectives is to construct a JFM Sea-Ice Concentration (SIC) time series for Disko Bay. I use the Sea-Ice Coverage Index (SIC Index) from The Greenland Ecosystem Monitoring (GEM) to get an idea of the sea ice around Disko Island. In addition, I am interested in the representation of the SIC Index to the sea-ice conditions in Disko Bay. Hence, I compare the SIC Index to two satellite-based SIC products for Disko Bay. The two satellite products are a 1k m spatial resolution product (SIC 1 km) by the University of Bremen (UoB) (Figure 3.2 and Table 3.1, Ludwig et al., 2019, 2020) and a 12.5 km spatial resolution product; (SIC 12.5 km) product by the European Space Agency (ESA) (Figure 3.3 and Table 3.1, Lavergne et al., 2023)

Table 3.1: *Sea ice data sets, their source, start and end date and spatial resolution. A dash in the End column indicates that the product is ongoing.*

Data set	Source	Start	End	Spatial Resolution
Sea-ice coverage	GEM, Visual Inspection	1991	-	NaN
SIC Climate Data Record V3	ESA, SSM/I & SSMIS	1991	2020	12.5 km
1 km resolution SIC	UoB, Modis & AMSR 2	2018	-	1 km

SIC 1 km is a combination of MODIS-Aqua (Thermal infrared) and AMSR2-GCOM_W1 (Passive Microwave) satellite data, providing three different SIC products: MODIS SIC, AMSR-2 SIC and a merged SIC from MODIS and AMSR-2. I use the merged SIC as this offers a continuous SIC product with a spatial resolution of 1 km. The uncertainty of SIC 1 km from February to April is 5%

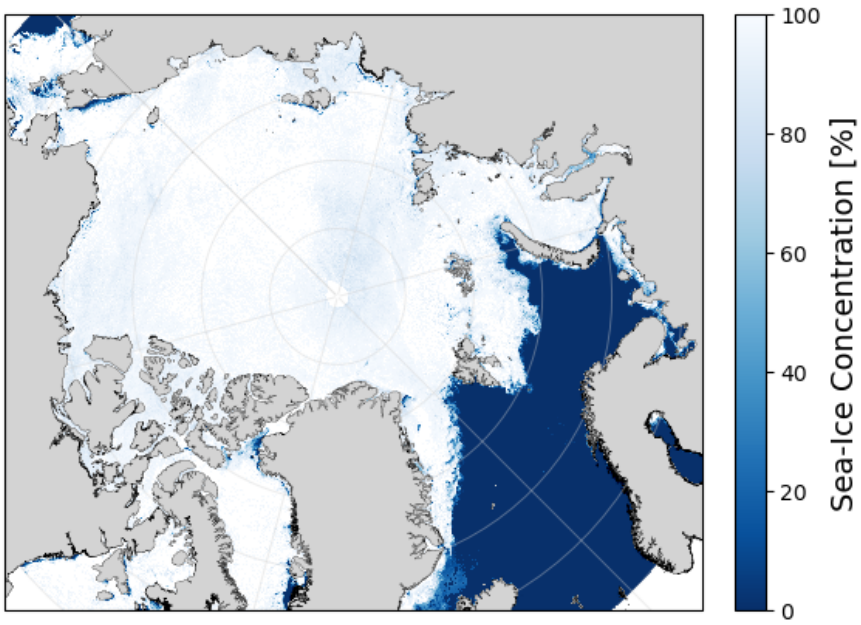

Figure 3.2: *Arctic sea-ice concentration of the 1 km sea-ice concentration product south to 60 °N on the 15th of March 2020 (Ludwig et al., 2019, 2020). Land is marked in light grey, and sea-ice concentration is in shades of blue. The high-resolution coastline is from NOAA, GSHHG (Wessel & Smith, 1996).*

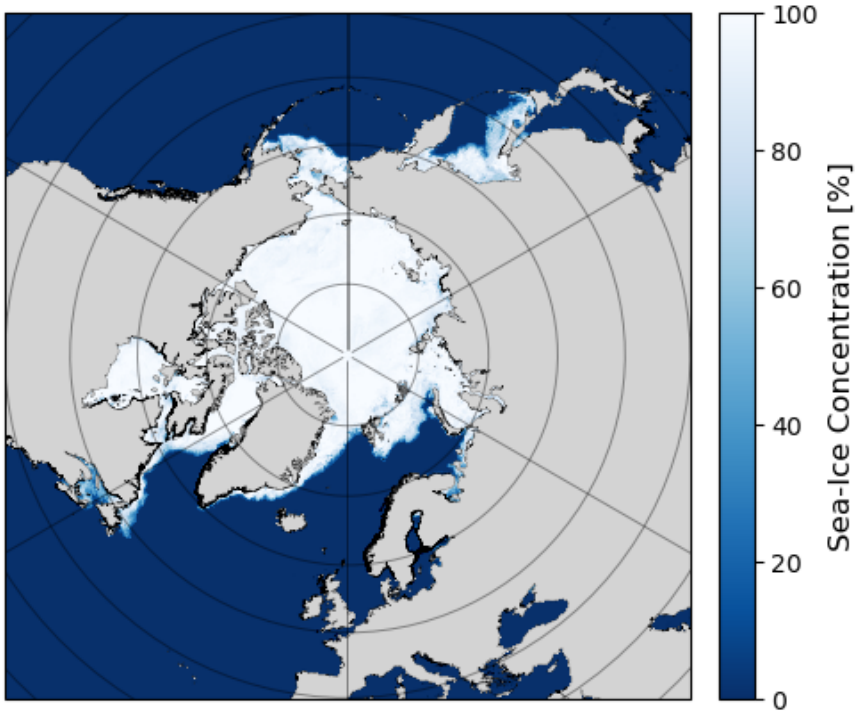

Figure 3.3: *Arctic sea-ice concentration of the 12.5 km sea-ice concentration product on the 15th of March 2020 (Lavergne et al., 2023). Land is marked in light grey, and sea-ice concentration is in shades of blue. The high-resolution coastline is from NOAA, GSHHG (Wessel & Smith, 1996).*

SIC 12.5 km is a recently published SEA Ice Climate Change initiative (Sea_Ice _cci:) High(er) Resolution Sea Ice Concentration Climate Data Record Version 3 (SSM/I and SSMS) product covering 1991 to 2020 (Lavergne et al., 2019, 2023). Sea-ice concentration is derived from SSM/I (Special Sensor Microwave/Imager) and SSMIS (Special Sensor Microwave Imager/-Sounder) radiometers. The SSM/I radiometer measures at multiple frequencies (19.3, 22.2, 37, and 85.5 GHz), with the first three having a pixel resolution of 25 km and the last one of 12.5 km. The SSMIS radiometer has comparable specifications to SSM/I but measures at 91.1 GHz instead of 85.5 GHz.

SIC 12.5 km offers two daily SIC products: the raw SIC and the main filtered SIC. I am interested in the main filtered SIC, which already went through several filters like an open water filter and post-processing steps (e.g. interpolation and thresholding). I extracted the main filtered SIC from 2003 to 2020. This product also provides three uncertainties. I calculated the uncertainty for JFM SIC in Disko Bay from 2003 to 2020 with their total mean uncertainty, which resulted in 2.34%.

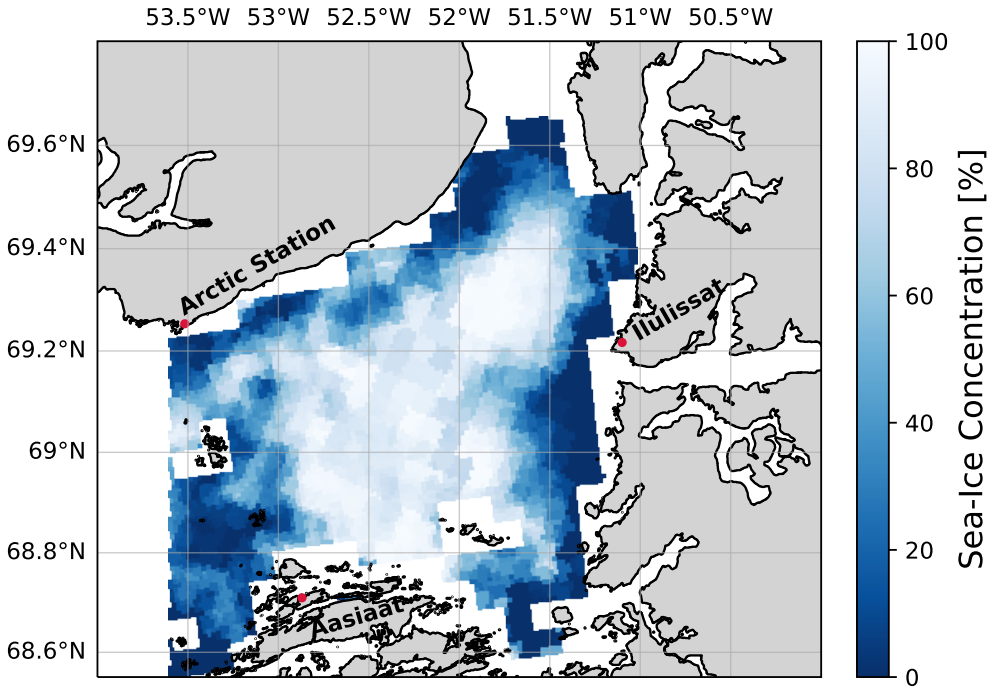

Figure 3.4: *Disko Bay sea-ice concentration with a spatial resolution of 1 km on the 15th of March 2020. Red dots mark Arctic Station, close to Qeqertarsuap, and the two closest cities, Ilulissat and Aasiaat. The high-resolution coastline is from NOAA, GSHHG (Wessel & Smith, 1996).*

The coordinates I used to extract SIC for Disko Bay are slightly different, resulting from the different projections offered by the two products (Figures 3.2 and 3.3). SIC 1 km is in North Polar Stereographic projection, and the coordinates are 68.55 to 69.58 °N and 50 to 53.3 °W (Figure 3.4). SIC 12.5 km is in Lambert Azimuthal Equal Area polar projection. The coordinates I used to extract SIC values slightly differ from SIC 1 km with 68.7 to 69.53 °N and 51.4 to 52.9 °W (Figure 3.5). Though I use other coordinates to extract SIC data, the acquired SIC area is very similar (Figures 3.4 and 3.5). However, it is possible that the extraction could lead to minimal deviations between the two SIC products.

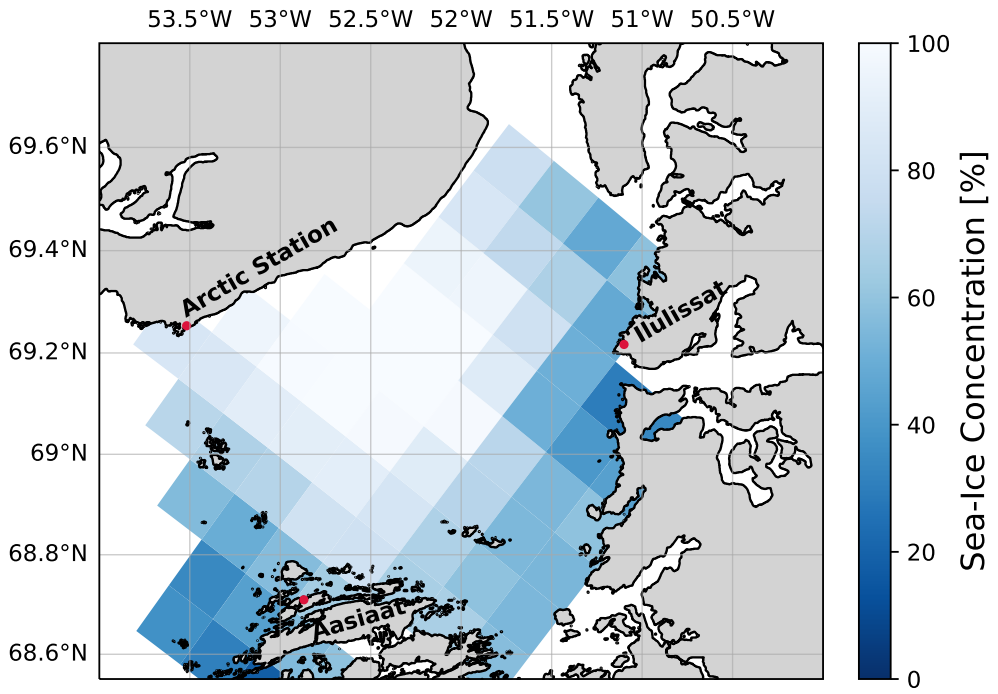

Figure 3.5: *Disko Bay sea-ice concentration with a spatial resolution of 12.5 km on the 15th of March 2020. Red dots mark Arctic Station, close to Qeqertarsuap, and the two closest cities, Ilulissat and Aasiaat. The high-resolution coastline is from NOAA, GSHHG (Wessel & Smith, 1996).*

These two data sets combined cover 2003 to 2023. Both SIC products cover 2018 to 2020; therefore, comparing their extracted SIC values to estimate their performance is possible. Furthermore, it is possible to do a pixel comparison of the closest available pixel to Arctic Station and compare this to the Sea Ice index to check how representative it is of the whole of Disko Bay.

SIC 1 km values need to be converted to latitude and longitude before SIC can be extracted, while SIC 12.5 km values have preassigned latitude and longitude coordinates. I created a mask based on the Disko Bay area (68.55 to 69.58°N, 50 to 53.3 °W). Afterwards, I applied the latitude and longitude mask on the data set, retrieving daily SIC. This results in a time series of daily SIC for 2003 to 2020 with a spatial resolution of 12.5 km and for 2018 to 2023 with a spatial resolution of 1 km. Lastly, I calculated weekly, monthly and JFM SIC (means).

Sea Ice Index

GEM provides hydrographic parameters and an index of a visual observation of the ice cover close to shore (SIC Index). These observations are daily, looking south from Arctic Station. They started on the 1st of January 1991 and are ongoing (GEM, 2020a). This data set has the potential to provide a long-time series of sea ice cover variability, providing good insight for the analysis. Nowadays, the station or scientific leader takes the visual inspection on the front porch (Figure 3.6) of the station. Visibility from the lookout stretches approximately 1.2 to 1.4 km south into QT, overseeing the sea ice in front of the station. Sea-ice cover is primarily documented in increments of 5% or 10 %.

Figure 3.6: *View from the porch facing Qeqertarsuup Tuna in front of Arctic Station used to inspect the sea-ice cover daily. Photograph taken by Lars H. Smedsrud on the 8th of March 2023.*

3.3 Ocean

To investigate the influence oceanic forcing has on sea-ice variability, I use observational hydrographic data from three different data sources. I am interested in temperature and salinity profiles inside Disko Bay (Figure 3.7) for January to March. Winter data is sparse; therefore, I was not able to acquire hydrographic data for every year. I was able to acquire data for nine out of 21 years. Most of my hydrographic profiles are from GEM, which has a fixed monitoring station (69.25 °N, 53.55 °W) close to Arctic Station. GEM conducts their measurements with a Sea-Bird CTD. From GEM, I have data for 2008 to 2012, 2018, and 2022. I obtained 30 CTD casts, ranging from one to six CTD casts during JFM and varying in depth between 160 and 270 dbar (Figure 3.7, GEM, 2020c,b).

From Ocean Melting Greenland (OMG), I use a CTD cast close to Ilulissat for 2020 (Figure 3.7, OMG, 2019). Lastly, I am using the 37 CTD casts we conducted during our fieldwork, which varied in depth between 12 and 200 dbar for 2023. Additional information about the single CTD casts, their dates, their bottom values and exact locations are found in Appendix B (Tables B.1 to B.9).

In total, I have 86 CTD casts spread over nine years for JFM. Two CTD casts in January (2010), 11 CTD casts in February (2008, 2009, 2010, 2011, and 2018), and 73 CTD casts in March (2008, 2009, 2010, 2011, 2012, 2018, 2020, 2022, and 2023). The location of the measurement is marginally spread out over Disko Bay (Figure 3.7). However, most CTD casts are located close to the inflow area to the western edge of Disko Bay, and only one CTD cast is towards the east, close to Ilulissat (Figure 3.1).

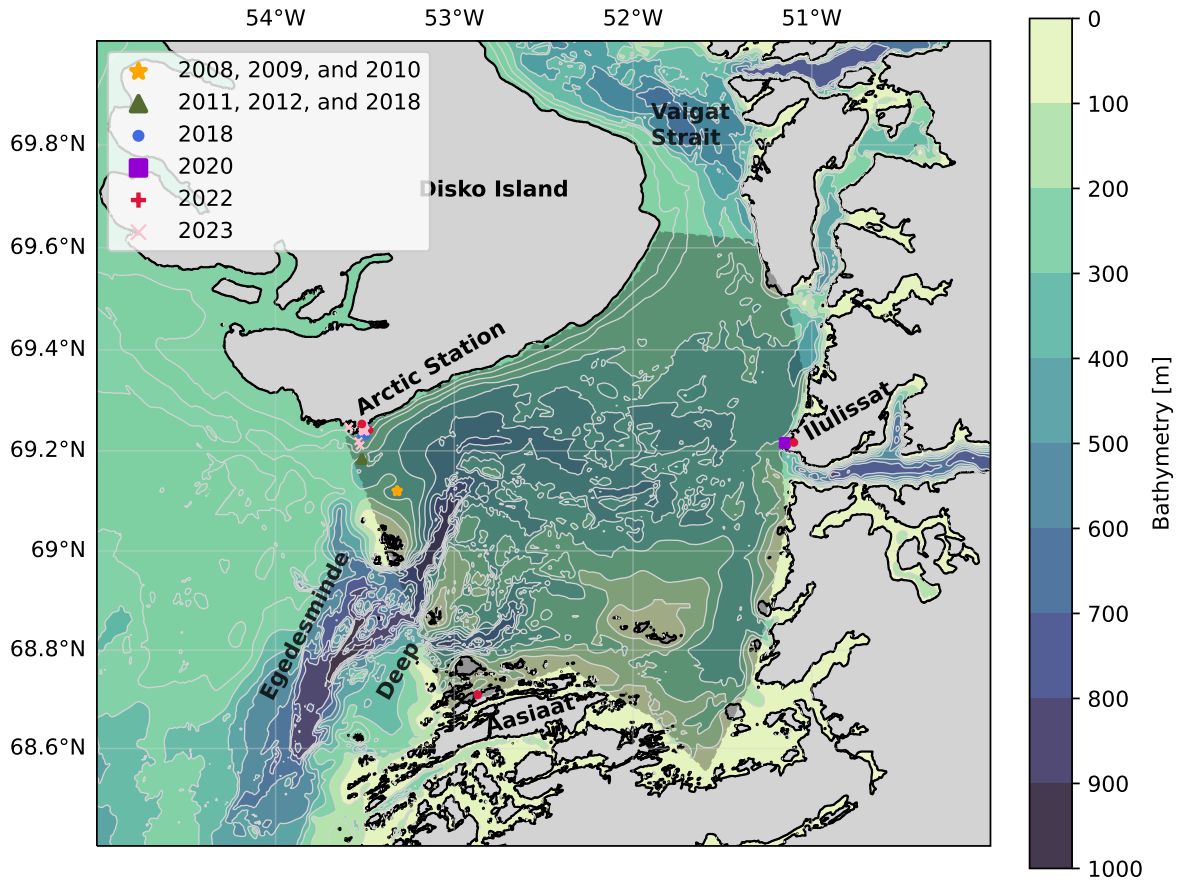

Figure 3.7: *Locations of all CTD stations of the hydrographic data. The area of interest inside Disko Bay is depicted as a lightly shaded polygon. A detailed map of the CTD casts near Arctic Station is shown in Figure 3.1. Notably, hydrographic measurements from 2008 to 2010 were taken at the same location and, thereby, are represented by a yellow star. Measurements of 2011, 2012, and 2018 were also taken at the same location and, therefore, are marked with a green triangle. Red dots mark Arctic Station, in Qeqertarsuap, and the two closest cities, Ilulissat and Aasiaat. The high-resolution coastline is from NOAA (GSHHG) (Wessel & Smith, 1996), and Bathymetry shading is from ETOPO 2022 (NOAA, 2022a) with isobaths in 100 m intervals in light grey. ETOPO 2022 estimates the bathymetry around Disko Island to be deeper than it is.*

Due to multiple CTD casts per day and varying CTD casts per month and year, I computed daily, monthly, and JFM means. If only one CTD cast was available for a month, I assumed this to be the monthly and JFM mean. The averaging process is the following:

1. Remove outliers greater than 2 standard deviations for temperature and salinity/conductivity
2. Convert depth to pressure [dbar], or pressure from psi to dbar
3. Calculate practical salinity from conductivity
4. Compute absolute salinity [g kg^{-1}]
5. Derive conservative temperature [°C]
6. Calculate potential density anomaly sigma0 [kg m^{-3}], with a reference pressure of 0 dbar

7. Bin the data into 1-dbar bins
8. Cut the top three dbar to remove any potential measurement errors
9. Calculate daily, monthly, and JFM means of the binned CTD profiles

I followed this procedure for each year. However, in 2011, the standard deviation was decreased to 1. Otherwise, the regular surface variation would have been removed. A Standard deviation greater than 2 worked best for the remaining years in removing extreme outliers while retaining surface variations in the top 10 to 20 dbar. If conductivity measurements were available, those were used to be more precise instead of pre-calculated salinity. If no conductivity values were given, step 3 was disregarded. While calculating the 1-dbar bins, I chose not to interpolate. Therefore, some of the daily means show gaps of no measurements (Figure 3.8). In the following, temperature represents conservative temperature [°C] and salinity absolute salinity [g kg^{-1}]. I ended up with daily, monthly and JFM means.

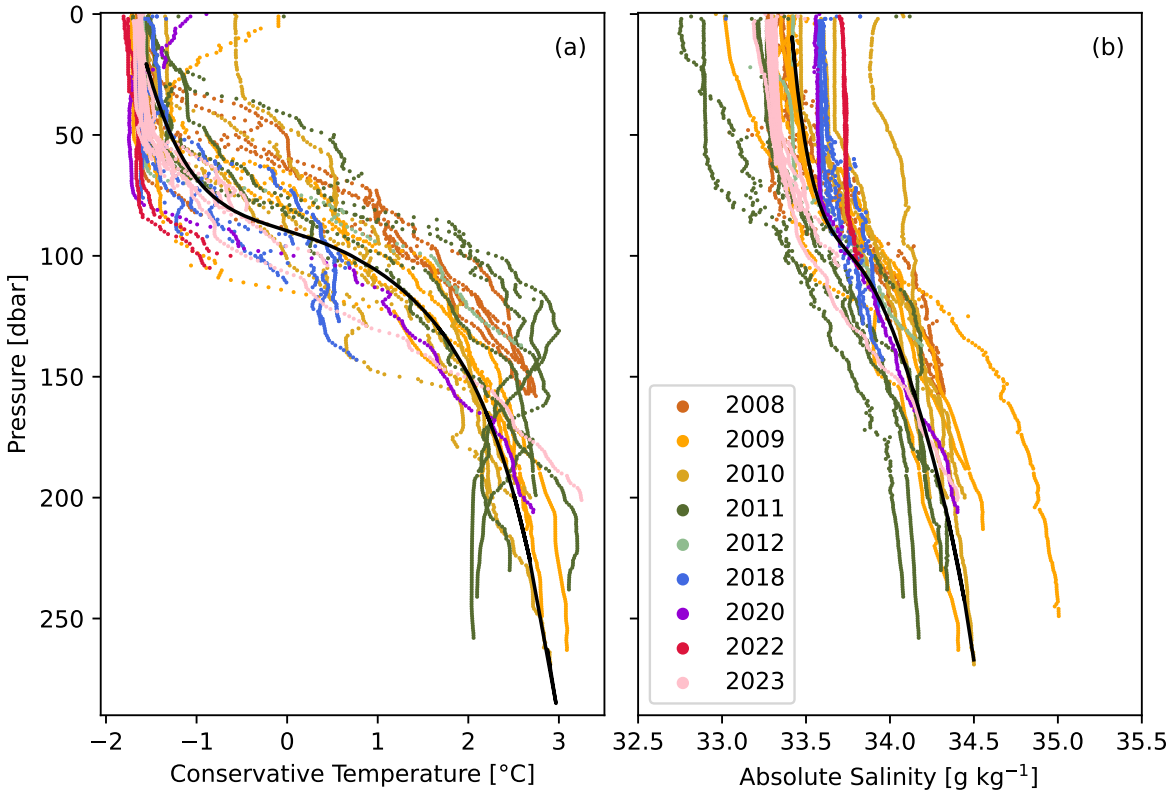

Figure 3.8: *Vertical profiles for temperature (a) and salinity (b) of the hydrographic data. Black solid lines represent the overall mean of a polynomial fit of the fifth degree for temperature and salinity.*

The hydrographic data were nearly all conducted close to or near Arctic Station. Therefore, I have no measurements from the deep parts or central Disko Bay. Moreover, most of the measurements are from March, and only a few are from January or February, which could lead to a small bias. This requires a spatial analysis of the hydrographic data.

Auxiliary Data sets

Additional datasets I used are a Bathymetry, a high-resolution coastline, and a higher-resolution sea surface temperature data set.

The Bathymetry data is from the ETOPO Global Relief Model. For the area around Disko Bay, I used the ETOPO 2022 15 Arc-Second Global Relief Model ice surface elevation (Figures 2.4, 3.1 and 3.7, NOAA, 2022a). For larger scales, I used ETOPO 2022 30 Arc-Second Global Relief mode ice surface elevation (Figures 1.2 and 2.3, NOAA, 2022b). The area around Arctic Station is not well captured in python'coastline cartopy package; therefore, I used the global Self-consistent, Hierarchical, High-resolution Geography Database (GSHHG) (Figures 2.3, 2.4, 3.1, 3.7, 4.10 and 4.11, Wessel & Smith, 1996).

I used the global ocean, OSTIA Sea Surface Temperature (SST) and Sea Ice Analysis product for sea surface temperature during the summer months, July, August and September (JAS). OSTIA provides daily gap-free maps of SST at a horizontal grid resolution of 0.05° x 0.05°. It utilises satellite, infrared and microwave radiometer measurements and in-situ measurements. I extracted SST for 68.55 to 69.8 °N and 50 to 53.6 °W. I computed a spatial average and calculated daily, weekly, and JAS means (Stark et al., 2007; Donlon et al., 2012; Good et al., 2020; CMEMS, 2023). I used GHRSST instead of ERA 5 as it has a finer spatial resolution but is only available from 2007.

3.4 Atmosphere

I use atmospheric variables from the ECMWF Reanalysis v5 (ERA5) data set to investigate the influence of atmospheric forcing on sea-ice variability. This data set is hourly on single levels from 1940 to the present (Hersbach et al., 2023, 2020; ECMWF, 2023). I downloaded the data based on my defined area in Disko Bay (68.55 to 69.8 °N, 50 to 53.6 °W) (Figure 3.7). Temperatures, winds, and several mean heat fluxes are of interest (Table 3.2). GEM also offers meteorological parameters; however, there is not one data set covering 2003 to 2023 that simultaneously includes temperature, wind direction and wind speed. Furthermore, the meteorological stations are placed in various locations, and the sensors for the same variable are placed at different heights at nearly every weather station. Additionally, they do not offer information about heat fluxes. Therefore, to minimise errors due to measurement variability, I focus on the ERA 5 data set.

Table 3.2: *Hourly exported parameters from the ERA 5 hourly on single levels data set for the defined area in Disko Bay (68.55°N to 69.8°N, 50°W to 53.6°W) and their units for JFM for 2003 to 2023. * the original units were converted to SI units.*

Atmosphere	**Unit***	**Abbrevation**
Temperature and pressure		
Sea Surface Temperatures	°C	SST
2 m Temperature	°C	T2M
Surface Pressure	hPa	SP
Wind		
10 m u wind	$m\ s^{-1}$	10U
10 m v wind	$m\ s^{-1}$	10V
Radiation and heat		
Surface net solar radiation	$W\ m^{-2}$	SSR
Surface net thermal radiation	$W\ m^{-2}$	STR
Surface latent heat flux	$W\ m^{-2}$	SLHF
Surface sensible heat flux	$W\ m^{-2}$	SSHF

Temperature and Pressure
I am interested in the Sea Surface Temperature (SST) and the Temperature at 2 m elevation (T2M). The former is the temperature of the water near the surface, and the latter is the temperature above the surface of land, sea or inland waters. I am also interested in Surface Pressure (SP), representing atmospheric pressure at the surface.

Wind
Winds are represented in the u and v-components at 10 m (10U, 10V), while u represents the eastward component of the wind, the horizontal speed of air moving towards the east, and v represents the northward component of the wind. I am interested in wind speed and wind direction. The 10 m wind speed is calculated with Equation (3.1).

$$|\vec{V}| = \sqrt{u^2 + v^2} \tag{3.1}$$

The wind direction is extracted with Equation (3.2) and represents the meteorological wind direction. The meteorological wind direction is the direction from which the wind is coming.

$$\theta = \frac{180 + \frac{180}{\pi}\text{atan2}(v, u)}{360} \tag{3.2}$$

The wind direction is calculated with the arctan, and by multiplying with 180 π^{-1}, I convert the wind direction from radians to degrees. The addition of 180 results in the meteorological convention of the wind direction. The division by 360 projects the wind direction onto a full circle.

Radiation and heat
The heat fluxes studied to explain sea-ice variability are the Surface Latent Heat Flux (SLHF), Surface Sensible Heat Flux (SSHF), Surface net Solar Radiation (SSR) and Surface net Thermal Radiation (STR). Vertical fluxes are available at ECMWF and are, by convention, positive downwards. SSHF represents the transfer of heat between the atmosphere and the Earth's surface through turbulent air motion. SSHF excludes the heat transfer, which is a consequence of condensation or evaporation. This is represented in SLHF. SSR is the quantity of solar radiation that reaches the Earth's surface minus the reflected solar radiation by the surface of the Earth. STR is the difference between downward and upward thermal radiation at the surface of the Earth. Sea ice controls how much SSR the ocean can absorb, as the sea ice has a high albedo and is very reflective. Consequently, the ocean absorbs less solar radiation with a sea-ice cover (Thomas, 2017).

I calculate the spatial average of each variable. In further calculations, I computed daily, weekly, and JFM means. I will use these to identify potential reasons for sea-ice variability in Disko Bay.

3.5 Correlation studies

I correlate hydrographic and atmospheric data to SIC to investigate whether oceanic or atmospheric forcing is the main driver for winter sea-ice variability in Disko Bay. For this, I use two statistical approaches. The first uses a statistical correlation model (Personal communication, Maritn Lindegren), and the second is a simple correlation (Thomson & Emery, 2014).

Statistical Correlation Model

The statistical correlation model includes three different approaches: a Linear regression Model (LM) (Wilkinson & Rogers, 1973; Chambers, 1992), a Generalised Additive Model with inte-

grated smoothness estimation (GAM) (Hastie, 1990), and a Random Forest model (RF) (Breiman, 2001). Initially, I wanted to use these correlation models to correlate atmospheric and oceanic forcing to SIC. However, due to sparse hydrographic data, it was not possible to correlate oceanic data to SIC. Therefore, I only correlate atmospheric forcing to SIC.

To correlate SIC to atmospheric forcing, I require a response and a predictor variable. The predictor variables are atmospheric variables, which are available for 2003 to 2023, and the response variable is SIC. In contrast to the atmospheric data, I do not have a continuous daily SIC time series of the same spatial resolution. The longest satellite-derived SIC time series is SIC 12.5 km, covering 2003 to 2020. As mentioned, SIC 1 km and SIC 12.5 km overlap from 2018 to 2020. This allows me to calculate the intercept and slope of the linear regression and then estimate the SIC for 2021 to 2023 with a spatial resolution of 12.5 km with Equation (3.3).

$$\mathrm{SIC}_{\mathrm{pred}} = \mathrm{intercept} + \mathrm{slope} \cdot \mathrm{SIC}_{1\,\mathrm{km}} \tag{3.3}$$

$\mathrm{SIC}_{\mathrm{pred}}$ are the computed SIC values for 2021, 2022, and 2023, and $\mathrm{SIC}_{\mathbf{1\,km}}$ are SIC values of SIC 1 km from 2021, 2022, and 2023 used as input variables. I predicted daily and monthly SIC values with a spatial resolution of 12.5 km for 2021 to 2023. The intercept and slope values for daily SIC are 29.20 and 0.72, respectively. I also calculated monthly SIC 12.5 km values; however, the RF was only possible to run for daily measurements as monthly data points were too few. In contrast, the LM and GAM were run for daily and monthly SIC and atmospheric forcing. To measure the performance of the three statistical approaches, I compare their explained variance and the Root Mean Square Error (RMSE) of each model (Figure 3.9, Thomson & Emery, 2014).

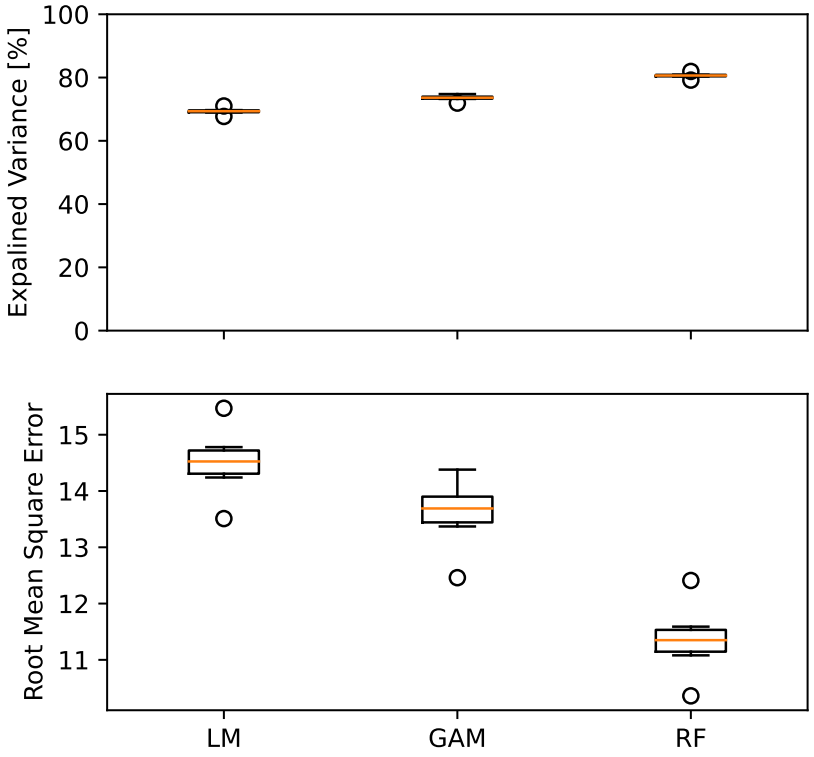

Figure 3.9: *Explained Variance and the Root Mean Square Error for three different statistical models, correlating daily atmospheric variable to daily sea-ice concentration. LM is a Linear regression Model; GAM stands for a Generalised Additive Model with integrated smoothness estimation, and RF for a Random Forest model.*

Explained variance indicates how well the model is able to explain the variability of the sea-ice concentration (response) with the atmospheric variables (predictors) on the training data set. All three models have an explained variance above 60%. However, the RF is the only model with an explained variance above 80%. The RMSE represents the difference between the predicted SIC and the observed SIC. The lower the score, the better the model performs (Thomson & Emery, 2014). The RMSE for each of the three models is below 20. The LM has the highest RMSE of 14.51, followed by GAM with 13.66, and the RF has the lowest RMSE of 11.34.

For my following analysis, I will only use the Random Forest model as it has the highest explained variance of about 82% and the lowest RMSE with 11.34.

Random Forest

A Random Forest model can be used for classification or regression purposes. I used the RF as a regression model to investigate the variable importance (%IncMSE) of the atmospheric variables to SIC.

A RF model combines the simplicity of decision trees with the flexibility of learning from training data and test data. The RF model first creates a bootstrapped data set. In the second step, a decision tree is applied to the bootstrapped data set. A RF model, by default, performs a cross-validation between the test and training data set, as for each decision tree, the test and training set are newly defined as the data set is permuted. In addition, the RF model only considers a certain number of predictor variables for each regression. These two steps are repeated for numerous individual decision trees. The results of all these decision trees are then averaged and presented as a final result (Breiman, 2001; Theodoridis & Koutroumbas, 2006; Hastie et al., 2009). The RF I used considers three predictor variables for each decision tree and achieves the best results with 500 trees. Further detailed and mathematical interpretations of the Random Forest are found in Breiman (2001) and Hastie et al. (2009).

To estimate the performance of the RF by a measure of the relative variable importance of atmospheric variables to SIC, I consider the %IncMSE. The %IncMSE is the Increased Mean Square Error and indicates how much worse a model performs if a certain variable is excluded. The higher the %IncMSE, the more important the variable is in describing the variability and the higher the MSE would increase if the variable were to be excluded (Breiman, 2001; Behrouz et al., 2022).

The %IncMSE is calculated in four steps. First, the RF model calculates the prediction error for the regression, the Mean Square Error (MSE). Second, the MSE is calculated after permuting the predictor variables. Third, the difference between the MSE of the first step and the MSE of the second step is calculated. This is then repeated for each decision tree and divided by the standard deviation of the difference, resulting in the %IncMSE (Breiman, 2001; Behrouz et al., 2022).

Correlation

Additionally to the Random Forest model, I calculated correlation coefficients r (Pearson Correlation, significance level = 0.05) between JFM atmospheric and oceanic variables and JFM SIC in Disko Bay. For winter SIC from 2003 to 2023, I used the linearly interpolated SIC with a spatial resolution of 12.5 km, which I utilised for the RF model. Furthermore, I include the NAO index (NOAA, 2023). The correlation coefficient r indicates the interrelationship between two variables (Thomson & Emery, 2014). r is dimensionless, and values can be between -1 and 1. The variables are either positively or negatively perfectly correlated if r is either +1

or -1. The two variables are not correlated when $r = 0$. Negative correlation values, between 0 and -1, indicate that when one variable changes in one direction, the other variable evolves in the contrary direction, while a positive correlation coefficient indicates that the two variables in the same direction evolve (Thomson & Emery, 2014).

Chapter 4

Results

In this chapter, I present my results in four sections. First, I compare photographs taken over Disko Bay to the visual observations of the Sea-Ice Coverage Index, SIC Index, to examine how representative it is of Disko Bay. In addition, I explore the closest available pixel (CAP) to Arctic Station of the SIC products (SIC 1 km and SIC 12.5 km) and compare them to the SIC Index for 2018 to 2020. Moreover, I compare SIC 1 km and SIC 12.5 km for Disko Bay for their overlapping years. Further, I present a constructed time series of JFM SIC of Disko Bay with SIC 1 km and 12.5 km (Section 4.1). Second, I investigate how representative the fieldwork data of March 2023 is to Disko Bay. Furthermore, I present the hydrography and water characteristics of Disko Bay in JFM. I also present a water mass analysis regarding Polar Water and West Greenland Irminger Water of the hydrographic data (Section 4.2). Third, I present the mean JFM evolution from 2003 to 2023 for SIC and the atmosphere of Disko Bay. Moreover, I present the correlation coefficients of SIC to atmospheric and oceanic parameters. Furthermore, I describe the results of the Random Forest model, which I used to determine the atmospheric variables with the largest %IncMSE concerning SIC variability (Section 4.3). Lastly, an investigation of years with high and low SIC aiming to find an explanation of how oceanic and atmospheric forcing influence SIC variability is presented (Section 4.4).

4.1 Sea Ice Observations

In this section, I present photographs taken over Disko Bay and compare them to the SIC Index to examine its representation of SIC in Disko Bay (Figures 4.1 and 4.2). Moreover, I compare the SIC Index to the CAP of SIC 1 km and SIC 12.5 km (Figures 4.3 and 4.4). Furthermore, I compare SIC 1 km and SIC 12.5 km of Disko Bay for the overlapping years of 2018 to 2020 (Figure 4.5). Lastly, I present a constructed time series of JFM SIC for 2003 to 2023 (Figure 4.6).

An analysis of the representation of the SIC Index to the CAP of the two satellite-derived SIC products revealed that the SIC Index represents the fast ice, and SIC 12.5 km the fast ice and the SIC in Disko Bay. While SIC 1 km solely represents the SIC in Disko Bay. The analysis of the SIC in Disko Bay detected by SIC 12.5 km and SIC 1 km showed a systematic difference of around 20% due to higher SIC estimated by SIC 12.5 km. This difference is evident at the beginning of January and at the end of March. However, the difference decreases when both determine the SIC to be about 75%. SIC in Disko Bay from 2003 to 2023 showed pronounced year-to-year variability, a small positive trend, and a small decadal variability.

Spatial extent of the SIC Index

The SIC Index offered by GEM is one available source of a continuous time series of JFM SIC of Disko Bay (Figure 4.1), and I want to investigate how spatially representative the SIC Index is for Disko Bay. Weather plays an important role as in bad weather conditions, visibility decreases, and in good weather conditions, it is possible to look 1 to 2 km into the distance (Figure 3.6).

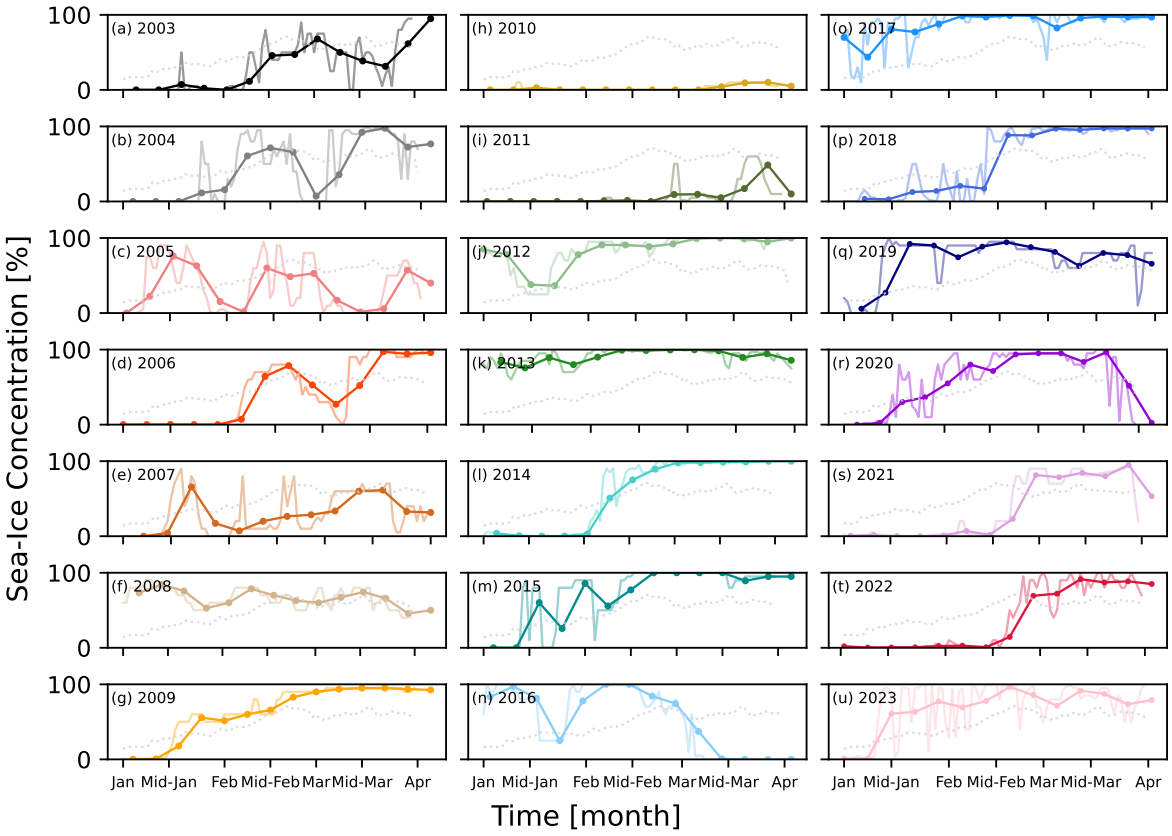

Figure 4.1: *Daily and weekly JFM SIC for 2003 to 2023 of the visual observed SIC Index as seen 1 to 2 km south of Arctic Station (GEM, 2020a). Solid lines represent weekly SIC means, lighter lines represent daily SIC means, and the dotted grey line represents the mean JFM evolution of SIC 1km and SIC 12.5 km from 2003 to 2023.*

Measurements of the SIC Index are taken by the scientific leader, who is employed for two to three years, indicating that there might be a personal bias in the data, as the inspection is subjective. Examples of what the SIC Index represents become evident on the day of arrival and departure in March 2023. For the arrival and departure days, the sea-ice cover estimated by the scientific leader was 80% for the former and 95% for the latter (Figure 4.1u). During our arrival and departure helicopter flights, I was able to take photographs (Figure 4.2 a, b, e, and f), and it was evident that SIC in the bay had quite different values.

On the 6^{th} of March, we flew north from Aasiaat to Qeqertarsuaq. We saw patches of thin, rafted, ridged, pancake ice, and an abundance of open water sections in between (Figure 4.2a and b). Most dominant was the visibility of open water and otherwise accumulations of thin sea ice. This would not be equivalent to a sea-ice cover of 80%.

The day we departed Qeqertarsuaq, on the 20th of March 2023, we flew east from Qeqertarsuaq to Ilulissat. Similarly to the arrival day, we saw large stretches of open water and accumulations of thin sea-ice patches (Figure 4.2e and f), which is not representative of a SIC of 95%. However, we did see more icebergs, as Jakobshavn Isbræ produces many.

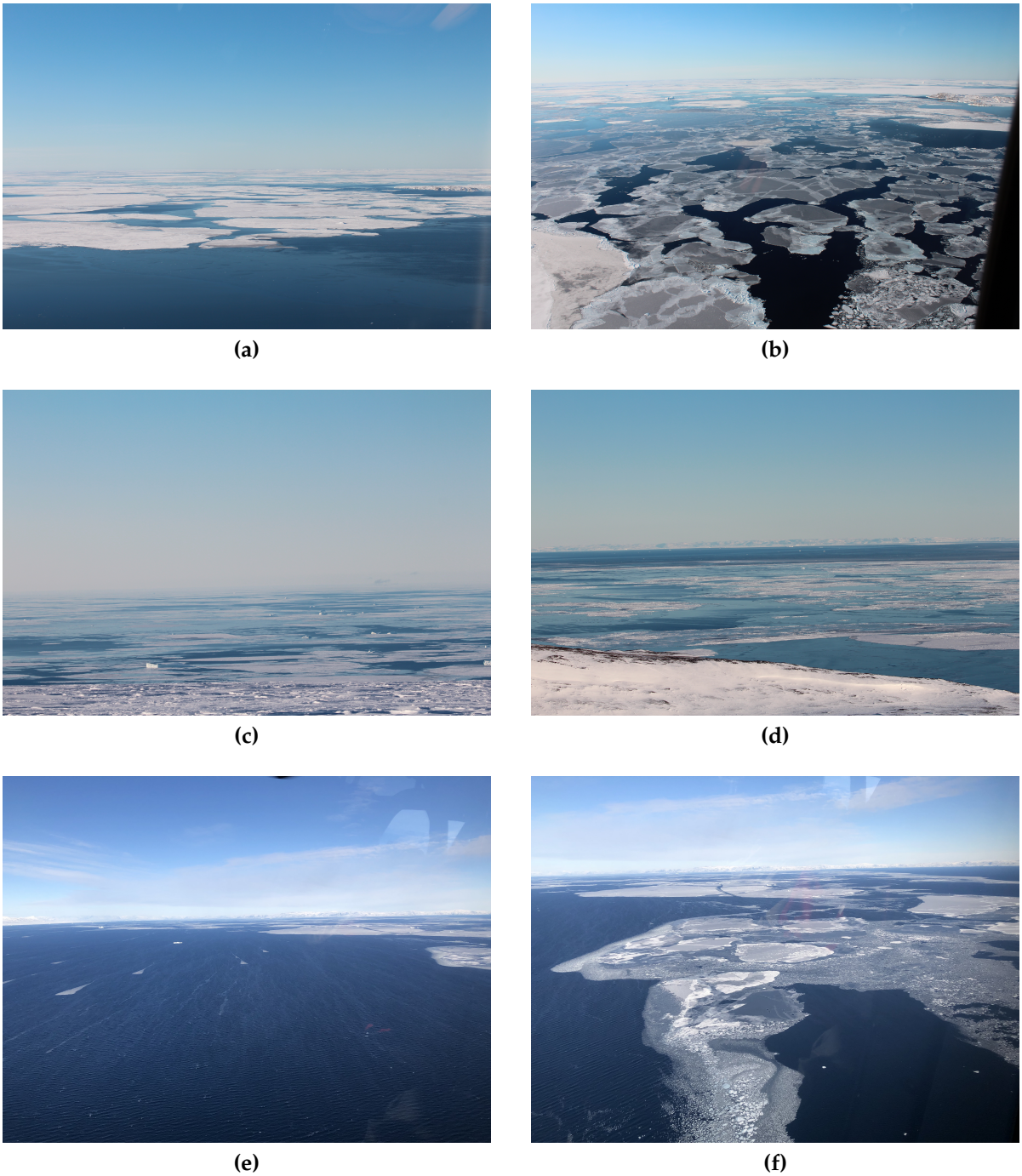

(a) **(b)** **(c)** **(d)** **(e)** **(f)**

Figure 4.2: *Sea-ice conditions seen from a helicopter on the 6th of March 2023 flying north from Aasiaat to Qeqertarsuap (a,b). Sea-ice conditions on the 12th of March from a mountain (c,d). Sea-ice conditions from the helicopter on the 20th of March 2023 flying east from Qeqertarsuap to Ilulissat (e,f).*

I had the opportunity to join an excursion to the southern-west side of Qeqertarsuap, where I took additional photographs (Figure 4.2c and d). They showed a few stranded icebergs near Qeqertarsuaq, originating from the Jakobshavn Isbræ (Figure 4.2c). The photographs also showed that the area close to the shore had higher sea-ice coverage than further out in the bay, which mainly consisted of open water (Figure 4.2d). Sea-ice conditions in March 2023 were characterized by various types and thicknesses of sea ice (Figure 4.2) and large stretches of open water.

Comparing SIC from Satellite and Visual Inspection

The SIC Index (Figure 4.1) appears to be representative of the fast ice in front of Arctic Station, but I am interested in the sea-ice cover in Disko Bay. Therefore, I selected the CAP of each SIC product (Figure 4.3), extracted daily SIC values for 2003 to 2023, calculated JFM means for each year and compared them to the SIC Index. I aim to estimate how representative the values of the SIC Index are compared to the closest satellite-derived SIC value.

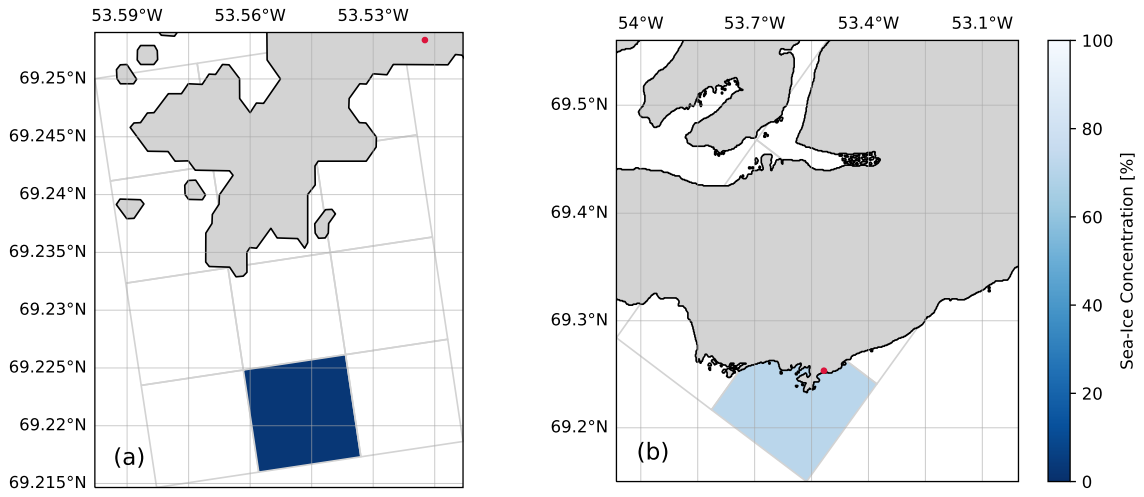

Figure 4.3: *The closest available pixel to Arctic Station for SIC 1 km (a) and SIC 12.5 km (b) on the 15th of March 2020. The red dot in (a) and (b) marks the location of Arctic Station.*

The CAP of SIC 1 km is around 4 km southwest of Arctic Station and does not include the area seen by the SIC Index (Figure 4.3a). In comparison, the CAP of SIC 12.5 km includes the area seen by the SIC Index and fast ice around Qeqertarsuaq (Figure 4.3b). The pixel from SIC 1 km is included in the pixel from SIC 12.5 km.

I analysed the CAP values in comparison to the SIC Index, as well as the CAP values between SIC 1 km and SIC 12.5 km, to better understand the difference between the SIC Index and the two SIC products for JFM of 2003 to 2023 (Table 4.1). Furthermore, I did an in-depth comparison of SIC 1 km and SIC 12.5 km CAP values to the SIC Index for the overlapping years of 2018 to 2020 to improve my understanding of where the differences originate from (Figure 4.4 and Table 4.2).

Table 4.1: *Comparison of the closest available pixel to Arctic Station for SIC 1 km and SIC 12.5 km to the SIC Index. JFM mean differences and JFM mean SIC values for each product and the available years. Negative differences in bold indicate a higher SIC of the second product than of the first product. In comparison, positive values indicate a lower SIC of the second product. There are two missing values in 2019 and two in 2022 in SIC 1 km. All values are given in percent [%].*

Year	SIC Index	SIC 12.5 km	SIC 1 km	ΔSIC 1 km - Index	ΔSIC 12.5 km - Index	ΔSIC 1 km - 12.5 km
2003	29.28	19.63	-	-	**-9.65**	-
2004	43.31	28.72	-	-	**-14.59**	-
2005	34.51	33.96	-	-	**-0.55**	-
2006	42.18	33.89	-	-	**-8.29**	-
2007	29.89	25.75	-	-	**-4.14**	-
2008	66.70	75.72	-	-	9.02	-
2009	64.39	67.88	-	-	3.49	-
2010	2.22	8.16	-	-	5.94	-
2011	7.58	9.66	-	-	2.08	-
2012	83.33	62.71	-	-	**-20.62**	-
2013	91.14	52.18	-	-	**-38.96**	-
2014	56.71	44.42	-	-	**-12.29**	-
2015	71.23	72.18	-	-	0.95	-
2016	56.63	33.16	-	-	**-23.47**	-
2017	88.37	75.10	-	-	**-13.2**	-
2018	55.81	46.73	34.38	**-21.43**	**-9.08**	**-12.35**
2019	72.06	59.94	37.82	**-34.24**	**-12.12**	**-23.44**
2020	60.87	28.74	23.03	**-37.84**	**-32.13**	**-5.71**
2021	30.14	-	16.93	**-13.21**	-	-
2022	39.41	-	30.54	**-8.87**	-	-
2023	70.94	-	55.17	**-15.77**	-	-
Mean	52.22	41.37	32.98	**-21.89**	**-9.87**	**-13.83**

Comparing SIC 1 km to the SIC Index for all available years, 2018 to 2023, it is evident that the SIC Index always measured higher SIC than SIC 1 km. The difference varied between 8.87% (2022) and 37.84 % (2020) (Table 4.1). The mean difference between SIC 1 km and SIC Index is 20%, indicating that the SIC Index estimates about 20% higher SIC values (Table 4.1).

SIC Index compared to SIC 12.5 km for 2003 to 2020 indicates that the SIC Index detected higher SIC values on 13 occasions, with differences of 0.55% (2005) to 38.96% (2013) (Table 4.1). In contrast, on five occasions, the SIC Index measured lower values than SIC 12.5 km, and the differences varied between 0.95% (2015) and 9.02% (2008) (Table 4.1). There is no clear indication when the SIC Index measured higher JFM averages than SIC 12.5 km, as some years had high SIC (2015 and 2008) while others had low SIC (2010 and 2011) (Table 4.1). Nevertheless, the differences are smaller for years when SIC 12.5 km detected higher SIC than the SIC Index.

SIC 12.5 km and the SIC Index agree reasonably well with a mean difference of about 10% (Table 4.1), suggesting that over 18 years, the SIC Index indicated 10% higher SIC than SIC 12.5 km. The comparison of the CAP values showed that for the overlapping years 2018 to 2020, SIC 12.5 km had consistently higher JFM mean values than SIC 1 km (Table 4.1). The differences varied between 5.71% (2020) and 23.44% (2019) (Tables 4.1 and 4.2). The mean

difference between the CAP values of SIC 1 and 12.5 km is about 15% (Tables 4.1 and 4.2).

To better understand where these systematic differences originate from, I examined the daily variability of the CAP of SIC 1 km, SIC 12.5 km and the SIC Index for 2018 to 2020 (Figure 4.4 and Figure 4.4).

Table 4.2: *Mean JFM SIC of SIC 1 km and SIC 12.5 km and the visual inspection of the SIC Index calculated from daily measurements for 2018 to 2020. For SIC 1 km and SIC 12.5 km, the closest available pixel to Arctic Station was used. All values are given in percent [%].*

Year	SIC 1 km	SIC 12.5 km	SIC Index
2018	34.38	46.73	55.81
2019	37.82	59.94	72.10
2020	23.03	28.74	60.87
Mean	**31.78**	**45.14**	**62.93**

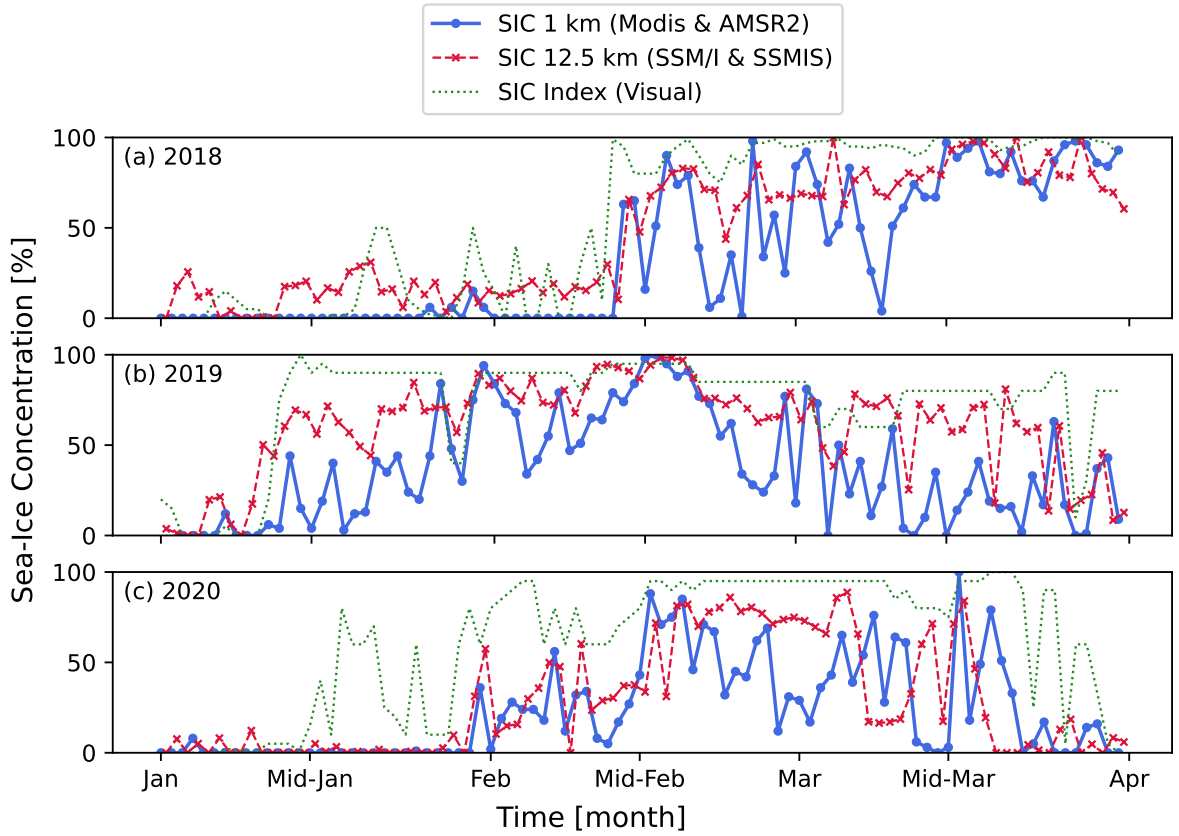

Figure 4.4: *Comparison of the closest available pixel to Arctic Station of SIC 1 km and SIC 12.5 km to the SIC Index for 2018 to 2020 for JFM. Blue solid lines represent SIC 1 km, red dashed lines represent SIC 12.5 km, and green dotted lines indicate the SIC Index. A cross and a dot mark the daily measured values of SIC 12.5 km and SIC 1 km, respectively.*

Between 2018 and 2020, the SIC Index indicated that mean JFM SIC were consistently higher than SIC determined by SIC 1 km (Figure 4.4 and Table 4.2). The mean SIC estimated by the SIC Index for JFM is about 60%, which is twice the average of the CAP of SIC 1 km estimated

at about 30% (Table 4.2). In comparison, the average determined by the CAP of SIC 12.5 km is 45%. These values indicate that SIC 12.5 km measured slightly higher values than SIC 1 km, but they primarily represent similar SIC. Meanwhile, the SIC Index generally showed the highest SIC values over the three years.

SIC Index and SIC 12.5 km tend to measure higher SIC than SIC 1 km. This is especially evident by examining the beginning of January. Specifically, in 2018 and 2020, SIC 12.5 km, and the SIC Index estimated SIC at 10% to 20 %, while SIC 1 km detected no SIC. For 2018, the variabilites of the three SIC products agree rather well (Table 4.2). For 2020, SIC 1 km and SIC 12.5 km agreed relatively well, whereas the SIC Index was more than twice that (Table 4.2). From mid-January to February 2020, the SIC Index indicated mean SIC of 30% to 50%, whereas SIC 1 km and SIC 12.5m estimated SIC to be 0% (Figure 4.4c). There are a few occurrences when SIC 12.5 km detected lower SIC compared to SIC 1 km, e.g. in March to mid-March 2020 (Figure 4.4c).

In 2019, the SIC Index suggested relatively constant values of 80% to 90% from mid-January to March and generally exhibited little variability. At the same time, SIC 1 km and SIC 12.5 km showed considerable variability. Furthermore, SIC estimated by SIC 12.5 km showed constant higher values compared to SIC 1 km (Figure 4.4b and Table 4.2). The SIC Index mean of 2019 was the highest, with about 70% compared to about 40% and 60% for SIC 1 km and SIC 12.5 km, respectively.

Overall, the largest difference occurred between the CAP for SIC 1 km and the SIC Index, with about 20% by the SIC Index. The smallest difference of 10% was between SIC 12.5 km and the SIC Index, and SIC 1 km and SIC 12.5 km differed by about 15%.

Comparing SIC 1 km and SIC 12.5 km for Disko Bay

The comparison of the CAP for SIC 1 km and SIC 12.5 km indicated that the SIC Index consistently measured higher SIC values, possibly reflecting the fast ice in front of Arctic Station. I am interested in the SIC in Disko Bay and want to use SIC 1 km and SIC 12.5 km to construct a time series of JFM SIC for 2003 to 2023. To estimate the differences between SIC 1 km and SIC 12.5 km and their representation of SIC in Disko Bay, I compare them for 2018 to 2020 (Figure 4.5 and Table 4.3).

Table 4.3: *Mean differences in JFM SIC between SIC 12.5 km and SIC 1 km product for the overlapping years of 2018, 2019, and 2020, and the mean JFM SIC estimated by SIC 1 km and SIC 12.5 km. Negative values indicate a higher SIC by SIC 12.5 km. All values are given in percent [%].*

Year	SIC 1 km	SIC 12.5 km	ΔSIC 1 km - 12.5 km
2018	46.06	61.42	-15.36
2019	45.65	66.41	-20.76
2020	27.37	46.05	-18.68
Mean	**39.69**	**57.96**	**-18.27**

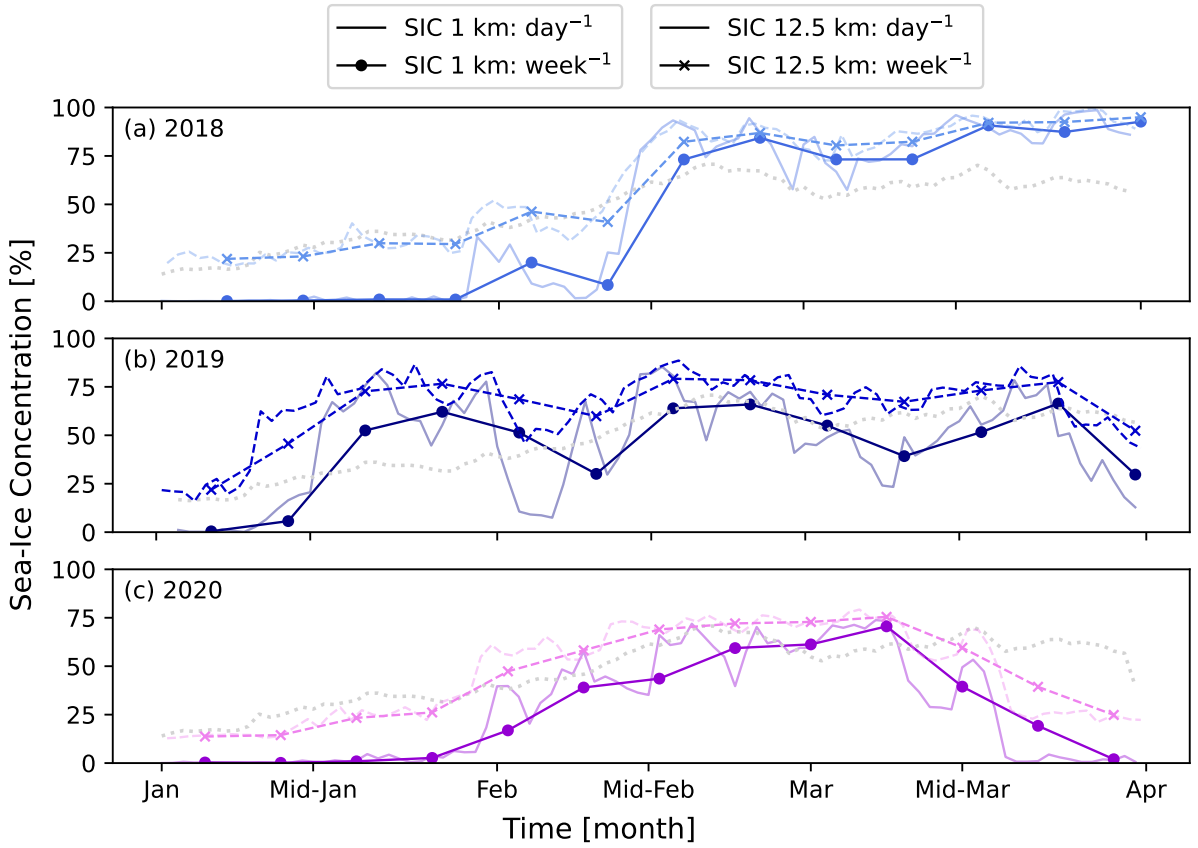

Figure 4.5: *Difference between SIC 1 km and SIC 12.5 km for JFM in Disko Bay for 2018, 2019, and 2020. Solid lines represent the weekly SIC means of SIC 1 km, and dashed lines represent the weekly SIC means of SIC 12.5 km. A cross and a dot mark the weekly measured values for SIC 12.5 km and SIC 1 km, respectively. Lighter lines represent daily means, and the dotted grey line represents the mean JFM evolution of SIC 1 km and SIC 12.5 km from 2003 to 2023.*

When comparing SIC 1 km to SIC 12.5 km, it is evident that SIC 12.5 km detected higher SIC values throughout 2018, 2019, and 2020 (Figure 4.5). There are only a few occurrences where weekly measurements of SIC 1 km and SIC 12.5 km agree well with each other, for instance, at the beginning of March to mid-March 2018 or in March 2020 (Figure 4.5a and c). In 2018, SIC 12.5 km measured slightly higher SIC than SIC 1 km for the first half of JFM in Disko Bay, while from around mid-February to the end of March, SIC 12.5 km and SIC 1 km agreed rather well (Figure 4.5a). The smallest JFM difference occurred in 2018, with 15% higher values by SIC 12.5 km. In contrast, in 2020, SIC 12.5 km was constantly higher than SIC 1 km by about 20%, except for one occurrence between March and mid-March (Figure 4.5c). 2019 also had about 20% higher SIC since SIC 12.5 km consistently detected higher SIC compared to SIC 1 km (Figure 4.5b). In general, SIC 12.5 km detected higher SIC than determined by SIC 1 km by about 20% for the three years

Time series of JFM SIC in Disko Bay for 2003 to 2023

I constructed a time series of JFM SIC for Disko Bay of daily and weekly extracted SIC of SIC 1 km and SIC 12.5 km to examine the variability between 2003 and 2023 (Figure 4.6). Additionally, I calculated the mean JFM evolution of SIC from 2003 to 2023 (Figures 4.5 and 4.6, grey dotted line). SIC for 2003 to 2017 are given by SIC 12.5 km. For the overlapping years of 2018 to 202, I calculated the mean JFM SIC per year and assumed that to be the year's JFM mean.

2021 to 2023 are given by SIC 1 km. The constructed time series of 2003 to 2023 revealed that there are a few years with predominantly low SIC, 2003, 2010, 2011, and 2021 (Figure 4.6a, h, i, and s) and even fewer years with consistently high SIC, 2008, 2012, and 2017 (Figure 4.6f, j, and o). Furthermore, there are clear indications of a seasonal cycle, with sea-ice formation in December and January and maximum SIC sometime in March (Figure 4.6).

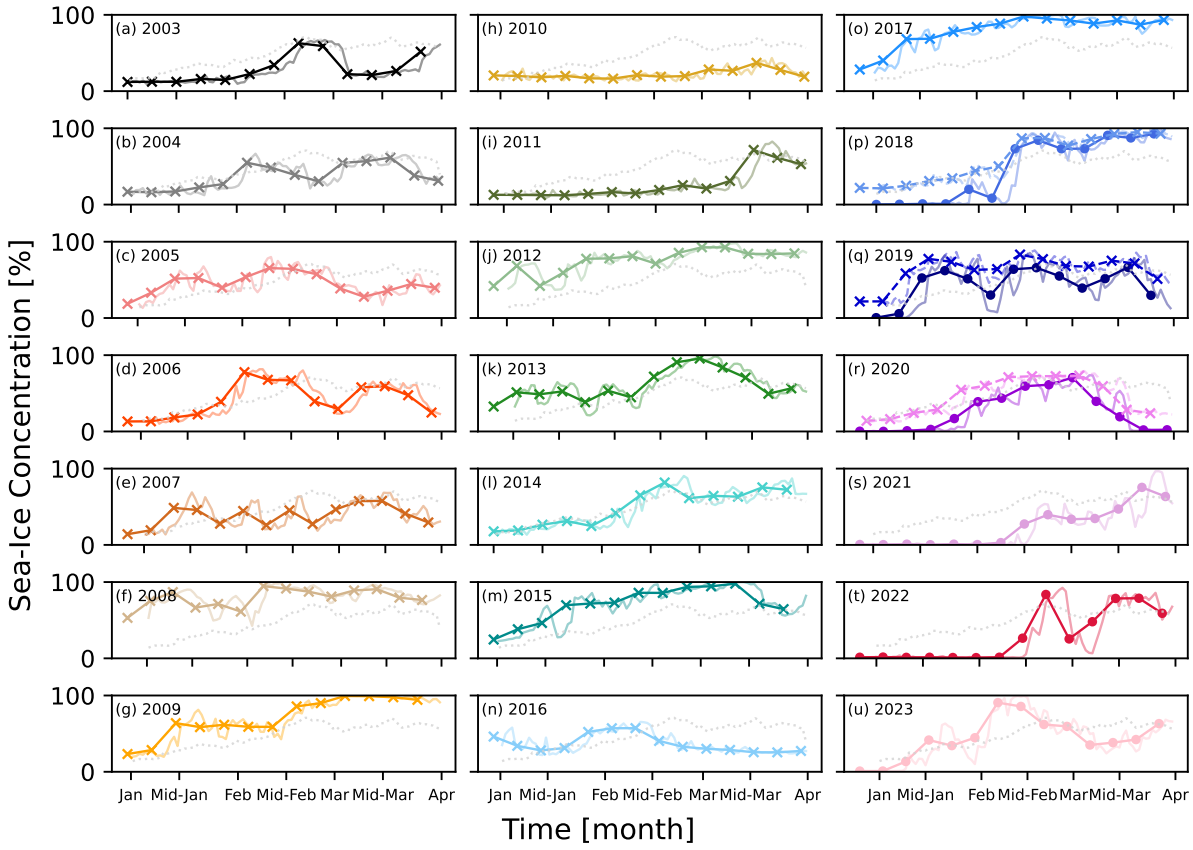

Figure 4.6: *Daily and weekly JFM SIC from SIC 1 km and SIC 12.5 km for Disko Bay from 2003 to 2023. Solid lines represent weekly SIC means, and the lighter lines present daily SIC means. The two markers represent the SIC products with different spatial resolutions. A cross marks SIC 12.5 km (a to r), (Lavergne et al., 2023), and a dot represents SIC 1 km (q to u) (Ludwig et al., 2019, 2020). The markers remain the same for the overlapping years (p, q, and r) of SIC 12.5 km and SIC 1 km. However, weekly SIC 1 km is displayed in solid lines and SIC 12.5 km in dashed lines. The dotted grey line represents the mean JFM evolution of SIC 1 km and SIC 12.5 km from 2003 to 2023.*

There is a pronounced year-to-year variability in SIC in Disko Bay during JFM from 2003 to 2023 (Figures 4.6 and 4.7). Most years indicate a seasonal pattern of sea-ice growth and when the sea-ice maximum is reached. The seasonality of sea-ice growth is evident as most years start with a relatively low SIC of below 20% (Figure 4.6a, b, d, and p to u), while only a few years start with SIC of more than 20% (Figure 4.6f, j, k, and o). This implies that in most years, sea ice started to grow in January, although, in some years, sea-ice growth started in December (e.g. Figure 4.6f and i). Further, most years reached their maximum in SIC between mid-February to mid-March. There appears to be some decadal variability (Figures 4.6 and 4.7).

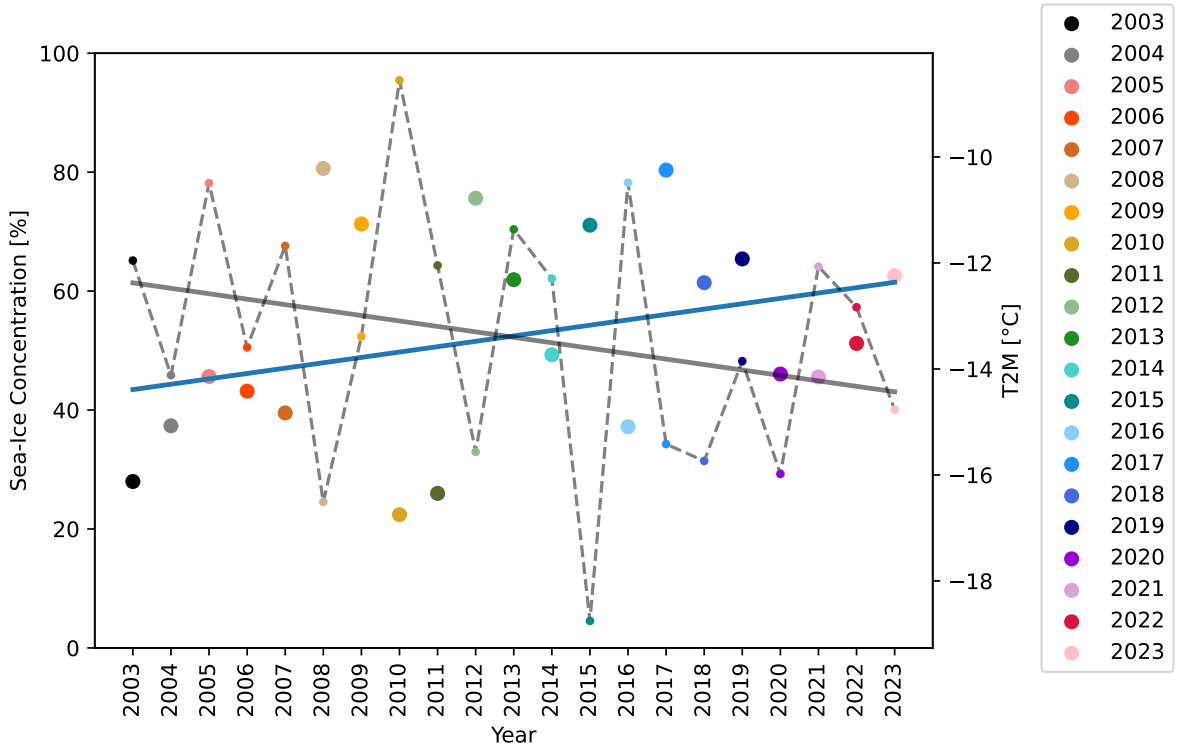

Figure 4.7: *Mean JFM SIC and T2M for Disko Bay from 2003 to 2023. SIC is the reconstructed time series of SIC with a spatial resolution of SIC 12.5 km. Large dots represent SIC, and small dots T2M. The blue line indicates a small trend in SIC with $\hat{y}$ = 43.44 + 0.90% (p-value > 0.05). The black line indicates a small trend in $\hat{y}$ = -12.37 - 0.10 °C (p-value > 0.05)*

In addition, I consider the JFM mean reconstructed SIC values (Section 3.5) for 2003 to 2023 with a spatial resolution of 12.5 km (Figure 4.7). I found a small positive trend of 0.9% per year (p-value > 0.05, 0.1643), indicating a small decadal trend. However, the p-value of 0.1643 is larger than 0.05. Indicating no statistical significance at a significance level of 5%. Further, I consider the JFM mean T2M from 2003 to 2023. For T2M, I see a small negative trend of -0.10 °C per year, indicating that the T2M decreases per year and gets colder. This trend of decreasing temperatures coincides with the increase in SIC (p-vale > 0.05, 0.2473). However, they both have a p-value above the significant level of 5%.

4.2 Ocean Observations

In this section, I present the results of the fieldwork in March 2023 in examining the representativeness of the data to Disko Bay. I compare measurements taken in two adjacent bays, Qeqertarsuup Tuna (QT) and Lyngmark Bugt (LB), near Arctic Station and investigate if they are subject to the same forcing (Figure 4.8). I analyse the difference between a CTD cast taken under sea ice and in open water CTD cast in close proximity since large parts of Disko Bay were not covered by sea ice (Figure 4.9). In addition, I present a repeated short transect, separated by 200 steps advancing towards the shore, to examine the horizontal homogeneity of the water (Figure 4.10). Further, I compare summer data taken in August 2019 inside Disko Bay to investigate the homogeneity of the water mass in deeper parts of Disko Bay and how representative the data we took close to shore is of the whole bay (Figure 4.11). Moreover, I present an inter-comparison of the CTD we used during fieldwork compared to the CTD used by the

Greenland Ecosystem Monitoring (GEM) program. Nearly all the rest of the hydrographic data was conducted with that CTD (Figure 4.12). Additionally, I present the general hydrography in Disko Bay during JFM (Figure 4.13), characteristics of the water column through the years (Figure 4.14) and a water mass analysis for the years with hydrographic data (Figure 4.15).

An analysis of the fieldwork data showed that the measurements near Arctic Station are representative of those further out in the bay and of open water conditions or with a very thin layer during JFM. A salinity-stratified water column with a vertical temperature gradient characterizes the hydrography of Disko Bay from 2003 to 2023 for JFM. Hydrographic data also showed a strong year-to-year variability in stratification, surface salinity and temperature, the thickness of the Polar Water (PW) layer, and if and at which pressure West Greenland Irminger Water (WGIW) is detected and a connection between the temperature of the upper 50 dbar ($T_{50\ \mathrm{dbar}}$) and SIC.

Ocean Observations March 2023

Even though we were able to conduct numerous CTD casts, we were normally limited by the extent of the sea ice in QT for our measurements, as we were only able to measure on the fast ice. The fast ice extended 1.2 to 1.4 km during the fieldwork. One day, we used a boat to go to deeper waters and further from the coast. Therefore, I examine how representative the data conducted in March 2023 is of Disko Bay. For the following analysis, I did not remove the top three dbar of the water column, as described in Section 3.3, as I am also interested in the surface variations.

I investigated the representativeness of the data acquired in March 2023 with a comparison of measurements taken in QT and LB, the difference between CTD casts taken in open water and under sea ice, a repeated transect towards the shore, summer data of 2019 for the whole bay, and compared the two CTD instruments used for nearly all of my hydrographic data. This analysis allows me to assume that the measurements taken during fieldwork in March are representative of JFM conditions in Disko Bay.

Spatial variability of measurements in Qeqertarsuup Tuna and Lyngmark Bugt

I am interested in whether the fieldwork measurements inside QT, in front of Arctic Station, and measurements in the adjacent bay, LB (Figure 4.8c) inhibit the same water mass and are subject to the same forcing. In QT, we conducted 33 CTD casts over a wider area. In contrast, we conducted four CTD casts in LB, which were taken at the same location (Figure 4.8).

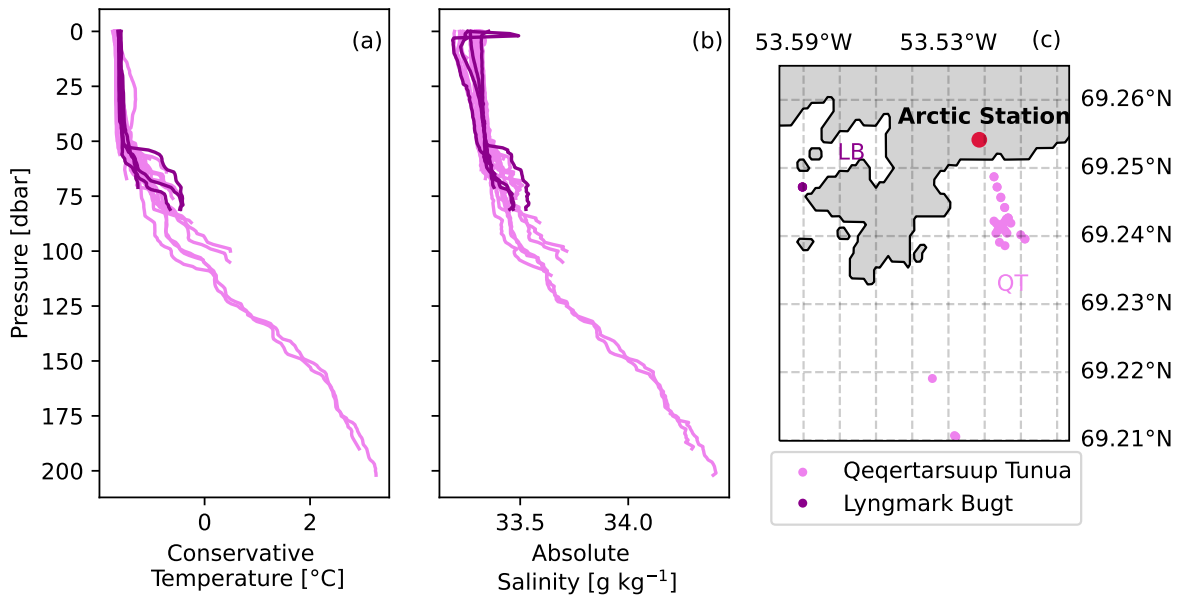

Figure 4.8: *Vertical profiles of temperature (a) and salinity (b) taken in Qeqertarsuup Tuna (QT) and Lyngmarkt Bugt (LB) (c). The colours in the profiles (a,b) indicate the stations marked with a dot in (c). The red dot marks the location of Arctic Station.*

Measurements taken in QT and LB show a similar structure in temperature and salinity (Figure 4.8a and b). Both reveal a slight warming in the lower part of the water column during the measurement period. The only visible difference is slightly higher salinity values at the surface in LB for one CTD cast (Figure 4.8b). The mean differences in temperature, salinity, and density between QT and LB are 0.001 g kg^{-1} in salinity, -0.067 °C in temperature, and 0.003 kg m^{-3} in density. A negative temperature difference indicates that the measurements in LB are slightly warmer. However, the temperature difference and especially the difference in salinity and density are minimal. Hence, an important result is that QT and LB occupy the same water mass and are subject to the same forcing as they both show a positive vertical gradient in temperature with pressure during the measurements.

Comparing CTD casts taken under sea ice and in open water

From satellite images of Disko Bay and visual inspection during the fieldwork, it is evident that a substantial part of Disko Bay was not covered in sea ice or only in a very thin layer during March 2023 (Figure 4.2). Therefore, we conducted two CTD casts near the sea-ice edge, one in open water and one under the sea ice, approximately 3 m apart (Figure 4.9). This allows me to examine the difference between measurements taken under the ice and in open water. It is important to mention that it was not entirely open water; it had a very thin layer of approximately 1 to 1.5 cm of frazil ice. However, this was the only sea-ice edge we could reach.

Comparing the two CTD casts at full length, I notice minimal differences in temperature and salinity (Figure 4.9a and b). The profiles vary for temperature the most after approximately 80 dbar, for salinity in the top 10 dbar, and then again after 80 dbar. However, the mean difference from open water to under sea ice is 0.022 °C for temperature, 0.003 g kg^{-1} for salinity, and 0.001 kg m^{-3} for density.

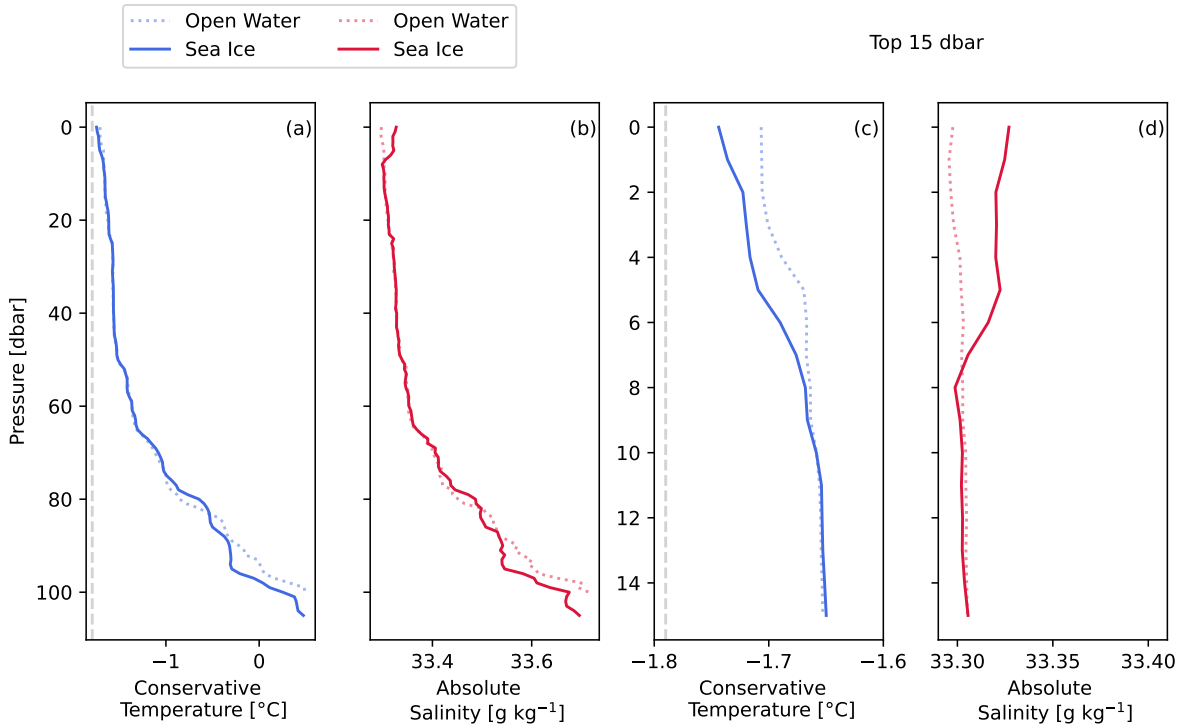

Figure 4.9: *Vertical profiles of temperature (a,c) and salinity (b,d) of a CTD cast taken in open water (blue) and one under the sea ice (red). (a,b) show the full vertical profile, and (c,d) show the top 15 dbar. Dotted lines represent measurements taken in open water, and solid lines represent measurements under sea ice. The grey dashed lines represent the freezing point at -1.79 °C.*

I am also interested in the variability in the top 15 dbar as sea-ice growth has the most considerable impact on this layer (Figure 4.9c and d). The variations in the top 15 dbar are more evident, especially in the top 8 dbar in salinity for the CTD taken under the sea ice (Figure 4.9d). The CTD cast taken under the sea ice is unstable in temperature and salinity from the surface down to 6 or 8 dbar. The difference between open water and under the sea ice is relatively small with 0.02 g kg^{-1}. The mean differences for the top 15 dbar are considerably smaller, with 0.010 °C, -0.008 g kg^{-1} for salinity, and -0.007 kg m^{-3} for density compared to the full profile. The negative differences in salinity and density indicate that the waters under the sea ice are slightly more saline and denser.

I am most interested in the salinity differences, which indicate stratification. For both the top 15 dbar and the entire profile, they are minimal. Hence, an important result is that measurements taken under the sea ice in JFM are representative of measurements with open water conditions or with a very thin layer of ice in Disko Bay.

Homogeneity of the water under fast ice

Due to the limited sea-ice coverage, most measurements are close to shore and less than 2 km out. Therefore, I want to investigate the homogeneity of the water under the ice towards the shore. We created a transect consisting of four stations, separated by increments of 200 steps progressing towards shore and repeated it five days later (Figure 4.10).

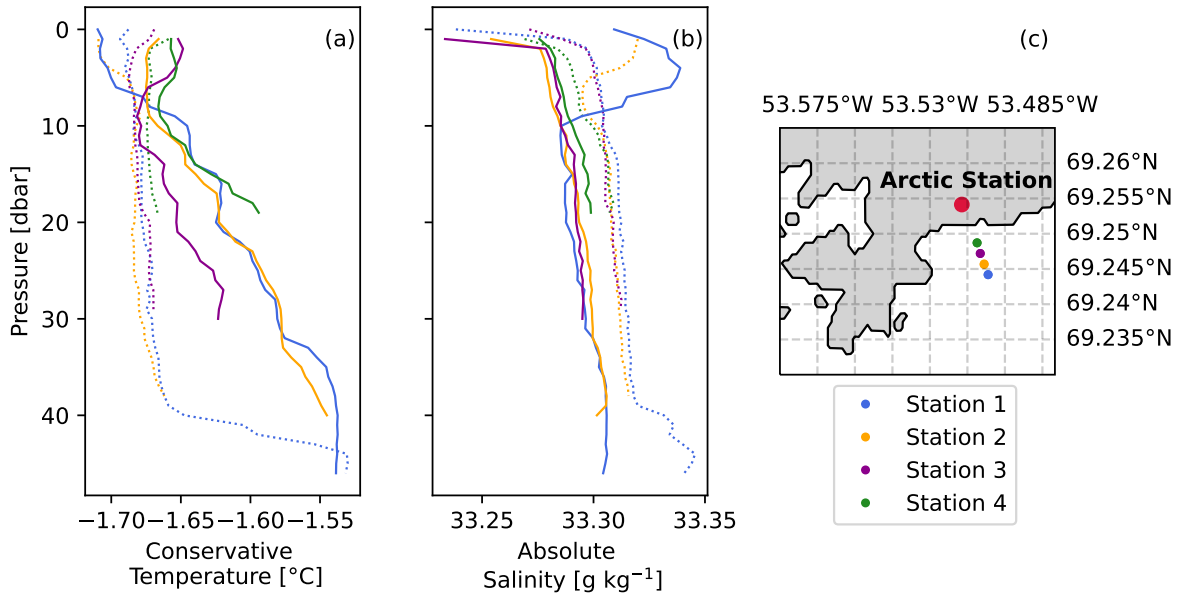

Figure 4.10: *Vertical profiles of temperature (a) and salinity (b) of the two transects taken on the 9th of March and 14th of March 2023. Dotted lines represent measurements of the first transect on the 9th of March, and solid lines represent measurements of the second transect on the 14th of March 2023. The colours in the profiles (a,b) indicate the stations marked with a dot in (c). The red dot marks the location of Arctic Station.*

The starting point of the transect was a CTD station close to a stranded iceberg (Figure 4.10c, Station 1), and the last CTD station was around 20 m from shore. The four stations have different bottom pressures, with the shallowest station (Station 4) reaching down to 19 dbar, while the deepest station (Station 1) reached down to 46 dbar. We conducted the first transect on the 9th of March and repeated the transect on the 14th of March 2023 (Figure 4.10).

Each transect indicates a rather homogeneous water mass under the ice and towards the shore, except for Station 1 during the first transect and Station 2 during the second transect. (Figure 4.10a and b). Both stations are located in an area with high sea-ice variability in terms of rafted and ridged ice and show slightly colder and more saline values than the rest of the stations on that day. Apart from this small difference, the salinity profiles show a homogeneous water column.

The mean difference from the mean on the 9th of March (not shown) is 0.001 °C for temperature, -0.0007 g kg^{-1} for salinity and -0.0006 kg m^{-3} for density. For Salinity, and therefore density, these are an order of magnitude lower than the accuracy of the instrument's sensors (Table 4.4) and, therefore, negligible. For the second transect, the salinity and density differences are of them (not shown) are very similar with -0.0006 g kg^{-1}, and-0.0005 kg m^{-3}, while the temperature variation is higher with 0.008 °C.

The mean differences between the stations are smaller than the accuracy for temperature and salinity, which are $\pm$ 0.003 mS cm^{-1} for conductivity and $\pm$ 0.002 °C for temperature (Table 4.4), except for temperature during the second transect. However, this difference is small. An important result is that the waters further from shore are the same as those close to shore, and the water under the fast ice is well mixed with a small temperature gradient.

Summer cruise around Disko Island in August 2019

Most of the hydrographic data from March 2023 is relatively close to shore. The transects we conducted in March 2023 gave insight into the stratification under the fast ice and towards the shore. However, information about the deeper parts ($\geq$ 200 dbar) of Disko Bay is needed to analyse the representation of the data to Disko Bay. Due to the limited data during winter, I examined data from August 2019, when GEM conducted a research cruise in Disko Bay and around Disko Island (Figure 4.11, GEM, 2019). I applied the same quality averaging process on the CTD cast as previously described in Section 3.3. However, I did not remove any outliers as the surface variation were larger than 1 standard deviation at all time.

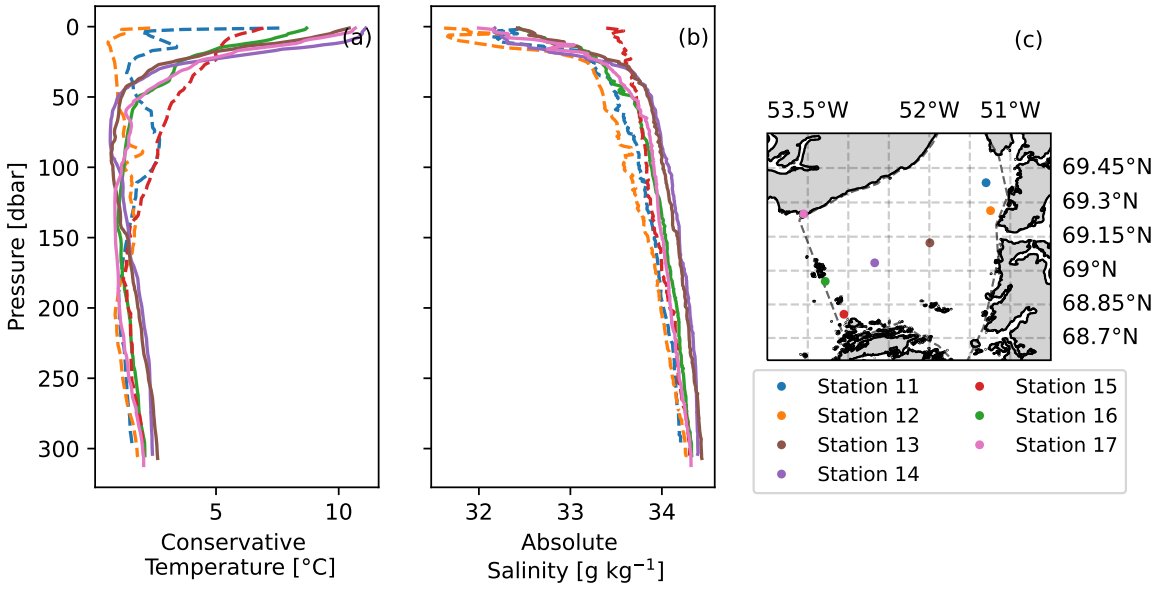

Figure 4.11: *Vertical profiles of temperature (a) and salinity (b) of CTD casts taken in August 2019 by GEM (GEM, 2019). The colours in the profiles (a,b) indicate the stations marked with a dot in (c). Dashed lines in (a,b) represent stations most likely affected by additional external factors (Station 11, 12, and 15). Dashed lines in (c) represent the borders of the area of interest in Disko Bay.*

I selected all stations inside Disko Bay (Figure 4.11c) and analysed their salinity and temperature profiles (Figure 4.11a and b). Even though this is summer data, it provides me with the opportunity to understand the spatial variability of the hydrography in Disko Bay better. For temperature and salinity, most stations show a rather homogeneous structure. Stations 11, 12, and 15 deviate slightly (Figure 4.11a and b). Stations 11 and 12 are located close to Ilulissat Icefjord and show colder and less saline waters. Station 15 is relatively close to Aasiaat and measures more saline and slightly colder values at the surface, and slightly warmer values around 50 to 150 dbar (Figure 4.11a and b). The standard deviation of the mean for salinity is $\pm$0.43 g kg^{-1}, $\pm$1.50 °C for temperature and $\pm$ 0.45 kg m^{-3} for density. These deviations indicate that the single profiles are warmer and more saline than the mean (not shown). However, compared to their temperature and salinity range, they are small and represent a homogeneous water mass. An important result is that the waters inside Disko Bay are relatively homogeneous, and the fieldwork data is representative of Disko Bay.

Inter-comparison of two CTD casts taken by different instruments

Except for 2020 and 2023, my hydrographic data is from GEM, and their measurements are taken with a Sea-Bird CTD. Therefore, we conducted three CTD casts simultaneously during fieldwork in March 2023. GEM conducts its CTD measurements with a Sea-Bird SBE 19plus V2, and the CTD we used during the fieldwork was a Sea & Sun CTD 48 M (Table 4.4).

Table 4.4: *CTD manufacturer and model, measured parameters, units, and accuracies. All information is from their respective manual (Sea & Sun Technology, 2020; Sea-Bird Scientific, 2022). The accuracy of pressure is on the full scale.*

Manufacturer & Model	Parameter	Unit	Accuracy
Sea & Sun	Conductivity	mS cm^{-1}	$\pm$ 0.003
Technology	Temperature	°C	$\pm$ 0.002
CTD 48 M	Pressure	dbar	$\pm$ 0.1%
Sea-Bird	Conductivity	mS cm^{-1}	$\pm$ 0.005
Scientific	Temperature	°C	$\pm$ 0.005
SBE 19plusV2	Pressure	dbar	$\pm$ 0.1 %

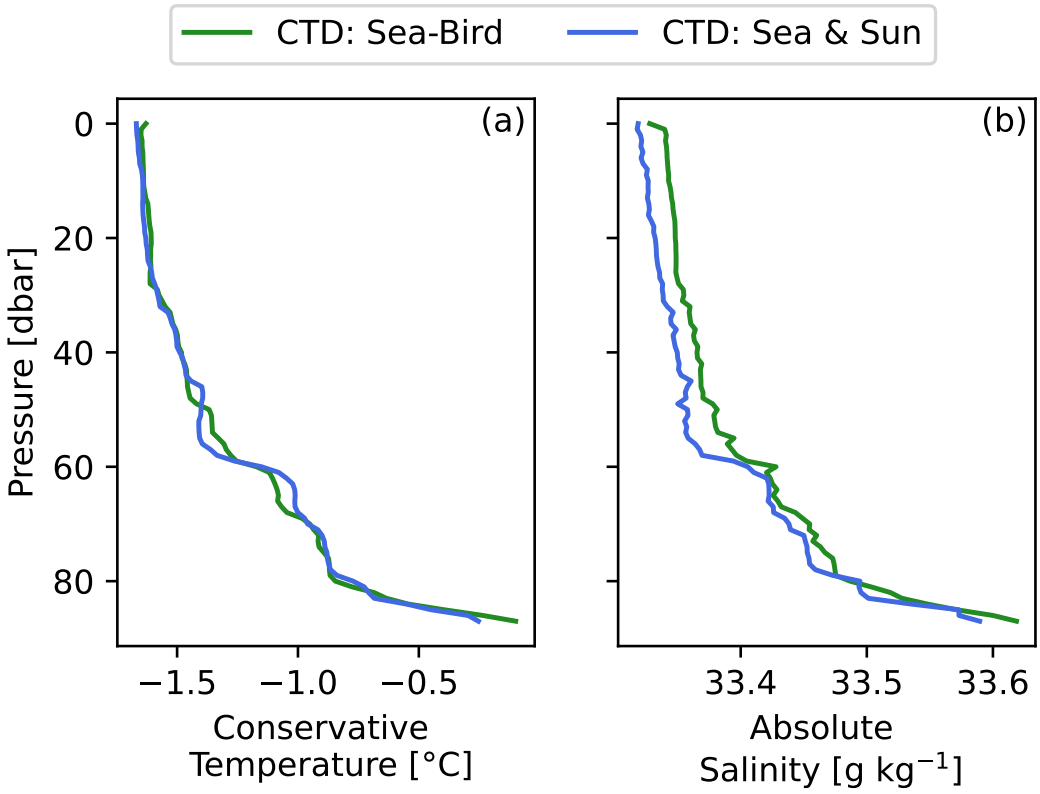

Figure 4.12: *Vertical profiles of temperature (a) and salinity (b) of two CTD casts taken simultaneously by different CTD instruments at the same location on the 18th of March 2023 taken. Green lines represent the CTD cast measured with the Sea-Bird, and blue represents the CTD cast measured with the Sea & Sun.*

Dates available for an inter-comparison are the 9^{th}, 14^{th}, and 18^{th} of March 2023. I compare the CTD cast for the 18^{th} of March 2023 (Figure 4.12) since the other two CTD casts were taken close to a stranded iceberg and showed an influence of fresh meltwater from the iceberg. Figures and salinity and temperature differences of the inter-comparison for the 9^{th} and 14^{th} of March 2023 can be found in Appendix B (Figures B.1 and B.2 and Table B.11).

The CTD by Sea & Sun has greater precision with an accuracy of $\pm$ 0.002 °C for temperature and $\pm$ 0.003 ms cm^{-1} for conductivity compared to $\pm$ 0.005 for temperature and conductivity by Sea-Bird (Table 4.4). At the same time, they share the same accuracy of $\pm$ 0.1% for pressure (Table 4.4).

With the Sea & Sun CTD, we were able to go closer to the ocean floor as this transferred instantaneous pressure values to the logging computer. For temperature, the two casts agree very well (Figure 4.12a), while there are some differences in salinity (Figure 4.12b). The mean difference between the Sea-Bird and Sea & Sun CTD cast for salinity is 0.016 g kg^{-1}, 0.005 °C for temperature and 0.013 kg m^{-3} for density. However, these are small compared to the range in salinity, and for temperature, the difference is close to the accuracy level (Figure 4.12b).

Furthermore, the accuracy of the Sea & Sun CTD sensors is higher compared to the Sea-Bird. Both CTD are thus confirmed to give good results. GEM data has thus also been exposed to an independent test, and we can safely progress using the slightly less accurate Sea-Bird CTD measurements.

Hydrography of Disko Bay in JFM

I computed an overall mean of the hydrographic data to improve my understanding of the average stratification during JFM in Disko Bay (Figure 4.13). I computed daily, weekly, and JFM means by averaging all available CTD profiles for 2008 to 2012, 2018, 2020, 2022, and 2023. Due to limited available data, the varying depth of the water column, and the different locations of the profiles, the overall mean shows a few unphysical artefacts, e.g. portraying lower salinities, temperatures and densities at 250 dbar compared to the deepest measurements (Figure 4.13, dashed lines). To remove those artefacts and create a more reasonable vertical profile, I used a polynomial fit of the 5th degree on the data (Figure 4.13).

Examining the fitted curves, it indicates a salinity-stratified water mass with fresher waters at the surface of about 33.4 g kg^{-1}, while more saline waters, 34.49 g kg^{-1}, are found at the bottom. Density follows salinity and varies between 26.74 kg m^{-3} at the surface and 27.36 kg m^{-3} at the bottom (Figure 4.13). The surface salinity allows me to calculate the mean freezing point of -1.79 °C for the winter months in Disko Bay from 2003 to 2023 (Figure 4.13, blue dotted line). There are low temperatures of -1.58 °C at the surface and higher temperatures of 2.96 °C at depth. Temperature shows a considerable increase downwards. At 89 dbar, temperatures are already above 0 °C; at 109 dbar, they are above 1 °C, and 2 °C are reached at 143 dbar (Figure 4.13).

Overall, the fitted profile provides valuable insight into the average stratification in JFM in Disko Bay and demonstrates the influence of salinity on the stratification. In addition, it reveals the rapid increase of temperature with pressure

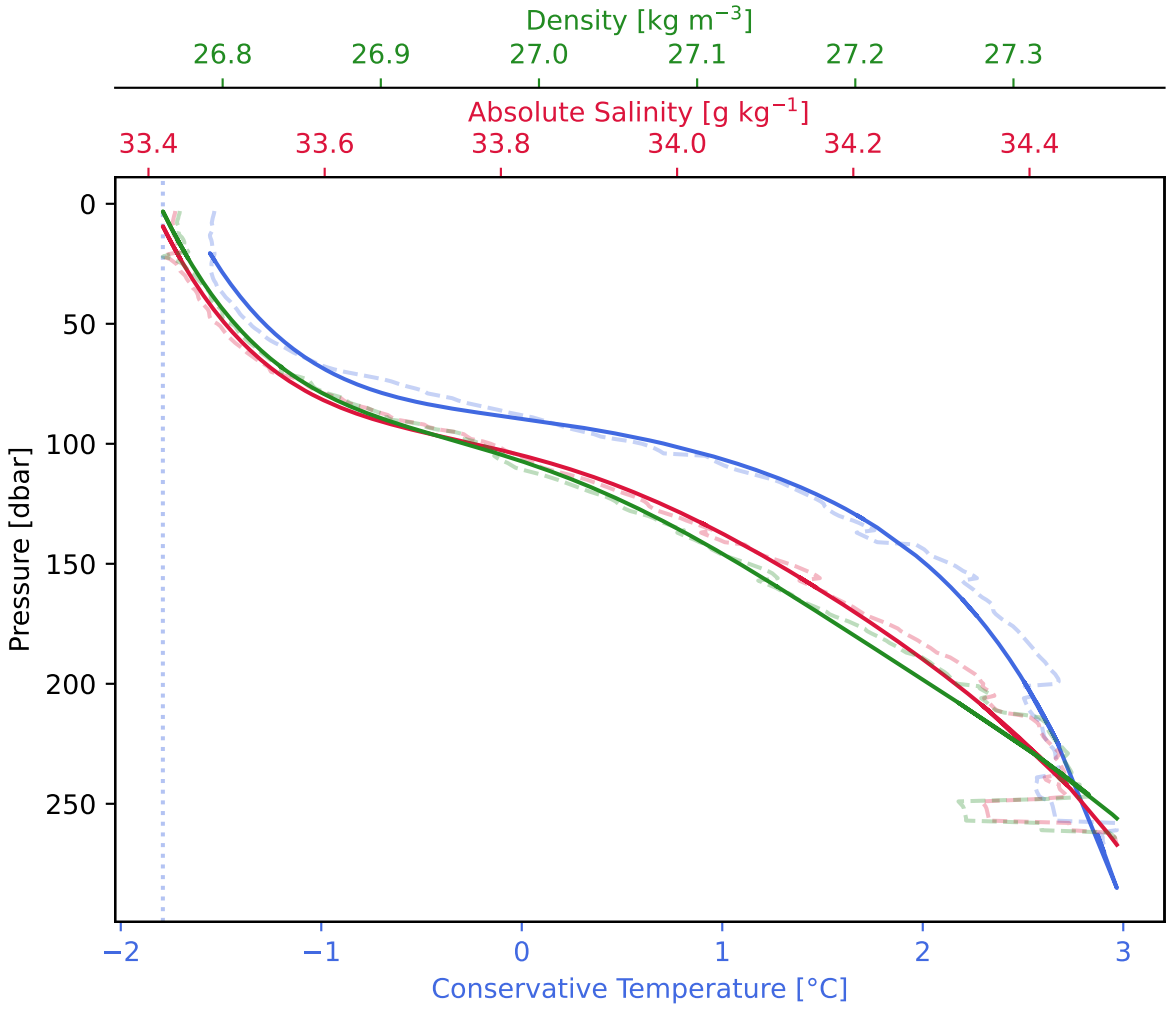

Figure 4.13: *Vertical profiles of temperature (blue), salinity (red) and density (green) for an overall mean of all hydrographic data for 2008 (12), 2009 (14), 2010 (8), 2011 (5), 2012(1), 2018 (6), 2020 (1), 2022 (5), and 2023 (37). The numbers behind the year indicate the number of profiles in that year for JFM in Disko Bay. Dashed lines represent the unfitted overall mean. Solid lines represent a polynomial fit of the 5th degree of the data. A vertical blue dotted line indicates the mean freezing temperature of -1.79 °C of Disko Bay.*

Characteristics of the hydrography over time

I used averaged JFM hydrographic data to obtain information about the characteristics of the JFM water column in Disko Bay to understand how hydrographic conditions are related to sea-ice growth (Figure 4.14). I found a pronounced year-to-year variability in both temperature and salinity, a varying thickness of the cold layer in the upper water column and the presence of warm waters towards the bottom. Through the years, the depth of the hydrographic profiles varied. The shallowest profile went down to 104 dbar (Figure 4.14, 2022), and the deepest reached 267 dbar (Figure 4.14, 2010). As described in the previous section, the averaging process of the hydrographic profiles with different depths led to artefacts. Similar artefacts of higher temperature and salinity than at the bottom are visible in temperature (Figure 4.14a, 2009, 2011, 2020, and 2023) and salinity (Figure 4.14b, 2009, 2011, and 2023).

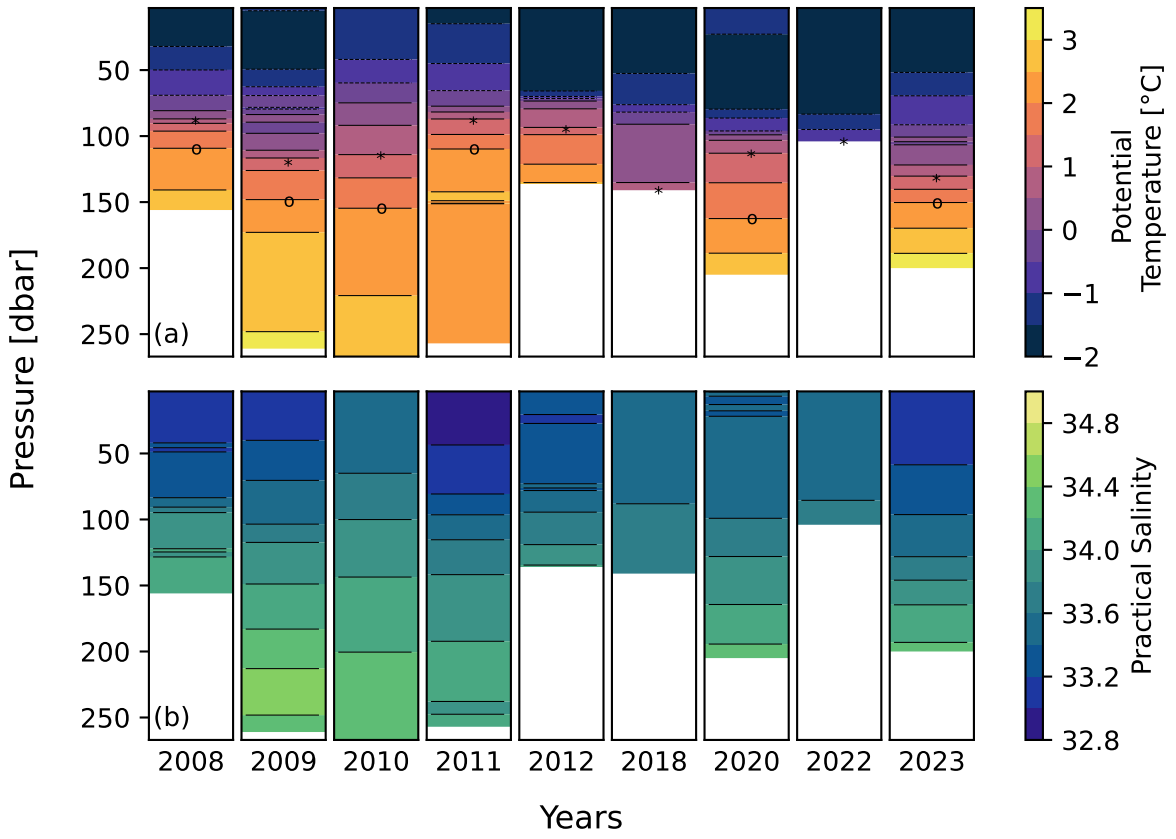

Figure 4.14: *Averaged CTD profiles of temperature (a) and salinity (b) for JFM each year in Disko Bay. Black horizontal lines represent contour lines in increments of 0.5 °C for temperature and 0.2 for salinity. Dashed lines in temperature correspond to temperatures below 0 °C. The star marks the depth of the 1 °C isotherm of the Polar Water (PW). For 2018 and 2022, the water was always colder than 1 °C, and the star marks the highest temperature. The circle marks the 2 °C isotherm, the upper extension of the West Greenland Irminger Water (WGIW).*

The top layer of the water column is characterised by cold water, with temperatures below -1.5 °C. The thickness of the cold water layer at the surface varies from year to year; some years have a relatively thick layer of more than 50 dbar (Figure 4.14a, 2012 and 2022), while in other years, it is shallow or completely absent (Figure 4.14a, 2010 and 2011). Temperatures increase rapidly to 0 °C, 1 °C, and 2 °C every year except for 2018 and 2020 (Figure 4.9a, 2008 to 2012, 2022, and 2023). 2018 was a cold year with maximum temperatures between -1 °C and -0.5 °C at around 100 dbar (Figure 4.14a, 2018). In addition, more than half of the water column is between the freezing point and -1.5 °C. 2020 was also cold compared to the other years; the highest temperatures were between 0 and 0.5 °C (Figure 4.14a, 2020). In 2022, the whole water column is characterized by temperatures below 0.5 °C (Figure 4.14a, 2022).

Generally, temperatures reached 0 °C at pressure values between 74 to 100 dbar throughout the years. Exceptionally high temperatures above 3 °C were found below 249 dbar in 2009 and in 2023 below 188 dbar (Figure 4.9a, 2009 and 2023). There is an evident year-to-year variability of how deep the cold water reaches from the surface and where higher temperatures are found in the water column.

Surface salinity exhibits more variability than surface temperature. In some years, salinity starts with a fresh layer at the surface between 33.2 and 33.4 (Figure 4.14b, 2008, 2009, 2012,

2020, and 2023), while in other years, the salinity varies between 33.4 and 33.6 (Figure 4.14b, 2010, 2018, and 2022). 2011 had the freshest surface layer with a salinity below 33 at the surface (Figure 4.14b, 2011). Salinity generally increases with depth in some years faster than in others. 2022 is nearly entirely homogeneous until it reaches 100 dbar (Figure 4.14, 2022).

Water mass analysis

To better understand the year-to-year variability of the hydrographic conditions in Disko Bay, I examined daily mean profiles to identify Polar Water (PW) and West Greenland Irminger Water (WGIW) (Figure 4.15). I found PW in every year we have hydrographic data and WGIW in six out of nine years (Figure 4.15 and Table 4.5), indicating a partial pressure dependency. The water mass analysis revealed the thickness of the Polar Water layer varied through the years, as does the depth at which I am able to detect West Greenland Irminger Water.

Table 4.5: *Thickness of the Polar Water (PW) layer, the first pressure where West Greenland Irminger Water (WGIW) was detected and the profiled bottom of the JFM hydrographic profile. All values are given in [dbar].*

Year	Thickness of PW layer	1st depth of WGIW	Bottom of the profile
2008	90	142	156
2009	111	161	261
2010	84	175	267
2011	87	201	257
2012	93	-	136
2018	111	-	141
2020	110	174	205
2022	104	-	104
2023	130	179	200

The colder and relatively fresh PW can generally be found in the upper layer of the water column down to around 130 dbar, and the warmer and more saline WGIW lies below. Furthermore, the waters between PW and WGIW lie on the mixing line between those two (Figure 4.15). For the years with hydrographic data, PW has been identified every year in Disko Bay. Additionally, WGIW was identified in 2008, 2009, 2010, 2011, 2020, and 2023, higher than 150 dbar (Figure 4.15 and Table 4.5). The years I was not able to detect WGIW were the three shallowest profiles, with 104 (2022), 136 (2012), and 141 dbar (2018), indicating a partial pressure dependency of WGIW detection.

In 2011, five profiles were available (Figure 4.15), and two of them showed the presence of WGIW; yet, the JFM mean did not reach the WGIW water. The thickness of the PW layer varied between 84 and 130 dbar down from the surface throughout the years (Table 4.5). In contrast, WGIW is found between 142 and 201 dbar to the bottom of the profile.

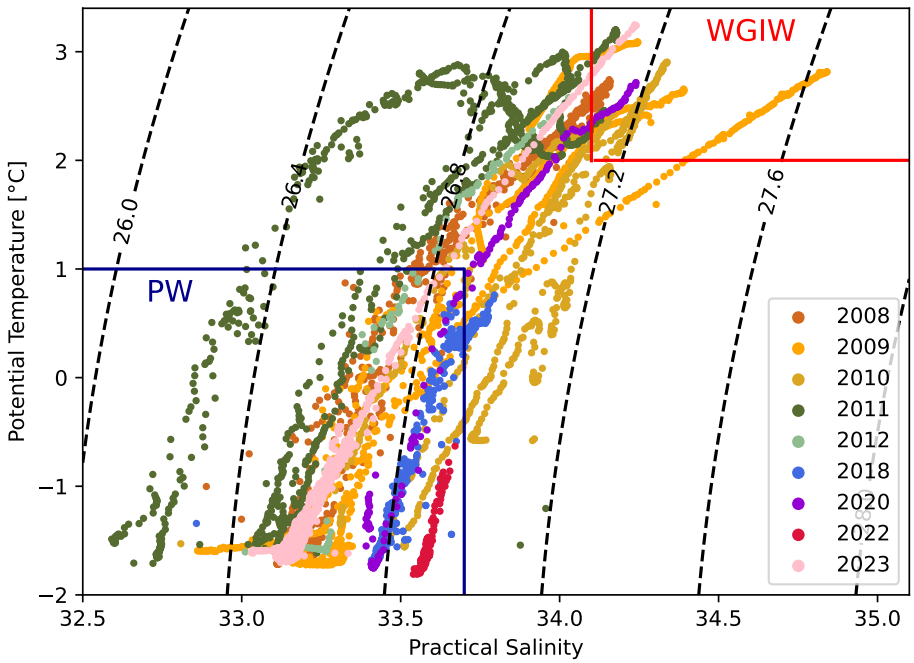

Figure 4.15: *Potential temperature-practical salinity (θ-S) diagram of daily averaged hydrographic data for each year with hydrographic data (2008 to 2012, 2018, 2020, 2022 and 2023). Each year is represented by a different colour. The red box marks the range of WGIW (θ > 2 °C and S > 34.1), and the blue box marks the range of PW (θ < 1 °C and S ≤ 33.7). Dashed lines represent density contours. Water mass characteristics are defined by Tang et al. (2004).*

Examining the contribution of the ocean to JFM SIC, I calculated the mean temperature of the top 50 dbar for JFM ($T_{50\ dbar}$) and found a linear relation to SIC (Figure 4.16).

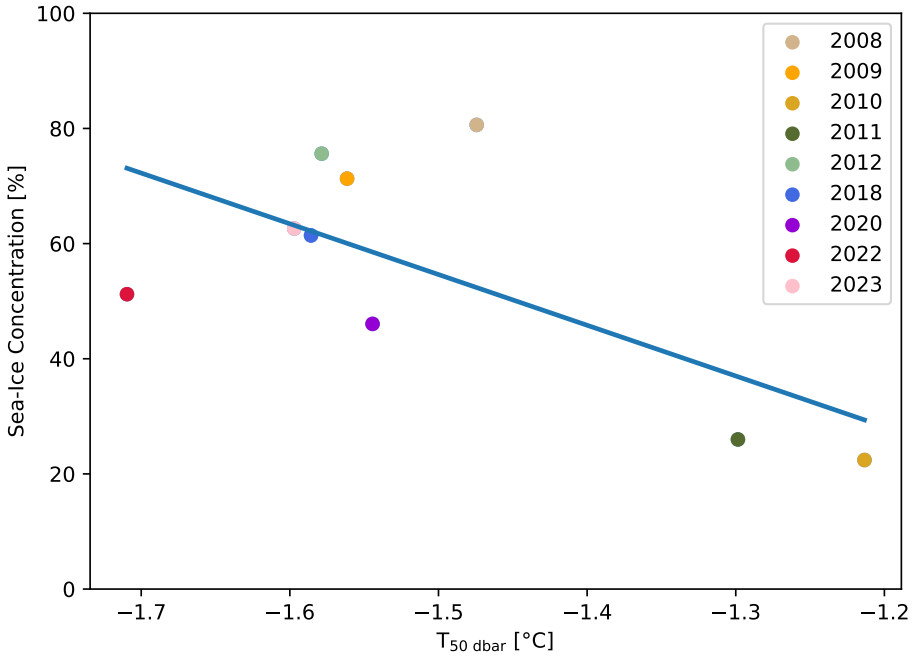

Figure 4.16: *Mean reconstructed SIC with a spatial resolution of 12.5 km and the mean temperature of the top 50 dbar ($T_{50\ dbar}$) for all hydrographic data. The blue line indicates the trend.*

SIC is the reconstructed time series of 2003 to 2023 with a spatial resolution of 12.5 km that I calculated for the RF model (Section 3.4). The linear relation between $T_{50\,dbar}$ and SIC indicates that higher temperatures are associated with lower JFM SIC (p-value > 0.05). The p-values indicate no statistical significance to a significance level of 5%. In most years $T_{50\,dbar}$ was between -1.50 °C and -1.60 °C. However, two years have relatively high $T_{50\,dbar}$. The temperature of 2010 and 2011 were between -1.30 °C and -1.20 °C. 2022 has the lowest $T_{50\,dbar}$ below -1.70 °C (Figure 4.16). Recent years were quite cold (Figure 4.16), 2022 and 2023). The linear relation between SIC and $T_{50\,dbar}$ suggests that if the temperature were to be around 1.0 °C, it would be associated with about 0% SIC.

4.3 Importance of Atmospheric and Oceanic Parameters

In this section, I present the mean JFM evolution of SIC to atmospheric variables extracted by ERA 5 (Figure 4.17) and the overall mean over values of atmospheric and oceanic parameters of 2003 to 2023 (Table 4.6 and Figure 4.18). Moreover, I present the correlation results between atmospheric and oceanic parameters to SIC (Table 4.7). Further, I describe the results of the RF model of daily atmospheric variables and SIC (Figures 4.19 and 4.20). I used the linear interpolated SIC with a spatial resolution of 12.5 km for both statistical approaches.

An analysis of the atmospheric conditions of the mean JFM evolution over 21 years showed a cold atmosphere and low wind speeds. The highest correlated variables to SIC are winter length, SST, T2M, $T_{50\,dbar}$, wind speed, and SLHF. The thickness of the PW layer and the preNAo were moderately correlated to SIC. The RF model determined SST, T2M, SSR, and SLHF are the four variables with the highest influence on the %IncMSE. In addition, the partial dependencies of the atmospheric variables are described.

Mean Winter Conditions

To analyse mean winter conditions during JFM, I calculated the mean JFM evolution over 21 years (2003 to 2023) for SIC, SST, T2M, SSR, and wind speed (Figure 4.17). In addition, I consider the NAO index between 2002 and 2023 (Figure 4.18) .

The mean JFM evolution is characterized by increasing SIC (Figure 4.17a), decreasing SST from -1 °C to around the freezing point (Figure 4.17b), and varying T2M between -10 °C and -15 °C (Figure 4.17c). SLHF are larger at the beginning of January, about -20 W m^{-2} and become smaller throughout JFM to below -10 W m^{-2} after mid-February (Figure 4.17d). This can be attributed to the continuous increase in SIC (Figure 4.17a). After mid-February, SLHF deviates around -10 W m^{-2} and SIC is around 70% to 80% (Figure 4.17a and d). SSR is below 1 W m^{-2} until mid-January and then increases continuously until the end of March (Figure 4.17e). Wind speed varies between 0 and 2 m s^{-1} through JFM. Nevertheless, winds are slightly higher at the beginning of January and lower in March (Figure 4.17f). The NAO is in a negative phase in ten years and in a positive phase in 12 years (Figure 4.18).

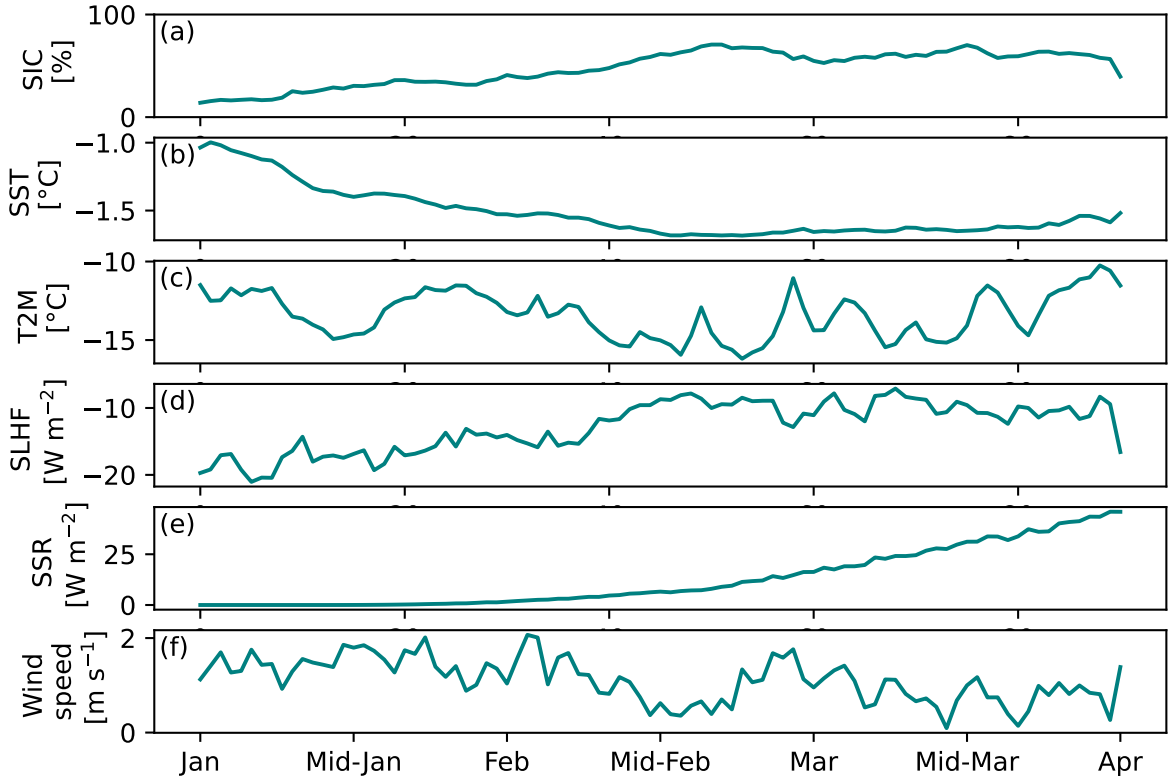

Figure 4.17: *Mean JFM evolution from 2003 to 2023 for SIC (a), SST (b), T2M (c), SLHF (d), SSR (e), and wind speed (f).*

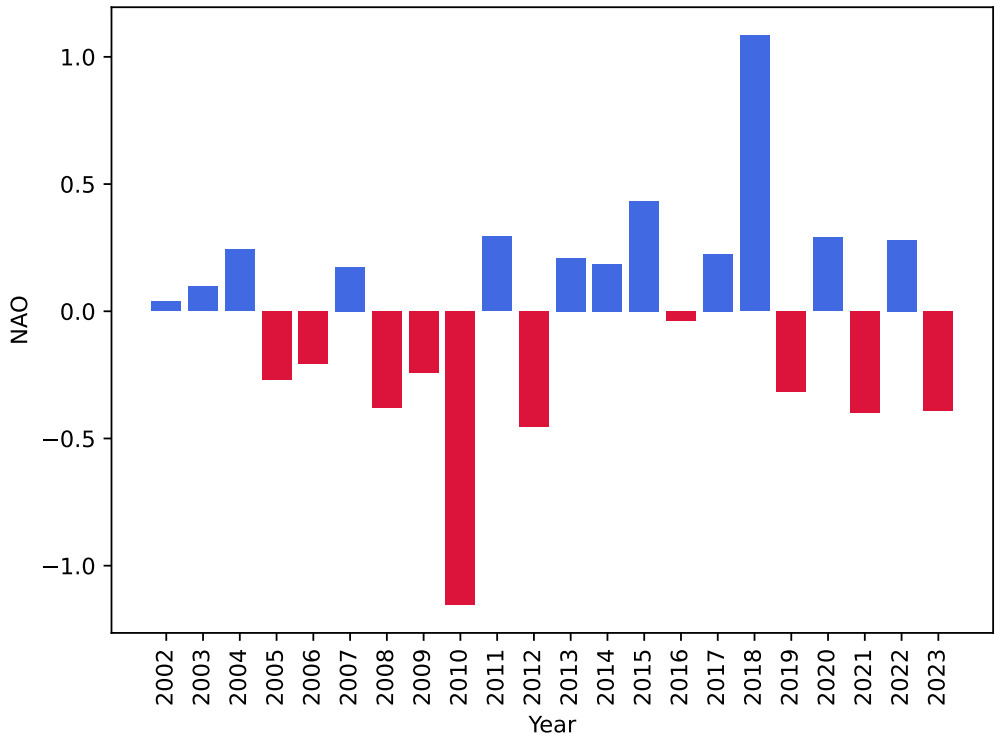

Figure 4.18: *NAO index for 2002 to 20233. Negative values are red and indicate a negative NAO phase, while positive values are blue and indicate a positive NAO phase.*

In addition to the mean JFM evolution, I calculated the overall JFM mean for 2003 to 2023 for each variable (Table 4.6).

Table 4.6: *Overall JFM mean for 2003 to 2023 for SST, T2M, SLHF, SSR, winter length, SIC, wind speed, previous years NAO, and SST of the preceding summer for 2007 to 2023.*

	Mean
SIC	48.36%
Atmosphere	
SST	-1.52 °C
T2M	-13.41 °C
winter length	63 days
SLHF	-12.76 W m^{-2}
SSR	12.53 W m^{-2}
wind speed	1.6 m s^{-1}
wind direction	NNE
Ocean	
$T_{50\ dbar}$	-1.50 °C
PW thickness	108 dbar
Previous Year	
JAS SST	4.60 °C
pre-NAO	-0.013

The overall JFM mean values indicate a SIC of 48.36%, SST at -1.52 °C, and T2M at -13.41°C. . In addition to SST and T2M, I consider the winter length to be important. I define the winter length as days T2M is below the freezing point of -1.79 °C (Figure 4.13), and SST is $\leq$ -1.58 °C during JFM. -1.58 °C is the average surface temperature determined by nine years of hydrographic data (Figure 4.13). For 2003 to 2023, the overall mean winter length is 63 days. Mean SSR is 12.53 W m^{-2} and SLHF 12.76 W m^{-2}. The overall mean wind speed over 21 years for JFM is 1.6 m s^{-1} with an average maximum of 6.6 m s^{-1}. The prevailing meteorological wind direction is Northern North-East. On average, the top 50 dbar of the water column is -1.50 °C determined by nine years of hydrographic data (Figure 4.16). The average thickness of the PW layer goes down to 108 dbar (Figure 4.13).

Statistical approaches

I calculated the correlation coefficients between atmospheric variables, the NAO index (Figure 4.18), oceanic parameters and SIC variability (Table 4.7). Sea ice is represented by the linearly interpolated SIC time series with a spatial resolution of 12.5 km, which I calculated in Section 3.5. SIC variability is the difference to the overall JFM mean (Table 4.6). I used JFM mean values since I wanted to incorporate the NAO of the previous year (pre-NAO), the NAO of the first six months (JFMAMJ) of the calendar year (6M-NAO), the winter length, $T_{50\ dbar}$, and the thickness of the PW layer (PW thickness), which are only available as JFM means (Table 4.7).

Table 4.7: *Correlation coefficients r of JFM SIC variability with a spatial resolution of 12.5 km to atmospheric variables from Table 3.2, pre-NAO, and 6M-NAO for 2003 to 2023. PW thickness, $T_{50\ dbar}$ are correlated for nine years (2008, 2009, 2010, 2011, 2012, 2018, 2020, 2022, and 2023). JAS SST is correlated for 2007 to 2023. P-values are related to a significance level of 5%. The number in the bracket is the actual p-value. Bold p-values indicate variables with statistical significance.*

	SIC variability *r*	p-value
Atmosphere		
SST	-0.76	**< 0.05** (6.64e-05)
T2M	-0.70	**< 0.05** (0.0004)
wind speed	-0.61	**< 0.05** (0.003)
SSR	-0.42	> 0.05 (0.060)
wind direction	-0.24	> 0.05 (0.300)
SP	-0.09	> 0.05 (0.686)
6M-NAO	0.18	> 0.05 (0.427)
SSHF	0.35	> 0.05 (0.123)
STR	0.55	**< 0.05** (0.0095)
SLHF	0.74	**< 0.05** (0.0001)
winter length	0.84	**< 0.05** (1.99e-06)
Ocean		
$T_{50\ dbar}$	-0.65	> 0.05 (0.057)
PW thickness	0.35	> 0.05 (0.3568)
Pre-conditioning		
JAS SST	-0.16	> 0.05 (0.5403)
pre-NAO	0.34	> 0.05 (0.131)

The analysis of the correlation found that winter length, SST, SLHF, T2M, and wind speed are the five atmospheric variables with the highest correlation coefficients ($r \geq \pm\ 0.60$) (Table 4.7). Their p-values indicate statistical significance as their p-values are below the significance level of 5%, for most of them even below 1%. SST, T2M, $T_{50\ dbar}$, and wind speed are negatively correlated (Table 4.7), while SLHF and the winter length are positively correlated (Table 4.7). SST (r = -0.76) and T2M (r = -0.70) have the highest negative correlation followed by $T_{50\ dbar}$ (r = -0.65,), wind speed (r = -0.61), and SSR (r = -0.42) (Table 4.7). Negative correlation coefficients indicate that the sea ice would be associated with lower SIC values with increased SST, T2M, $T_{50\ dbar}$, SSR, and wind speed. SSR and $T_{50\ dbar}$ have a p-value above 0.05, indicating no statistical significance to a significance level of 5%.

The highest positive correlated variables (r > +0.60) are winter length with (r = 0.84) and SLHF (r = 0.74). They indicate that an increase in winter length and smaller SLHF correlate to an increase in SIC. SLHF is, by definition, positive downwards; hence, an increase in SLHF represents smaller heat flux values. Further, I found a moderate correlation between the pre-NAO and SIC variability (r = 0.43). However, the p-value is above 0.05, indicating no statistical significance to a significance level of 5%. SIC variability and JAS SST show a very small correlation.

In addition to the correlation, I used a RF model to find the atmospheric variables with the highest %IncMSE related to JFM SIC in Disko Bay from 2003 to 2023 (Figure 4.19).

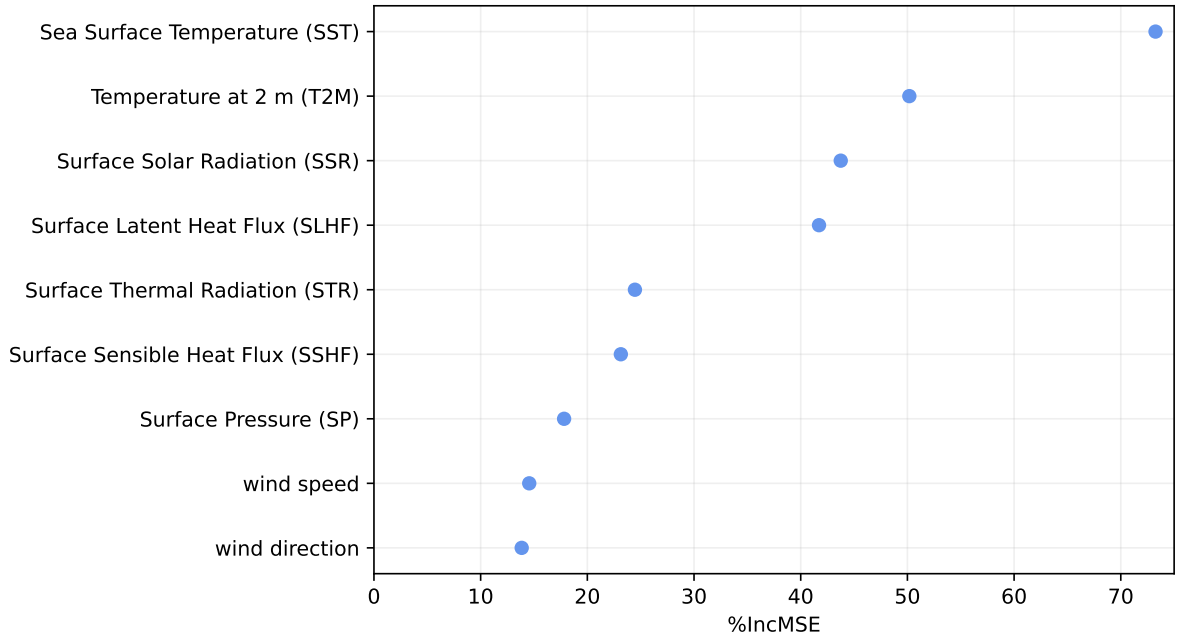

Figure 4.19: *%IncMSE of all atmospheric variables from Table 3.2.*

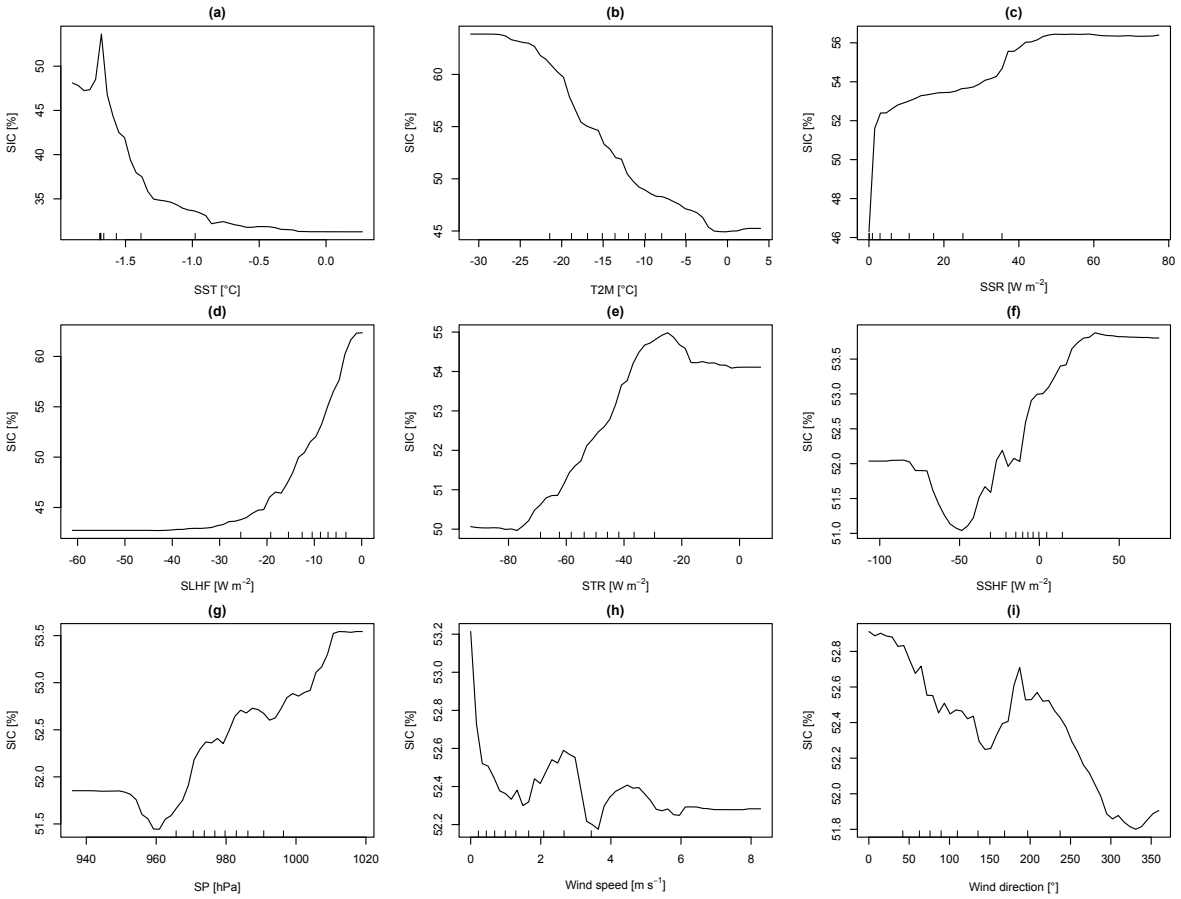

Figure 4.20: *Partial dependencies of SST (a), T2M (b), SSR (c), SLHF (d), STR (e), SSHF (f), SP (g), wind speed (h), and wind direction (i) in predicting SIC.*

Examining the RF revealed that SST, T2M, SSR, and SLHF are the four variables with an %IncMSE above 40% (Figure 4.19). T2M and SST have an %IncMSE of 50.18% and 73.26%, respectively. For SSR and SLHF, the %IncMSE is between 40% and 50%. The variables with the lowest influence on the MSE are wind speed, wind direction, and Surface Pressure (SP), with values of below 20% (Figure 4.19). In addition to the %IncMSE, I considered the partial dependency for each atmospheric variable in explaining JFM SIC (Figure 4.20). Partial dependencies show how much the variability of an atmospheric variable is able to explain the predicted SIC while the other variables are kept at their mean. A larger spread in SIC indicates that the variable is better at explaining the variability (Figure 4.20).

The spread of predicted SIC is largest for SST, SLHF, T2M, and SSR (Figure 4.20a, b, c, and d). In SST, low temperatures coincide with high SIC and high temperatures around 0 °C coincide with low SIC (Figure 4.20a). Similar is visible in T2M, with an even higher relation between low temperature and high SIC (Figure 4.20b). SSR shows that high solar radiation coincides with high SIC, which appears to represent a false interrelationship (Figure 4.20c). For SLHF, the RF model shows that low fluxes coincide with high SIC and high fluxes with low SIC (Figure 4.20d). STR, SSHF, SP, wind speed and wind direction are only able to predict change in the range of 2% to 5 % in SIC (Figure 4.20e, f, g, h, and i).

4.4 Events of Low and High SIC

In this section, I examine years with low and high SIC (Table 4.8). I then analyse atmospheric conditions and oceanic parameters during JFM for two events of low and high SIC (Figures 4.21 and 4.22). I define years with high SIC with JFM SIC above 75% and low SIC years with less than 30% SIC (Table 4.8).

Table 4.8: *Years with high SIC, above 75% and low SIC, below 30%. Years in bold indicate years with hydrographic data. All SIC are given in percent [%].*

High		**Low**	
Year	SIC	Year	SIC
2008	80.62	2003	27.98
2017	80.35	**2011**	25.99
2012	75.62	2021	22.62
		2010	22.41

High SIC years are 2008 and 2017 with above 80%, and 2012 with about 75%. Low SIC years are 2010 and 2021 with around 22%, 2011 with roughly 25%, and 2003 with approximately 28% (Table 4.8). Atmospheric forcing is available for all the above years. However, I do not have hydrographic data for all years. I chose years which had hydrographic data available for my investigation. Those are 2008 and 2012 for years with high SIC and 2010 and 2011 for years with low SIC (Table 4.8).

To understand the correlation between atmospheric variables and SIC for low and high SIC years, I analyse the atmospheric variables and oceanic parameters to the overall mean of 21 years (Table 4.6) and the mean JFM evolution (Figure 4.17). I first investigate SST, T2M, and the winter length to examine the atmospheric conditions during that winter. Then, I consider the influence of SLHF, SSR, and wind speed and their influence on SIC. To study the connection of oceanic forcing in years with high and low SIC, I consider the temperature of the top 50 dbar, $T_{50\ dbar}$, and the thickness of the PW layer. A cold surface is an essential prerequisite for

sea-ice growth, and a thick PW layer could indicate better insulation against the warmer and more saline WGIW. The profiles of the four years have different depths; hence, I only consider the water column to the common deepest measurement, 136 dbar. In addition, I consider the pre-NAO (Figure 4.18) and the SST of July, August, and September (JAS) of the previous year to analyse the pre-conditioning of the ocean surface during summer (CMEMS, 2023).

Figures showing seasonal changes and tables with the mean, minimum, and maximum values for SST, T2M, SLHF, SSR, wind speed, JAS SST, NAO Index, and the water mass analysis for low and high SIC years can be found in Appendix C (Figures 4.18 and C.1 to C.7 and Tables C.1 to C.6).

Low SIC years

An investigation into two years with low SIC, 2010 and 2011, revealed that during JFM, they experienced higher-than-average T2M, SST, SLHF, and a shorter winter length compared to the overall JFM mean and the mean JFM evolution. The PW thickness was below 90 dbar, and $T_{50\,\mathrm{dbar}}$ was higher than the average over nine years. SSR and wind speed do not show an apparent connection to SIC. In terms of pre-conditioning, the mean JAS SST is higher than the overall JAS mean and the mean JAS evolution. The NAO of the previous year was in a negative phase for both years (Figure 4.21).

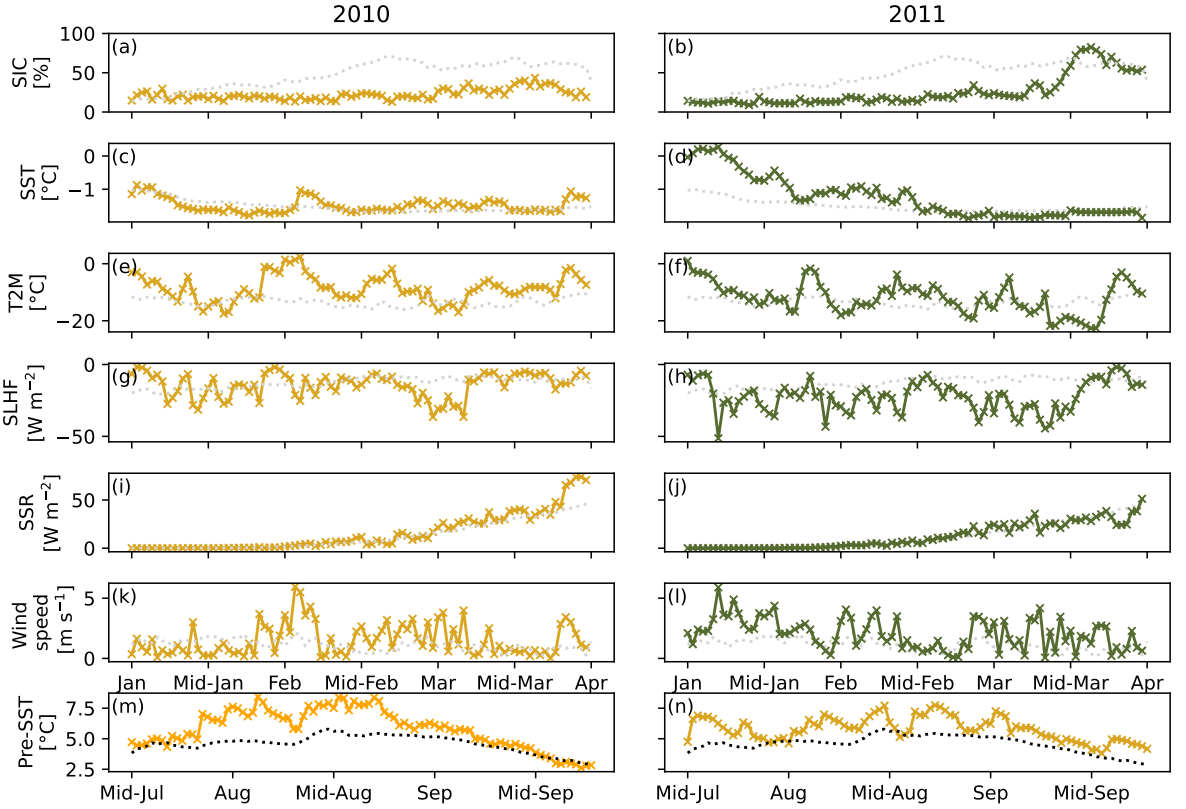

Figure 4.21: *SIC (a,b), T2M (c,d), SLHF (e,f), SSR (g,h), SLHF (i,j), and wind speed (k,l) for JFM 2010 (a, c, e, g, i, and k) and JFM 2011 (b, d, f, h, j, and l). Grey dotted lines (a to l) indicate the mean JFM evolution of SIC 1 km and SIC 12.5 km from 2003 to 2023. (m,n) show the JAS SST of 2009 (m) and 2010 (n). The black dotted line (m, n) indicates the mean JAS evolution from 2007 to 2023.*

The two years with low SIC I examine are 2010 and 2011, with a mean SIC of 22.41% and 25.96%, respectively (Figure 4.21 and Table 4.8). In 2010, SIC was consistently below the overall JFM mean of 48.36% and the mean JFM evolution (Figure 4.21a). Around mid-March, a slight increase occurred but decreased quickly back to around 20% at the end of March (Figure 4.21a). At the beginning of 2011, SIC was stable between 10 and 20% until around mid-February (Figure 4.21b). After this, SIC increased and decreased in a couple of days until it steadily increased around mid-March and reached a maximum of around 80%

The mean JFM SST in low SIC years is higher than the overall JFM mean of SST in Disko Bay (Figure 4.21c and d, Tables 4.6 and C.1). The overall JFM mean is -1.52 °C, and the average SST for 2010 and 2011 were -1.49 °C and -1.24 °C, respectively (Table C.1c and d). In 2010, SST varied around the mean JFM evolution (Figure 4.22c). Between February and mid-March, SST is mostly above the mean JFM evolution and was below the mean from mid-March until six days before the end of March, coinciding with a slight increase in SIC (Figure 4.21a and d). The last six days of the winter are above the mean JFM evolution (Figure 4.21c). SST in 2011 started close to 0 °C and dropped below the mean JFM evolution around mid-February (Figure 4.21d). After this, SST was below -1.53 °C (Figure 4.21d). At the same time, SIC started to slowly increase (Figure 4.21b). Maximum SST was above -1 °C with -0.87 °C in 2010 and 0.27 °C in 2011, indicating higher temperatures and potential warming and melting. For 2011, the highest values above 0 °C were reached at the beginning of January, while the highest temperature for 2010 was reached between February and mid-February.

Atmospheric temperatures, T2M, indicate that in years with low SIC, the temperatures are above the overall JFM mean, with -8.55 °C for 2010 and -12.05 °C for 2011 and mostly above the mean JFM evolution (Figure 4.21e and f, Tables 4.6 and C.2). In 2010, T2M showed a lot of variability and was mostly above the mean JFM evolution except for two occasions. Once around mid-January and a second time at the beginning of March (Figure 4.21e). An increase in T2M at the beginning of February, where T2M reached its maximum at +2.38 °C, is also associated with an increase in SST a few days later (Figure 4.21c and e). In 2011, T2M started with its highest temperature of +1.01 °C and throughout JFM showed a lot of variability around the mean JFM evolution. T2M dropped below the overall JFM mean of -13.41 °C and the mean JFM evolution of T2M on several occasions (Figure 4.21f and Table 4.6). Around mid-March, T2M reached its minimum at about -20 °C but increased again towards the end of March to about -12 °C. The coldest T2M values were -17.52 °C for 2010 and -22.65 °C for 2011 (Figure 4.21 and Table C.2).

For years with low SIC, the winter length was below the average of 63 days, with 43 days for 2010, the second shortest winter between 2003 and 2023, and 44 days for 2011 during JFM (Table 4.6). The first day of potential freezing in 2010 was the 13^{th} of January, and the last day was the 26^{th} of March. The first potential freezing day in 2011 was on the 16^{th} of February. The time after is associated with increased SIC (Figure 4.21b).

Years with low SIC have larger JFM mean SLHF values compared to the overall JFM mean of -12.7 W m^{-2}, with -14.1 W m^{-2} for 2010 and -22.5 W m^{-2} for 2011 (Figure 4.21, Tables 4.6 and C.3). SLHF varied considerably in 2010, yet when SIC increased at the beginning of March, SLHF became smaller (Figure 4.21a and g). In 2011, SLHF expressed more variability than in 2010 (Figure 4.21g and h). However, it is also observed that when SIC started to increase in mid-March, SLHF values decreased (Figure 4.21h and b).

Mean SSR values were slightly higher, with 12.9 W m^{-2} in 2011 and 15.4 W m^{-2} in 2010, than overall JFM mean of 12.5 W m^{-2} (Figure 4.21, Tables 4.6 and C.4). SSR in 2010 was very similar

to the mean JFM evolution except for an increase in SSR at the end of March (Figure 4.22i). In 2011, SSR showed a similar pattern to that in 2010, except that at the end of March, there was a small decrease in SSR. Both years had higher SSR at the end of JFM. Nevertheless, I do not see an apparent connection between SSR and SIC in either 2010 or 20111.

The mean wind speed of 2010 was 1.5 m s^{-1}, thus slightly lower than the overall JFM mean. Winds at the beginning of 2010 were weak and below the overall JFM mean of 1.6 m s^{-1} (Table C.5). An event of higher wind speed occurred at the end of January until the first week of February, with wind speeds of above 5 m s^{-1} (Figure 4.21k). Around the same time, the data indicated lower SLHF, higher T2M and, with a few days delay, an increase in SST (Figure 4.21c, e, g, and k). After February, winds were higher than the overall JFM mean until mid-March. Around mid-March, wind speeds were close to zero, SLHF showed smaller values, and SST showed decreased values (Figure 4.21c, g, and k). In 2011, wind speeds were, on average, higher than the overall JFM mean with 2.1 m s^{-1} (Table C.5), which is evident from January to mid-February. For the rest of JFM, wind speeds were mostly above the overall JFM mean and the mean JFM evolution (Figure 4.21l).

The thickness of the PW layer in 2010 in a water column down to 267 dbar covered the top 84 dbar. In 2011, the thickness of the PW layer reached down to 87 dbar in a water column down to 257 dbar (Figure C.7). The temperature of the top 50 dbar in JFM of 2010 and 2011 were the highest two $T_{50\,dbar}$ measured compared to the nine years of data (Figure 4.16). With -1.21 °C in 2010 and -1.30 °C in 2011, they were also higher than the overall JFM mean of -1.50 °C (Figure 4.16).

The mean JAS SST of the preceding summer were 1 °C higher, with 5.67 °C in 2009 and 5.77 °C in 2010, compared to the overall JAS mean of 2007 to 2023, with 4.60 °C (Tables 4.6 and C.6). In addition, for 2010, SST was consistently higher than the mean JAS evolution until a few days before the end of September. When temperature decreased to its lowest value of 2.74 °C (Figure 4.21n and Table C.6). In 2010, JAS SST was mostly above the mean JAS evolution, and the temperature at the end of the summer was around 4.16 °C (Figure 4.21n and Table C.6). Nearly 2 °C higher than at the end of 2009. The NAO of 2009 and 2010 were both in a negative phase with index values -0.24 and -1.15 (Figure 2.5). The NAO index of 2010 was the lowest NAO index between 2003 and 2023 (Figure 4.18).

High SIC years

An investigation into two years with high SIC, 2008 and 2012, revealed that during JFM, they experienced lower-than-average T2M, SST, SLHF, a longer winter length, the PW layer was slightly thicker, and $T_{50\,dbar}$ was lower or approximately the same as the nine-year mean. SSR does not show an apparent correlation to SIC. Wind speed suggests that, on a few occasions, an event of high wind can be associated with large SLHF, higher T2M, SST, and a decrease in SIC. During JAS, SST was slightly higher than the 17-year mean, and the pre-winter NAO was in a positive phase for both years. Compared to the overall JFM mean and the mean JFM evolution, SIC was consistently higher, SST lower, and T2M mostly below (Figure 4.22).

The two years with the highest SIC are 2008 with 80.62% and 2012 with 75.62% (Table 4.8). For 2008 and 2012, SIC was consistently above the overall JFM mean and the mean JFM evolution (Figure 4.22a and b). In 2008, SIC were between 80% and 100% after mid-February (Figure 4.22a). In 2012, SIC varied mostly between 60% and 100% (Figure 4.22b) and on one occurrence in mid-February when SIC decreased for a few days, it was below the mean JFM evolution.

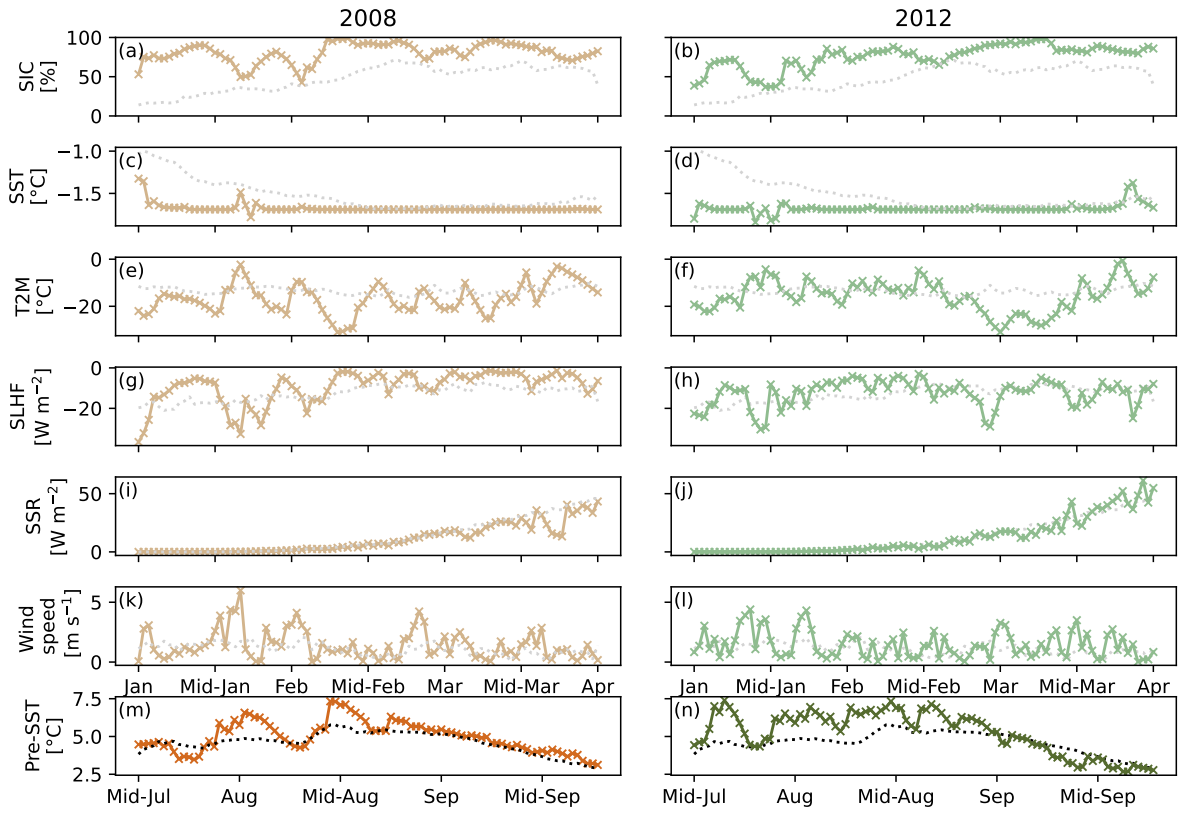

Figure 4.22: *SIC (a,b), T2M (c,d), SLHF (e,f), SSR (g,h), SLHF (i,j), and wind speed (k,l) for JFM 2008 (a, c, e, g, i, and k) and JFM 2012 (b, d, f, h, j, and l). Grey dotted lines (a to l) indicate the mean JFM evolution of SIC 1 km and SIC 12.5 km from 2003 to 2023. (m,n) show the JAS SST of 2009 (m) and 2010 (n). The black dotted line (m, n) indicates the mean JAS evolution from 2007 to 2023.*

The mean SST values for years with high SIC were lower than the overall JFM mean of SST with -1.52 °C, with -1.67 °C and -1.68 °C in 2008 and 2012, and the mean JMF evolution (Figure 4.22c and d and Tables 4.6 and C.1). This is evident as SST was already well below the mean JFM evolution of SST at the beginning of January. Around mid-February in both years, SST and the mean JFM evolution of SST showed the same pattern and were below the overall JFM mean of SST. Maximum SST in high SIC years were around -1.3 °C, reached in 2008 at the beginning of January and in 2012 at the end of March (Figure 4.22c and d, and Table C.1). In 2008, SST was well below the overall JFM mean and the mean JFM evolution of SST (Figure 4.22c). In 2012, the mean SST was -1.68 °C and only went above the overall JFM mean and the mean JFM evolution at the end of March (Figure 4.22d).

Atmospheric temperatures, T2M, with a mean value of -16.51 °C in 2008 and -15.56 °C in 2012, were colder than the overall JFM mean of -13.41 °C and mostly below the mean JFM evolution of T2M (Figure 4.22e and f, and Table 4.6). In 2008, T2M was mostly below the overall JFM mean of -13.41 °C. Between mid-January and February, an event of higher temperatures for three days with maximum temperatures of -2.31 °C occurred. At the beginning of February and mid-March were occasions of temperatures above the overall mean and the mean JFM evolution for a couple of days (Figure 4.22e). The minimum temperature for 2008 was about -30.98 °C, reached shortly before the beginning of March (Figure 4.22e and Table C.2). After mid-March, T2M was above the overall JFM mean but decreased again, and at the end of March, T2M was below -13 °C (Figure 4.22e). In 2012, T2M varied moderately along the mean JFM evolution except for considerably low temperatures between the end of February and the

beginning of March, where T2M reached a temperature of -30.91 °C. Until mid-March, temperatures stayed below the overall JFM mean and the mean JFM evolution. Afterwards, they increased and decreased, and shortly before the end of March, reached the T2M maximum value of -0.68°C in 2012. At the end of March, T2M was slightly above the overall mean and the mean JFM evolution (Figure 4.22f).

For 2008 and 2012, the length of the winter determined by T2M and SST was 89 days of potential freezing, the longest winters detected between 2003 and 2023. Both JFM in 2008 and 2012 had 91 days; this suggests that there were only two days without the potential of freezing.

Mean JFM SLHF values were small for years with high SIC. For 2008, the SLHF was -9.5 W m^{-2} and therefore smaller than the overall JFM mean of -12.7 W m^{-2}. After February, SLHF was mostly above the mean JFM evolution, indicating a smaller SLHF. In contrast, in 2012, the mean SLHF was slightly smaller with -12.44 W m^{-2} than the overall JFM mean. SLHF deviated around the mean JFM evolution (Figure 4.22, Tables 4.6 and C.3). The smallest SLHF values coincide with the highest SIC. Mean SSR were slightly larger for 2012 with 12.8 W m^{-2} compared the overall JFM mean of 12.53 W m^{-2} and slightly lower in 2008 with 10.7 W m^{-2} (Figure 4.22i and j, and Table C.4). Comparing the SSR of 2008 and 2012 to the mean, JFM evolution shows minimal deviation from the mean, except for an occasion at the end of March 2008, around mid-March in 2012. In addition, I am not able to establish a connection between SSR and SIC.

The mean JFM wind speeds for 2008 and 2012 were 1.4 m s^{-1} and 1.5 m s^{-1}. Hence, they were lower than the overall JFM mean with 1.6 m s^{-1} (Figure 4.22k and l and Table 4.6). However, both years indicate events of higher winds. In addition, they mostly show higher winds than the mean JFM evolution (Figure 4.22k). In 2008, between the 16^{th} and 21^{st} of January, there was an event of higher winds between 3.8 m s^{-1} and above 5 m s^{-1}, coinciding with larger SLHF, higher T2M, an increase in SST, and a decrease in SIC (Figure 4.22a, e, g, j, and k). This is illustrated in a sequence of daily wind speed and direction and SIC in Appendix A (Figure A.1). This wind event indicates that Disko Bay shows features of a coastal polynya. However, not all high wind events exhibit this pattern, as similar wind events at the end of February in 2008 and in mid-January in 2012 show.

The thickness of the PW was 90 dbar in 2008 in a water column down to 156 dbar, and in 2012, the PW reached 93 dbar, with a profile down to 136 dbar (Table 4.5 and Figure C.7). In 2008, $T_{50\,bar}$ was -1.47 °C, slightly higher than the nine-year average, while in 2012, it was -1.58 °C, lower than the nine-year mean of -1.50 °C (Figure 4.16).

The mean SST for years with high SIC were above the overall JAS mean of 4.60 °C (2007 to 2023). For 2010, the mean JAS SST was 4.96 °C, only slightly warmer than the mean. At the end of the summer, the surface had cooled to 3.12 °C, agreeing with the mean JFM evolution. In 2011, the mean JAS SST was 5.18 °C, and at the end of September, the surface temperature had cooled considerably to 2.77 °C and was lower than the mean JAS evolution (Figure 4.22 and Table C.6). The NAO of 2007 and 2011 were in a positive phase with index values of 0.17 and 0.29, respectively (Figure 4.18a and e). The positive NAO index in 2007 is the only positive NAO index between 2005 and 2010 (Figure 4.18). The positive NAO index of 2011 follows after three years with a negative index and a record low in 2010 (Figure 4.18).

Chapter 5

Discussion

In this chapter, I first discuss the spatial and temporal variability of the JFM sea ice in Disko Bay for 2003 to 2023 (Sections 5.1 and 5.2) and then the temporal and spatial variability of the JFM hydrography in Disko Bay (Sections 5.3 and 5.4). Furthermore, I assess the temporal variability of atmospheric and oceanic parameters correlated to SIC (Section 5.5). Lastly, I discuss oceanic and atmospheric coupling towards SIC (Sections 5.6 and 5.7) and consider the possibility of Disko Bay showing features of a coastal polynya (Section 5.8).

5.1 Spatial Variability of JFM Sea Ice

I examined three different sea-ice concentration (SIC) products (SIC Index, SIC 1 km, and SIC 12.5 km) and their representation of the SIC in Disko Bay. My analysis of the spatial extent of the SIC Index and a comparison of the closest available pixel (CAP) of SIC 1 km and SIC 12.5 km showed that the SIC Index represents the fast ice in front of Arctic Station and possibly the fast ice around Disko Island (Section 4.1, Figures 4.1 and 4.4, and Table 4.1). An in-depth comparison of the CAP of SIC 1 km and SIC 12.5 km to the SIC Index for 2018 to 2020 showed a systematic difference of above 20% between the SIC Index and SIC 1 km and 10% between SIC 12.5 km and the SIC Index. The comparison of the CAP for the SIC 1 km and SIC 12.5 km and a comparison of SIC in Disko Bay revealed a difference of 20% between the two products. The difference is attributed to the beginning and the end of the freezing season in JFM and that SIC 12.5 km represents the fast ice around Disko Bay and SIC in Disko Bay, and SIC 1 km only represents the SIC in Disko Bay (Section 4.1, Tables 4.1 and 4.2, and Figure 4.5). In addition, I found a pronounced year-to-year variability in JFM SIC between 2003 and 2023, with a small positive trend, accompanied by a small trend of decreasing atmospheric temperatures (Section 4.1, Figures 4.6 and 4.7).

I compared the mean JFM SIC values of the SIC Index to the CAP, near Arctic Station, of SIC 1 km and SIC 12.5 km. This revealed that the SIC Index represents the fast ice south of Arctic Station (Section 3.3, Figure 3.6 and Section 4.1, Figure 4.1). The analysis of the three products also showed that SIC 12.5 km represents the fast ice and the sea ice in Disko Bay, while SIC 1 km only represents the sea ice in Disko Bay (Section 3.2, Figures 3.4 and 3.5, and Section 4.1, Figure 4.4). This was further expressed in consistently higher JFM SIC determined by the SIC Index of approximately 20% compared to SIC 1 km and about 10% compared to SIC 12.5 km (Section 4.1, Table 4.2). An in-depth comparison of the overlapping years of all three products, 2018, 2019, and 2020, allowed insight into where these differences most likely stem from. The comparison of daily JFM SIC for 2018 to 2020 showed considerable differences at the start of the freezing season in January and at the end of March (Section 4.2, Figure 4.4). The SIC Index predominantly detected SIC before SIC 1 km and SIC 12.5 km. This most likely occurred since

the SIC Index covers a smaller area than SIC 12.5 km and SIC 1 km. For SIC 1 km, the closest pixel was further away than the general visibility from Arctic Station (Section 4.1, Figure 4.3a). Hence, the area close to shore is not included by SIC 1 km, and sea ice growth occurs later further out in the Bay. Moreover, the SIC Index showed consistently higher values over time and a different temporal variability than SIC 1 km and SIC 12.5 km. This can be attributed to its representation of the fast ice. The variability of SIC 1 km and SIC 12.5 km was similar when SIC reached around 40%, indicating that at that time, the sea ice covered more than the fast ice and is therefore also represented in SIC 1 km (Section 4.1, Figures 4.3 to 4.6).

The limitations associated with a visual inspection of the SIC Index have not been directly discussed; however, Heide-Jørgensen et al. (2007b); Mosbech et al. (2007); Møller & Nielsen (2019); Møller et al. (2023) used either solely satellite-derived SIC products (Mosbech et al., 2007; Heide-Jørgensen et al., 2007b) or used satellite-derived SIC products in addition to the SIC Index to describe SIC in Disko Bay (Møller & Nielsen, 2019; Møller et al., 2023). And Hansen et al. (2006) used the SIC Index to describe the fast ice surrounding Disko Island.

The comparison of weekly and daily JFM SIC means for Disko Bay of SIC 1 km, and SIC 12.5 km for 2018 to 2020 confirmed that SIC 1 km enables higher precision in identifying sea-ice variability due to its finer spatial resolution. Furthermore, both products show similar variability throughout JFM and thus, both represent the SIC in Disko Bay similarly (Section 3.2, Figures 3.4 and 3.5; Section 4.2, Figure 4.6 and Table 4.3). Nevertheless, SIC 12.5 km measured consistently higher SIC values than SIC 1 km, by about 20%. This is most likely related to the detection of fast ice associated with the coarser resolution of 12.5 km. This hypothesis is supported by the around 20% to 25% higher SIC values by SIC 12.5 km to SIC 1 km at the beginning of January and at the end of March. The degree to which SIC 12.5 km measured higher values seems to be year-dependent and to decline when SIC 1 km and SIC 12.5 km estimate SIC to be above 75% (Section 4.1, Figure 4.5). The uncertainty of the satellite-derived SIC should also be considered. The uncertainty of a grid cell value for SIC 12.5 km for JFM of 2003 to 2023 is 2.34% (Section 3.2). For SIC 1 km, the uncertainty between February and April is estimated to be 5% to 10% (Section 3.2). The percent-wise uncertainty of SIC 1 km is larger than SIC 12.5 km. Nevertheless, compared to the area the uncertainty covers in a grid cell, which for SIC 12.5 km is an area of around 300 m x 300 m, while for SIC 1 km, it is about 50 m x 50 m, SIC 1 km is still more precise.

Generally, the three products agree quite well with a systematic difference of about 15%. This is somewhat unexpected as there are apparent differences between the three products. It also concluded that each product has its advantages. The SIC Index works well if one is interested in local conditions around Qeqertarsuaq. For detailed information about the SIC in Disko Bay, SIC 1 km is the best option due to its fine spatial resolution. If someone is interested in the broad sea-ice coverage of Disko Bay, including the smaller island in the middle and the coast, then SIC 12.5 km is the product to use.

5.2 Temporal Variability of JFM Sea Ice

The constructed time series of JFM SIC for 2003 to 2023 revealed an evident year-to-year variability, where some years are characterised by low SIC while other years by high SIC (Section 4.1, Figures 4.6 and 4.7). Few studies address SIC specifically in JFM, as they often consider winter to last until April or May (Hansen et al., 2006; Møller et al., 2023). Nevertheless, such variability in winter SIC in Disko Bay is well documented and was found independently of winter length definition and the considered period (Hansen et al., 2006; Møller & Nielsen, 2019; Møller et al., 2023). Moreover, they agree on a seasonal cycle of sea-ice growth in Jan-

uary, and the sea-ice maximum is reached sometime in March (Andersen, 1981; Hansen et al., 2006; Heide-Jørgensen et al., 2007b; Møller & Nielsen, 2019; Møller et al., 2023). The same seasonal cycle was visible between 2003 to 2023. The constructed time series of SIC with a spatial resolution of 12.5 km between 2003 and 2023 indicates a small positive trend of 9% per decade. However, a p-value > 0.05 (0.1643)indicates no statistical significance related to a significance level of 5%. This increase in SIC is accompanied by a cooling of atmospheric temperature of -1.0 °C per decade, which was unexpected (Section 4.1, Figure 4.7). The decrease of T2M has a considerably larger p-value (0.2473) and thus is not statistically significant related to a significance level of 5%. I do not expect this cooling and increase in SIC to continue, as atmospheric temperatures are increasing all over the Arctic. This statistical insignificance might be connected to the period I consider, as many other papers have found a decrease in the sea ice and an increase in temperature (Hansen et al., 2006). In addition, I consider the winter to last from January to March, which might also have an influence. Hansen et al. (2006) found a decrease in the sea ice cover between 1994 and 2004 and Møller et al. (2023) noted a reduction of the sea ice cover between 1986 and 2019, especially in January and May in Disko Bay. Large changes in the Arctic sea ice were visible in the 1990s and the 2000s (Section 2.1, Figure 2.2b). Both of these periods are at least partly included in Hansen et al. (2006) and (Møller et al., 2023). This would imply that my time series might be too short to detect these long-term trends. Another possibility is that the results may vary as Møller et al. (2023) considered the sea-ice cover from January to May and investigated the number of days with more than 40% sea-ice cover for their analysis. Hansen et al. (2006) also considered that the winter season lasted until May. In addition, Hansen et al. (2006) used the SIC Index as a representative of the fast ice of Disko Island and found a reduction in the sea ice cover, indicating that there might have been a decline in the fast ice but not in the sea ice in Disko Bay.

5.3 Spatial Variability of JFM Hydrography

I investigated several types of spatial variability in Disko Bay with hydrographic observations. This data was acquired in March 2023 in Qeqertarsuup Tuna (QT) and Lyngmarkt Bugt (LB), in open water and under sea ice, during a repeated transect towards the shore, and by two different CTD instruments. In addition, I consider summer data of the whole Bay in 2019. The analysis indicated that the measurements taken during fieldwork in March 2023 are representative of JFM in Disko Bay as there is little spatial variability (Section 4.2, Figures 4.8 to 4.12).

The analysis of measurements in QT and LB revealed similar vertical profiles, except for one profile that displayed higher salinity values (Section 4.2, Figure 4.8b). The responsible CTD cast was conducted on the first fieldwork day in a water column where, a few hours previously, three biological nets were heaved up and down. This could have led to the uplifting of warmer and more saline water from the deep to the surface. Another more probable possibility is that the higher salinity values result from brine release due to the formation of new sea ice since we saw newly formed ice when we arrived back at the site.

The difference between a CTD cast taken under sea ice and open water showed slightly colder and more saline values down to 10 dbar in the water column under the sea ice(Section 4.2, Figure 4.9c and d). This difference is most likely the result of new sea-ice growth. An indication for this is that the temperature at the surface is close to the freezing point (Figure 4.9a and c, grey dashed lines), and the increased salinity could be attributed to brine release (Figure 4.9b and d).

A repeated transect of four stations separated by increments of 200 steps showed that dur-

ing each transect, the water mass under the fast ice varied little, except for one station for each transect (Section 4.1, Figure 4.10a and b). These stations showed colder and more saline values, which could be associated with new sea-ice formation as both stations were located in areas with high sea-ice variability.

In addition, I analysed CTD casts from a cruise in August of 2019, covering the whole of Disko Bay (Section 4.2, Figure 4.11). Three stations, Station 11, 12, and 15, showed slightly deviating profiles from the rest (Figure 4.11a and b). Stations 11 and 12 showed fresher and colder values. Due to their location to the east of the Bay, near the mouth of Ilulissat Icefjord (Figure 4.11c), they were most likely influenced by water leaving Ilulissat Icefjord (Figure 4.11c). The influence could result from submarine melt of Jakobshavn Isbræ, subglacial discharge, or submarine melt of the glacier or icebergs or ice-ocean interaction (Beaird et al., 2017). The exact circumstances are outside of the scope of this thesis. Station 15 is relatively close to Aasiaat (Figure 4.11c) and is known to have unique features and show a lot of variability (Personal Communication, Linda Latuta).

A similar approach to examine measurements conducted near Arctic Station to the waters of Disko Bay has been made by Hansen et al. (2012). They considered the period of May 1996 to June 1997. They concluded that measurements taken at the permanent research station from GEM largely represent the deeper parts of Disko Bay due to the homogeneity in temperature and salinity across the Bay below 150 m. However, they also discussed that the top 100 m showed apparent differences throughout the year, as the depth of the cold layer varied across Disko Bay, and the water west of Ilulissat Icefjord had higher temperatures and lower salinities.

5.4 Temporal Variability of JFM Hydrography

Oceanic data showed a pronounced variability in temperature and salinity over nine years of hydrographic data spanning the time between 2008 and 2023 (2008 to 2012, 2018, 2020, 2022, and 2023) (Section 4.2, Figures 4.14 and 4.15). The general hydrography of the waters in JFM indicates a salinity-stratified water column (Section 4.2, Figure 4.13). A cold and relatively fresh Polar Water (PW) layer lies at the surface. PW covers, on average, the surface down to 108 dbar. Below the PW, temperature rapidly increases until it reaches 2 °C, then increases at a slower rate. Salinity increases steadily, nearly linearly. I find warmer and more saline waters, West Greenland Irminger Water (WGIW), at depth. In contrast, to Heide-Jørgensen et al. (2007b), who described the water column as "well mixed" during winter, the average JFM water column indicates a salinity-stratified water column with a large temperature gradient. This could potentially stem from the definition of winter to last until May by Heide-Jørgensen et al. (2007b).

Buch (1990) discussed that the water at the bottom ($\geq$ 200 m) of Disko Bay would not exceed 2 °C, which he associated with a restricted inflow of warm and saline waters. A later study by Hansen et al. (2012) indicated that this had changed in the mid-1990s. The bottom waters of Disko Bay showed higher temperatures and more influence of the warm water originating from the Atlantic. This change of bottom water temperatures above 2 °C is also visible in (Gladish et al., 2015b, Figure 6, DB typical σ_θ). They showed that June, July, and August temperatures in Disko Bay at 250 m from 1997 to 2014 were mostly above 2 °C, some even above 2.5 °C. Observed summer temperatures at 250 m between 2002 and 2018 were, except for three years, above 2 °C as seen in (Khazendar et al., 2019, Figure 3d). This change in temperate has been associated with an increase in the warm and saline waters transported by the WGC through a shift in the NAO (Myers et al., 2007; Holland et al., 2008). This shift in

the NAO influenced the ocean circulation and resulted in an increased inflow of warm and saline waters into Disko Bay (Hansen et al., 2012; Gladish et al., 2015a; Khazendar et al., 2019). Khazendar et al. (2019) found that between 2014 and 2016, the top 250 m of the water column in Disko Bay decreased by almost 2 °C below 150 m. Nevertheless, the average JFM profile between 2008 and 2023 showed that temperatures above 2 °C are found below 150 dbar even in winter months (Section 4.2, Figure 4.13), showing that these warm conditions in the water column are normally found here nowadays.

Moreover, the JFM hydrography showed that stratification, especially surface salinity and temperature, played a role. Below the surface, the temperature of the top 50 dbar, the thickness of the PW layer, and whether and where WGIW can be found in the water column varied throughout the years (Section 3.3, Figure 3.8 and Section 4.2, Figures 4.14 and 4.15). I detected PW in all nine years; however, I only identified WGIW in six years (2008 to 2011, 2020, and 2023) (Section 4.2, Table 4.5). WGIW is found between 142 and 201 dbar down to the bottom of the profile. The detection of WGIW is thus partly depth-dependent. In the three years with shallower CTD profiles, 104, 136, and 141 dbar, I was not able to identify WGIW (Section 4.2, Table 4.5). In 2011, the JFM mean did not identify WGIW; however, two out of five CTD casts detected it. The dates of the profiles taken in 2011 are the 21^{st} of February (241 dbar), the 3^{rd} (258 dbar), the 14^{th} (230 dbar), the 24^{th} (199 dbar), and the 28^{th} (238 dbar) of March. On the 14^{th} and 28^{th} of March 2011, I detected WGIW. On the former, the first trace of WGIW was detected at 210 dbar, suggesting that between the 3^{rd} and the 14^{th}, an inflow event of WGIW south of Disko Island must have had occurred. This could explain why it was not measured on the two previous dates, even though they would have been sufficiently deep. On the latter date, the 28^{th}, WGIW was detected at 191 dbar. A potential explanation for this could be that another inflow event of WGIW further up in the water column occurred. The detection of WGIW is thus partly depth dependent; nevertheless, a horizontal source of advective properties of WGIW into Disko Bay has to have occurred sometime before (Figure 4.15 and Table 4.5). In addition, examining the first pressure values at which WGIW has been detected throughout the years showed that WGIW seems to be deepening throughout the years but is characterised by interannual variability (Figure 4.15 and Table 4.5).

5.5 Correlation of SIC to the Atmosphere and the Ocean

The highest correlation coefficients between SIC variability and the atmosphere were found for the winter length, SST, SLHF, T2M, and wind speed with $r \geq \pm 0.60$. The p-values for the winter length, SST, T2M, and SLHF were well below the significance level of 5%, with a p-value below 0.001 and below 0.01 for wind speed, which indicates statistical significance related to a significance level of 5%. I found a moderate correlation to the pre-NAO of r = 0.34 (p-value > 0.05). However, a p-value above 0.05 indicates no statistical significance related to a significance level of 5%. For the oceanic contribution to SIC variability, the correlation estimated a relatively high correlation to $T_{50\,\mathrm{dbar}}$ (r = -0.65, p-value > 0.05) and a moderate correlation to the thickness of the PW layer (r = 0.35, p-value > 0.05). Both have a p-value above 0.05, indicating no statistical significance related to a significance level of 5%. This might be related to only nine years of available hydrographic data in comparison to the 21 years of data for the atmospheric variables.

The RF model estimated an %IncMSE above 40% for SST, T2M, SSR, and SLHF, suggesting that if they were removed from the model, they would have the largest influence in increasing the MSE of the model performance. The partial dependencies of SSR showed a questionable relationship to SIC (Section 4.3, Figure 4.20c). It indicated that a large SSR value is associated with high SIC. This is unexpected as we would expect lower SIC with increased

SSR. However, by investigating the partial dependency, it is evident that the RF portrays the connection between the increase of SIC and SSR throughout JFM, as both have high values at the end of March. SSR starts to increase at the end of January, and SIC increases in most years at the beginning of January. In March, both reached their maximum values during JFM, and this relationship is seen in the partial dependency. This shows that correlation does not mean causation, and it only represents the seasonal cycle of SIC and SSR (Figure 4.17a and e, Figure 4.20c).

In general, the results of the RF have to be considered under the assumption that the RF model has no information about the interconnection between other parameters and how they influence each other. In addition, the RF does not have any information about the physical conditions of the parameters. The RF considers SIC and has no information about the thickness, which is also seen in the partial dependencies, as it misinterpreted the interrelationship between SLHF, SSHF and SIC. For SLHF, the partial dependency showed that small values of SLHF are associated with high SIC and large values are related to low SIC. This is attributed to a high SIC cover and a smaller possibility for heat extraction, indicating a small SLHF. With low SIC, more open water is available, and more heat can be extracted, as large SLHF fluxes suggest. However, this does not indicate how thick the sea ice cover is. Because at the same time, when SLHF become smaller, SSHF will continue to show high values, as heat is still being conducted through the ice, but evaporation does not occur anymore, thus lowering SLHF values. Therefore, the model will assign larger importance to the decreasing values of SLHF, which coincide with the increase of SIC, than with SSHF.

The RF and the correlation coefficients determined a high correlation between SIC variability and SST, T2M, and SLHF. The connection between the sea-ice cover and atmospheric conditions in Disko Bay has been observed and discussed over various periods (Hansen et al., 2006; Heide-Jørgensen et al., 2007b,a; Myers et al., 2007; Holland et al., 2008; Lloyd et al., 2011; Hansen et al., 2012; Gladish et al., 2015a). However, these two statistical approaches attributed different levels of importance to the variables and were calculated with different inputs. The correlation was calculated for JFM means but included more atmospheric variables and oceanic parameters. The oceanic parameters were also only available for nine years, and JAS SST for 17 years. Yet, the correlation captures the variables'interrelationship better than the RF as the input is only one value per JFM. Meaning that it is not possible to detect seasonal changes. On the other hand, the RF is a more convoluted approach and was run for daily SIC and atmospheric variables. I did not include a time lag, except for JAS SST and the pre-NAO. This could be important as some variables influence other variables after some time, and the effects on SIC would be seen later. It is important to consider the physical relationship between variables when determining the correlation between atmospheric and oceanic parameters and SIC.

I found a moderate correlation between the SIC variability and the pre-NAO of 0.34 (p-value > 0.05), indicating that the pre-NAO does not show a statistical significance related to a significance level of 5% However, the connection between winter sea ice, atmosphere, and the NAO is well documented on a regional and a large scale (Stern & Heide-Jørgensen, 2003; Hansen et al., 2006; Myers et al., 2007; Heide-Jørgensen et al., 2007a; Holland et al., 2008; Lloyd et al., 2011; Hansen et al., 2012; Gladish et al., 2015a; Onarheim et al., 2018; Møller & Nielsen, 2019). Sea-ice variability in Baffin Bay/Gulf of St.Lawrence relates to atmospheric variabilities, like the NAO (Onarheim et al., 2018). In literature, the pre-NAO and the previous winter NAO index are used. Stern & Heide-Jørgensen (2003) found a strong correlation between the March ice concentration and the one-year lagged winter NAO index in Baffin Bay. Similar conditions were found in Davis Strait, where the correlation to the NAO of the previous winter was high,

indicating that the coming winter sea-ice condition can only be speculated with the NAO index of the current winter (Stern & Heide-Jørgensen, 2003). Between 1991 and 2004, an increase in the mean air temperature and a reduction in the sea ice cover were observed in Disko Bay. These changes were mainly detected in winter and related to the NAO index (Hansen et al., 2006). The influence of the NAO was seen in the atmosphere, on the sea ice, in the ocean circulation, and in the inflow of warm waters in Disko Bay (Myers et al., 2007; Holland et al., 2008; Hansen et al., 2012). In addition, the effect of the NAO index is related to the temperature below the surface and affects the West Greenland shelf with a delay (Gladish et al., 2015a).

Møller & Nielsen (2019) found that the sea-ice cover is correlated to the 6M-NAO and the pre-NAO. Changes in the NAO index have been related to shifts in ocean temperature in Disko Bay (Holland et al., 2008; Gladish et al., 2015a). Hansen et al. (2006) found that monthly mean atmospheric temperatures derived from Arctic Station and the NAO index correlate reasonably well to temporal variations in winter. There also seems to be a link between the NAO and atmosphere conditions during winter independent of whether the winter comes early in the season or later (Hansen et al., 2006). However, the connection between the NAO and SIC relationship is convoluted as large a shift in the NAO in the 1960's (Lloyd et al., 2011; Hansen et al., 2012) was not reflected in bottom temperature (Lloyd et al., 2011; Hansen et al., 2012). Hansen et al. (2012) suggest that "other more local feedback mechanisms are also influencing conditions" that are influential in Disko Bay. This might be a possible explanation for a p-value above 0.05. It suggests that the pre-NAO is correlated to the SIC variability but is not the only influencing factor, as the previous winter NAO index could also play a role or other atmospheric variabilities.

A linear relationship between SIC and $T_{50\ dbar}$ has been established (Section 4.2, Figure 4.16). A p-value above 0.05 (0.057) suggests that $T_{50\ dbar}$ shows no statistical significance related to a significance level of 5%. However, as previously discussed, this might originate from the fact that it is only data of nine years. And the p-value is only slightly above the significance level. $T_{50\ dbar}$ were relatively cold at the surface, and the only two high temperatures below the overall JFM mean of -1.50 °C were found in 2010 and 2011. The connection between SIC and $T_{50\ dbar}$ also indicates that a warming of 0.2 °C to a temperature of -1 °C in the top 50 dbar would theoretically be associated with a JFM SIC of 0%.

5.6 Events of Low SIC

An investigation of events of low and high SIC showed that T2M, SST, SLHF, the winter length, $T_{50\ dbar}$, the thickness of the PW, and the pre-NAO all show a relation to SIC. It also showed that the SIC seems to control the atmospheric heat fluxes during winter.

Events of low SIC for 2010 and 2011 showed that the SST, T2M, and SLHF mean were higher than the overall JFM mean and the mean JFM evolution (Section 4.4, Figure 4.21). Moreover, 2010 and 2011 had the second and third shortest winter length of 2003 to 2023. 2010, the year with the lowest SIC, is associated with the highest T2M, largest SLHF, and the shortest winter length. Due to the higher atmospheric temperatures and reduced freezing time, it was harder for sea ice to grow. In addition, the summers preceding 2010 and 2011 had a higher SST mean than the overall JAS mean. The NAO of the previous year was negative for both years (Section 4.4, Figure 4.18), suggesting potentially more transport of warm waters and generally warmer SST in the south, lower east and west of Greenland and thus potentially in Disko Bay (Section 2.4, Figure 2.5). $T_{50\ dbar}$ had the highest two values for 2010 and 2011 of all nine years (Section 4.2, Figure 4.16), indicating that the surface and upper water column were warmer (Section 4.2, Figure 4.14 and Appendix C, Figure C.7). The ocean and the atmosphere

were generally warmer than the overall JFM mean and the mean JFM evolution. Milder atmospheric temperatures during winter and a potential inflow of warmer and more saline water from the WGC in Disko Bay were associated with reduced sea ice before and have been discussed by Nielsen et al. (2001).

The low SIC in Disko Bay during JFM 2010 can be related to observations by Gladish et al. (2015a,b). They found high SST characterised the summer of 2009 in Baffin Bay, warmer waters were found in Disko Bay, and temperatures were considerably warmer than the WGC. Increased temperatures of the warm and saline waters transported by the WGC result in more open water areas and a reduction in sea-ice cover along the coastal areas of West Greenland (Parkinson, 1995; Heide-Jørgensen et al., 2007b). The following winter, 2009/2010, was associated with a low NAO index at the beginning, high sea level pressure values over Baffin Bay, and higher air temperatures than usual in Davis Strait and in the southeastern part of Baffin Bay. This was associated with low sea ice in the south and southeast Baffin Bay (Gladish et al., 2015a,b). Another possibility for the low SIC is that the inflow of warm and saline waters continued, increasing temperature and salinityin the water column. Warmer and more saline waters can lead to a later freeze-up date and, inherently, to a reduced freezing period (Hansen et al., 2006; Mosbech et al., 2007; Holland et al., 2008; Motyka et al., 2011; Hansen et al., 2012) The hydrographic data of 2010 indicates that the surface was the warmest for all years, and it had the shallowest cold and fresh layer. The thickness of the PW layer was 84 dbar, the shallowest PW layer in nine years and lower than the mean of 108 dbar. In addition, the salinity was relatively high, between 33.4 to 33.6. Higher salinity indicates more cooling is needed until sea ice can grow. The mean temperature of the top 50 dbar was highest in 2010 at -1.21 °C. This also means sufficient cooling during autumn must happen until the water is at the freezing point. The winter length was 43 days, indicating a reduced time for sea ice to form. To sum up, warmer and more saline waters in the top 50 dbar were connected to a milder winter, and a low NAO index are most likely the reason for low SIC in 2010.

The low SIC in the following year, 2011, is related to a record low of the NAO in 2010. In addition, summer SST in the eastern Baffin Bay were still high. Indicating that throughout the autumn and at the beginning of winter, sufficient cold atmospheric temperatures were needed to cool down the water column for sea-ice growth to occur early during winter. Atmospheric temperatures in Davis Strait and southeast Baffin Bay in the winter of 2010/2011 were still higher than the mean, and the waters of the WGC during the summer of JFM 2010 were warmer than usual (Ribergaard, 2011). This resulted in low SIC in the south and southeast of Baffin Bay (Gladish et al., 2015a,b). Gladish et al. (2015a) found summer SST to be 1 °C lower than the year with the highest temperatures. Yet, at the end of September, SST in Disko Bay was still at 4.16 °C (Section 4.4, Figure 4.21n) Gladish et al. (2015a) explained the lower temperatures in Disko Bay with a freshwater inflow from the Baffin Bay current origination from the Canadian Arctic at the end of 2009. This freshwater inflow is most likely the cause of the relatively fresh 50 to 80 dbar of the water column in 2011 compared to the other years. Suggesting that the water column was highly stratified, with a salinity of 32.8 in the top 35 dbar. This also indicates a shallow thermocline, which would increase the possibility for sea ice to grow as a shallower thermocline is easier to cool to the freezing point. The inflow of freshwater describes a negative feedback mechanism of more melt leading to a higher stratification by the freshwater, decreasing the salinity at the surface, which makes it easier for sea ice to grow. This input of fresh water can also be the result of a warmer ocean is more submarine melting from Jakobshavn Isbræ entering Ilullisat Icefjord and, therefore, Disko Bay (Hansen et al., 2006; Mosbech et al., 2007; Holland et al., 2008; Motyka et al., 2011; Hansen et al., 2012) In contrast to the low salinity values, the surface temperature was slightly higher than in other years. The temperature in the top 50 dbar was -1.30 °C, the second-highest temperature in the

nine years we have data for. The thickness of the PW layer was down to 87 dbar, the second shallowest PW thickness.

The low SIC in 2011 can be related to a record low of the NAO index, warmer SST in the summer, a shorter winter length, warmer T2M and increased temperatures in the top 50 dbar. Even though surface temperatures were warm, the surface salinity showed relatively fresh values compared to the other years. This fresh surface layer of about 32.8 might be related to the considerable sea ice growth that occured after mid-March.

5.7 Events of High SIC

Events of high SIC, 2008 and 2012, describe years with lower SST and T2M than the overall JFM mean and the JFM evolution. A longer winter length and slightly smaller SLHF. The ocean shows a minimally higher $T_{50\,dbar}$ for 2008 and a lower value for 2012 than the overall JFM mean. In addition, the thickness of the PW was above 90 dbar, lower than the overall JFM mean of 108 dbar but deeper than the PW thickness of low SIC years. Additionally, the previous years's NAO were both in a positive phase (Section 2.4, Figure 2.5a), suggesting that the surface waters east and south of Greenland are cooler and the warm waters do not reach as far towards Greenland and are flowing stronger towards Scandinavia and the Russian the Arctic (Figure 2.5a). Summer SST temperatures at the end of September for 2007 were slightly above the mean JFM evolution and, in 2011, below the mean (Section 4.4, Figure 4.22n).

The longest winter, the smallest SLHF, and the coldest T2M are related to the highest SIC (2008). A long and continuous winter season translates to favourable conditions for sea-ice growth. The water column in 2008 showed low temperatures and a fresh surface layer, which are excellent conditions for sea ice growth. In 2012, the water column was colder at the surface, thicker, and slightly more saline. The water column of winter 2011 showed a very fresh and less cold surface because of this there might have been only a thin, warm upper layer during the summer, which cooled down towards the end of the summer would have been easier to cool down during autumn (Gladish et al., 2015a,b), (Figure 4.22n). This would indicate that the Autumn cooling is more important than the pre-conditioning during the summer at the surface. $T_{50\,dbar}$ in 2012 was -1.58 °C, and the temperature at the end of September was 2.77 °C, considerably lower than in other years. Indicating that a weaker autumn cooling might have been enough to cool the surface enough for sea ice to grow.

Generally, years with high SIC are correlated with lower than the mean water column SST and T2M. Low SST values indicate a higher chance of sea-ice growth (Section 4.4, Figure 4.22). The influence from the ocean is related to the temperature in the top 50 dbar, $T_{50\,dbar}$ wither temperature in the upper water column. These indicate good conditions for sea-ice growth, and a slightly thicker layer might insulate against the layer of warmer water below. In addition, in high SIC years, I found a few events of higher winds associated with a decrease in SIC, higher SST, T2M, and larger SLHF, which indicate that Disko Bay might show features of a coastal polynya.

5.8 Disko Bay - Coastal Polynya?

Two wind events in 2008 indicate that under the right conditions, Disko Bay shows features of a coastal Polynya. I consider a wind event which occurred between the 13^{th} and 21^{st} of January 2008 (Section 4.4, Figure 4.22a, c, e, g, and k, and Figure A.1). Wind speed started to slightly increase on the 13^{th} of January and reached 3.88 m s^{-1} on the 17^{th} of January. At

that time, SIC is at 78.69%, SST at -1.69 °C, T2M at -22.01 °C and SLHF is -15.72 W m^{-2} (Figure 4.22a, c, e, g, and k). One day later, the wind speed dropped to 1.25 m s^{-1}, and T2M increased by nearly 10 °C to -13.10 °C. SIC decreased to 73.35%, and SLHF increased slightly to -18.91 W m^{-2}. This could indicate that a part of the sea ice was exported out of the Bay due to the previous higher winds. The now open water stretches are exposed to cold atmospheric temperatures and induce vertical mixing in the ocean water column. This leads to an extraction of heat to the atmosphere, which a slightly larger SLHF value indicates. SST remained the same. On the 19^{th} of January, wind speed increased again and reached 4.36 m s^{-1}. T2M were slightly less cold with -12.94 °C, while SIC decreased to 71.16% and SLHF increased by 10 W m^{-2} to -28.37 W m^{-2}. SST remained at -1.69 °C. These values indicate that the vertical mixing and the extraction of heat continued and slightly increased the heat content in the atmosphere. The next day, on the 20^{th} of January, the wind continued to be above 4 m s^{-1}, T2M increased by 8 °C to -5.82°C. SLHF decreased minimally to -27.11 W m^{-2}, while SIC decreased to 61.75%. SST was at -1.67 °C. This suggests that more sea ice has been exported, and more heat has been extracted to the atmosphere, increasing T2M due to a larger SLHF. On the 21^{st} of January, the highest wind speed in JFM 2008 of 5.99 m s^{-1} is detected. SIC was at 49.62% that day. SLHF is larger with -32.66 W m^{-1}, and SST dropped to -1.49 °C, and T2M is -2.31°C (Figure 4.22a, c, e, g, and k). This suggests that due to the higher winds of the past days, around 30% of the sea ice in Disko Bay was exported, resulting in vertical mixing and extraction of heat from the ocean to the atmosphere to grow more sea ice and hence increasing the atmospheric temperature, and SST to -1.49 °C (Figure 4.22a, c, e, g, and k, and Figure A.1). After the 21^{st} of January, winds decrease to nearly 0 m s^{-1}, after which another wind event of 7 to 8 days followed, showing a similar pattern.

Higher wind speeds likely lead to an export of sea ice out of the Bay; the cold wind induces vertical mixing, extracting heat from the ocean, releasing it to the atmosphere, and warming the atmosphere and the surface. As the high winds persisted, more ice was exported. The sea ice starts to grow new sea ice until the next wind event before the beginning of February occurs, lasting nearly a week. This also showed that Disko Bay during the winter of 2008 did not contain a lot of heat as T2M quickly increased with larger SLHF.

The possibility of Disko Bay showing features of a polynya has been mentioned before by Mosbech et al. (2007); Heide-Jørgensen et al. (2007b). Mosbech et al. (2007) proposed the possibility as Disko Bay displays characteristics of a polynya to the west of Disko Island and in front of Disko Bay when the melt season starts. They also consider that the waters at the entrance of Disko Bay might be a polynya. In line with this was the mentioning of Disko Bay as a polynya in Heide-Jørgensen et al. (2007b). In addition to the wind event in 2008, the prevailing winds in JFM of Disko Bay for 2003 to 2023 come from the Northern North-East (Section 4.3, Table 4.6). This could also indicate a coastal polynya because if sufficiently low air temperatures accompany the wind direction, Disko Bay could have characteristics of a coastal polynya (Thomas, 2017), as long as the conditions persist. Due to the prevailing wind direction, the sea ice could be exported through the entrance of Disko Bay or southwest of Arctic Station. At the same time, atmosphere temperatures are low, and sea-ice formation is likely to occur (Thomas, 2017). This process would continue as long as the air temperatures remain low and sea ice can be exported out of Disko Bay. In this way, Disko Bay showed similar features to a polynya in Svalbard, created by winds from the North-East transporting cold air (Skogseth et al., 2009).

Chapter 6

Concluding remarks

This thesis provided insight into Sea-Ice Concentration (SIC) in Disko Bay from January, February, and March of 2003 to 2023 using three different SIC products, hydrographic data for nine years and atmospheric reanalysis data. An investigation of the three SIC data sets established that there are systematic differences. The SIC Index from Arctic Station represents the fast ice area locally close to Qeqertarsuup Tuna. The two satellite-derived products (SIC 12.5 km and SIC 1 km) show a systematic difference of about 20%, with SIC 12.5 km indicating higher SIC. This is reflected in SIC 12.5 km, which, in addition to the SIC in Disko Bay, also represents the fast ice, while SIC 1 km only represents the sea-ice concentration in Disko Bay. A thorough analysis of hydrographic data conducted in March 2023 allowed me to conclude that it represents the waters of Disko Bay, as these are quite homogeneous.

An investigation into the highest correlated daily atmospheric variables with a Random Forest Model on daily SIC revealed that SST (73.26%), T2M (50.18%), SSR (43.75%) and SLHF (41.72%) have the highest %IncMSE. A Pearson correlation of yearly SIC to atmospheric variables and the NAO revealed that the winter length (r = 0.84), SST (r = -0.76), SLHF (r = 0.74), T2M (r = 0.70) and wind speed (r = -0.61) are highly correlated with SIC. Further, I found a moderate correlation to the NAO of the previous year (r = 0.34). Ocean forcing correlated to the SIC variability revealed that the temperature of the top 50 dbar(r = -0.65) was highly correlated. The thickness of the cold and fresh Polar Water (PW) layer (r = 0.35) was moderately correlated.

My first research question concerns the changes in SIC in Disko Bay during January, February and March over 21 years. My analysis based on two satellite-derived SIC products (SIC 1 km and SIC 12.5 km) revealed a pronounced year-to-year variability and a clear seasonal cycle of ice growth. For the mean JFM SIC, a small positive trend of 9% per decade was found, associated with a 1 °C decrease of T2M per decade.

For my second research question, I examined the ocean conditions during JFM and examined the variability. I was able to compare data for nine out of 21 years from 2008 to 2012, 2018, 2020, 2022, and 2023. These indicated that throughout the years, there is an evident year-to-year variability in stratification, surface salinity and temperature, the temperature of the top 50 dbar $T_{50\,\mathrm{dbar}}$, the thickness of the Polar Water layer, and if and where West Greenland Irminger Water can be found in the water column. The temperature of the top 50 dbar showed a linear relationship to sea-ice concentration, in which low $T_{50\,\mathrm{dbar}}$ were associated with high sea-ice concentration.

With my third research question, I aimed to answer whether oceanic or atmospheric forcing was the main driver for sea-ice variability in Disko Bay from 2003 to 2023. Examining two

different statistical approaches and a composite of low and high SIC years suggests an interrelationship between atmospheric and oceanic drivers. The contribution of the atmosphere is related to SST, T2M, and the length of the winter, as these were highly correlated. The phase of the NAO of the previous year showed a moderate correlation. The analysis also showed that the sea ice was controlling the atmospheric heat fluxes at the air-ice-ocean interface. The contribution of the ocean is attributed to the temperature of the top 50 dbar, $T_{50\ dbar}$ During years with high SIC, higher wind speeds over a couple of days have the potential for Disko Bay to show characteristics of a coastal polynya. Determining atmospheric and oceanic drivers influencing SIC variability showed that all these variables are closely correlated and influence each other. Therefore, I conclude that a combination of oceanic and atmospheric forcing drives the sea-ice variability in Disko Bay.

Future work

Expanding the winter season to include April and May and extending the time series back to the 1990's could be beneficial. It could be interesting to see if, by including these two months, thus the start of the melting season, the variability and trends would still agree with my result or previous work. Extending the time series to the 1990's would allow for a more comprehensive understanding of the changes in SIC. Moreover, by expanding the time series to 30 or 50 years, it is possible to examine multidecadal variability

A tremendous help would be oceanographic current data to understand when, where, at what strength, and depth West Greenland Irminger Water (WGIW) enters the bay and if there is a seasonal cycle. This information would provide a deeper understanding of the connection between the inflow of WGIW and SIC in Disko Bay. Additionally, more spatially varying data collected during winter might provide more insight into the spatial variation of Disko Bay during winter.

A more detailed analysis of event of high and low SIC with a focus on autumn cooling would be beneficial to enhance the understanding of the beginning of the freezing season as a prerequisite of sea ice formation in Disko Bay. Autumn cooling seems to be the main factor as a prerequisite for the winter in Disko Bay.

Additionally, It would be intriguing to expand the use of the Random Forest and include sea-ice thickness or volume to observe how the importance of the variables might change. Additionally, to include a time lag for certain variables, e.g. SSR and wind speed, to see the effects of certain variables over time and on other variables. Furthermore, a more detailed study of wind events to analyse the potential to which extent Disko Bay can show features of a coastal polynya.

Abbreviations

Currents:
BIC = Baffin Island Current
EGC = East Greenland Current
IC = Irminger Current
WGC = West Greenland Current
NAC = North Atlantic Current
NwAC = Norwegian Atlantic Current

Sea Ice terms:
SIC = Sea-Ice Concentration

Water masses:
PW = Polar Water
WGIW = West Greenland Irminger Water

Atmospheric Terms:
NAO = North Atlantic Oscillation
T2M = Temperature at 2m
SST = Sea Surface Temperature
SLHF = Surface Latent Heat Flux
SSHF = Surface Sensible Heat Flux
SSR = Surface net Solar Radiation
STR = Surface net Thermal Radiation
pre-NAO = NAO of the previous calendar year

Oceanic Terms:
$T_{50\ dbar}$ = Temperature of the top 50 dbar
PW thickness = Thickness of the Polar Water Layer

Other abbreviations:
JFM = January, February and March
JAS = July, August and September
CAP = Closest Available Pixel

Appendices

Appendix A

Sea Ice

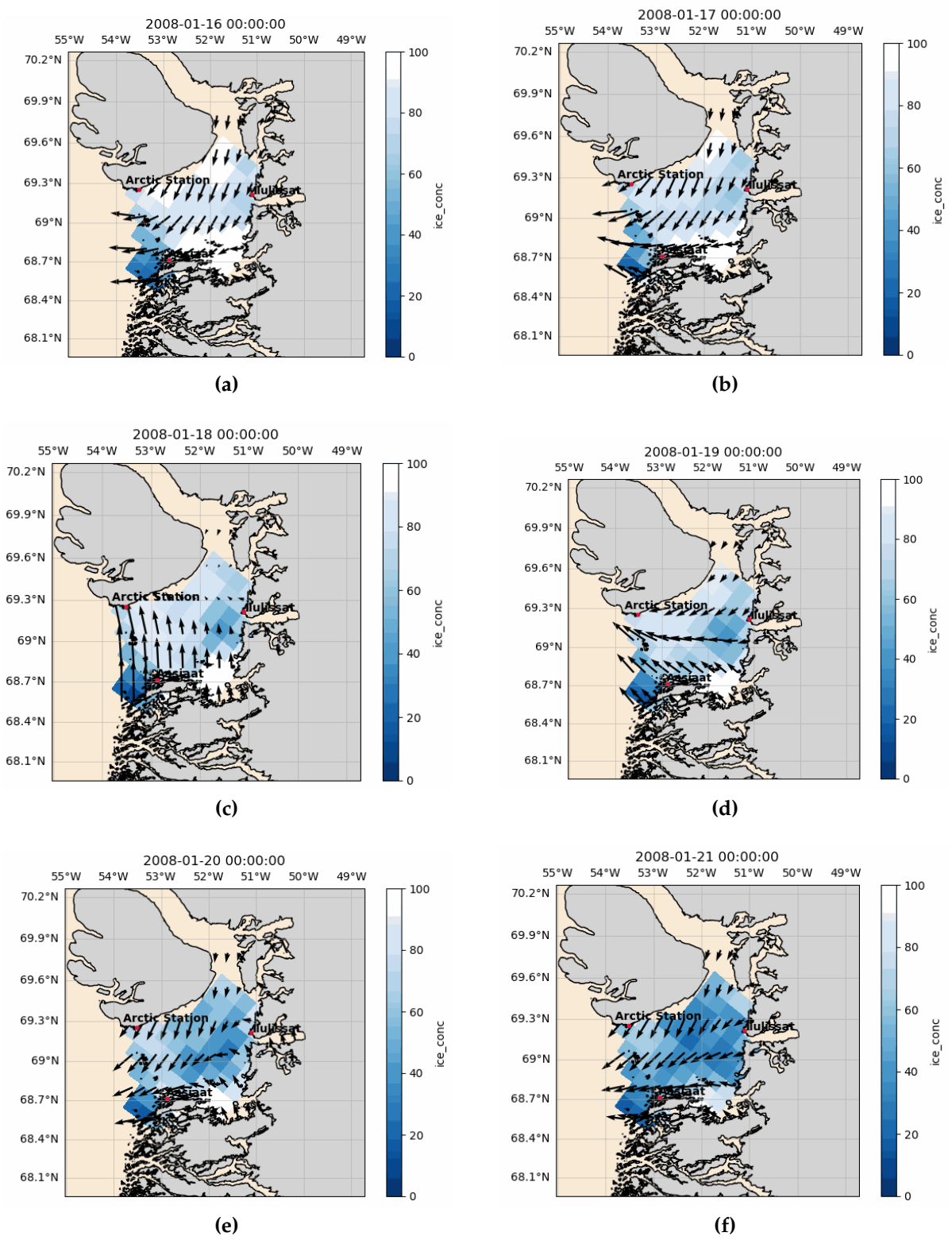

(a) **(b)** **(c)** **(d)** **(e)** **(f)**

Figure A.1: *Wind and SIC form the 16th to the 21th of January 2008-*

Appendix B

Ocean

Table B.1: *List of data sources and their respective dates, and the number of casts available. all were taken at, GEM is the Greenland Ecosystem Monitoring Station, OMG is Ocean Melting Greenland.*

Year	January	February	March	Casts	Data Source
2008	-	21 , 27	07 19 , 23 , 24	12	GEM
2009	-	10, 24	09, 10, 21, 26	14	GEM
2010	22	18	17, 29	8	GEM
2011	-	21	03, 14, 24, 28	5	GEM
2012	-	-	07	1	GEM
2018	-	27	07, 16, 21, 26, 30	6	GEM
2020	-	-	27	1	OMG
2022	-	-	25, 30	2	GEM
2023	-	-	07, 08, 09, 10, 13, 14, 15, 16, 18	37	Fieldwork
Sum	**2**	**11**	**73**	**86**	

Table B.2: *Date and bottom value of all hydrographic measurements from 2008. All CTD casts were taken at 69.117°N, 53.3181°W.*

2008	Date	Bottom value [dbar]
February	21	60.84
		60.98
	27	124.31
		125.15
March	07	154.89
		155.31
	19	156.43
		156.57
	23	154.89
		155.59
	24	156.15
		156.01

Table B.3: *Date and bottom value of all hydrographic measurements from 2009. All CTD casts were taken at 69.117°N, 53.3181°W.*

2009	Date	bottom value [dbar]
February	10	259
		261
	24	46
		50
March	09	44
		49
	10	187
		182
	21	211
		208
	26	48
		247
		54
		244

Table B.4: *Date and bottom value of all hydrographic measurements from 2010. All CTD casts were taken at 69.12°N and 53.32°W.*

2010	Date	bottom value [dbar]
January	22	197.47
		198.12
February	18	198.53
		196.73
March	17	198.49
		197.61
	29	264.64
		266.58

Table B.5: *Date and bottom value of all hydrographic measurements from 2011. All CTD casts were taken at 69.1836°N and 53.5169°W.*

2011	Date	bottom value [dbar]
February	21	238
March	03	255
	14	227
	24	196
	28	235

Table B.6: *Date, bottom depth, latitude and longitude of the hydrographic measurement from 2012.*

2012	Date	bottom value [dbar]	Latitude [°N]	Longitude [°W]
March	07	134	69.251	53.31

Table B.7: *Date and bottom value of all hydrographic measurements from 2018. All CTD casts were taken at 69.1836°N and 53.5169°W.*

2018	Date	bottom value [dbar]
March	03	93
	07	141
	16	126
	21	126
	26	125
	30	125

Table B.8: *Date, bottom value, latitude and longitude of the hydrographic measurement from 2020.*

2020	Date	bottom value [dbar]	Latitude [°N]	Longitude [°W]
March	27	204.64	69.25169	51.1509

Table B.9: *Date, bottom value, latitude and longitude of all CTD casts taken during the two-week fieldwork in March 2023*

2023	Date	bottom value [dbar]	Latitude [°N]	Longitude [°W]
March	07	80.90	69.2472	-53.590417
	08	81.68	69.2472	-53.590417
		63.51	69.24265	-53.505283
		63.35	69.24265	-53.505283
	09	46.02	69.244183	-53.506733
		38.32	69.245633	-53.508333
		29.19	69.2472	-53.509867
		19.53	69.248717	-53.511167
		81.47	69.2472	-53.590417
	10	70.08	69.2419	-53.50415
		60.79	69.24265	-53.505283
		206.7	69.2105	-53.52695
	13	195.80	69.210667	-53.5275
		138.50	69.219067	53.536667
		63.42	69.242417	-53.506083
		46.93	69.2442	-53.506717
	14	40.06	69.245717	-53.5083
		30.31	69.2472	-53.50985
		19.29	69.2487	-53.5111
		88.48	69.238583	-53.5066
	15	113.27	69.239567	-53.498267
		113.13	69.239583	-53.498433
		12.37	69.241033	-53.509317
		70.84	69.240783	-53.509667
		72.90	69.2404	-53.51035
		76.67	69.240983	-53.507017
		73.99	69.240767	-53.506567
	16	79.10	69.240417	-53.505783
		13.31	69.241917	-53.5071
		64.54	69.242133	-53.50665
		61.51	69.242517	-53.505967
		64.01	69.2417	-53.509517
		61.99	69.241867	-53.510183
		69.24	-53.51115	64.793
	18	81.737	69.247217	-53.590533
		101.58	69.240183	-53.5001
	19	80.82	69.239083	-53.508883

Heat content

I additionally calculate the heat content (Equation (B.1)) to the common deepest depth of 136 dbar for the water column, the heat content in the Polar Water layer to their respective depth of the Polar Water layer, and the heat content of the Polar Water layer to the common deepest depth of 80 dbar (Table B.10). This analysis, unfortunately, did not provide any insight into

the values that vary for each year. Even in years with low or high SIC, no pattern is evident.

$$H = \rho \cdot c_p \cdot T - T_{ref} \tag{B.1}$$

Table B.10: *Heat content for three experiments.*

Heat content	to 136 dbar	PW Layer	PW Layer to 80 dbar
2008	1.04· 10^6 J	7.96· 10^6 J	6.42· 10^6 J
2010	-1.72· 10^6 J	8.58· 10^6 J	8.58· 10^6 J
2011	-1.33· 10^6 J	8.53· 10^6 J	7.66· 10^6 J
2012	2.27· 10^6 J	7.21· 10^6 J	4.78· 10^6 J

Fieldwork

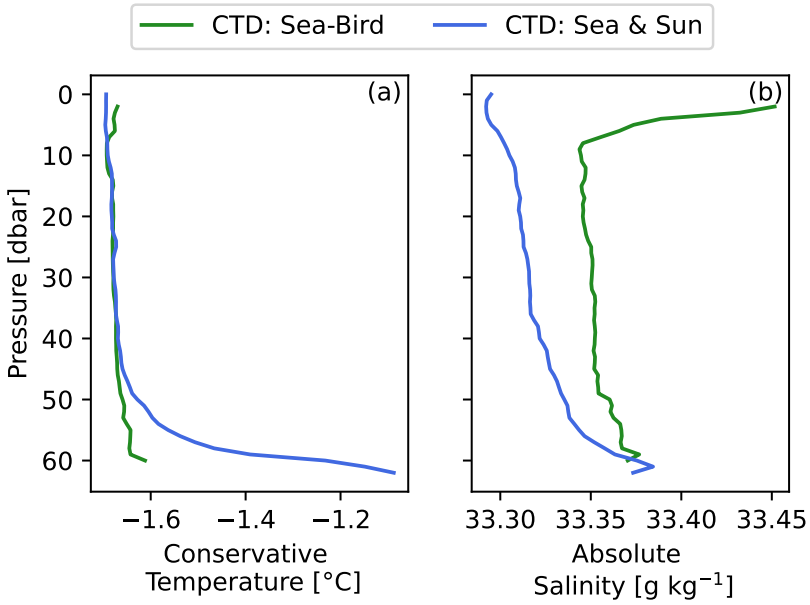

Figure B.1: *Vertical profiles of temperature (a) and salinity (b) of two CTD casts taken by two different instruments at the same location on the 09th of March 2023. Green lines represent a CTD cast measured with a Sea-Bird CTD, and blue represents the CTD cast measured with the Sea & Sun CTD.*

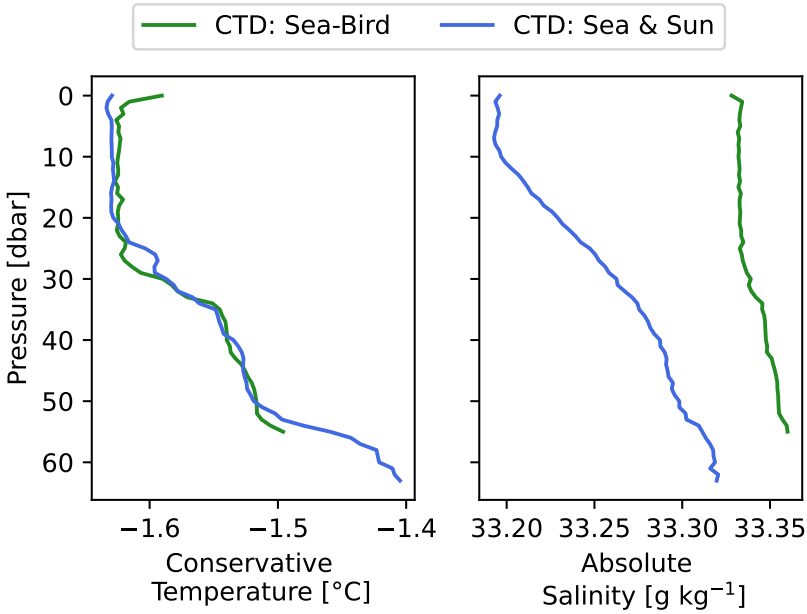

Figure B.2: *Vertical profiles of temperature (a) and salinity (b) of two CTD casts taken by two different instruments at the same location on the 14th of March 2023. Green lines represent a CTD cast measured with a Sea-Bird CTD, and blue represents the CTD cast measured with the Sea & Sun CTD.*

Table B.11: *Averaged difference between CTD measurements by Sea-Bird Scientific and Sea & Sun Technology*

Date	**Difference**	
	Salinity [g kg^{-1}]	Temperature [°C]
09.03.2023	0.037	-0.024
14.03.2023	0.091	-0.0005
18.03.2023	0.016	0.005
Mean	0.048	-0.006

Appendix C

Events of Low and High SIC

SST

Table C.1: *Mean, minimum and maximum SST for January to March for high SIC years(2008, 2012) and low SIC(2010, 2011) years.*

Year	mean [°C]	min [°C]	max [°C]
2008	-1.67	-1.78	-1.33
2012	-1.68	-1.84	-1.38
2010	-1.49	-1.79	-0.87
2011	-1.24	-1.88	0.27

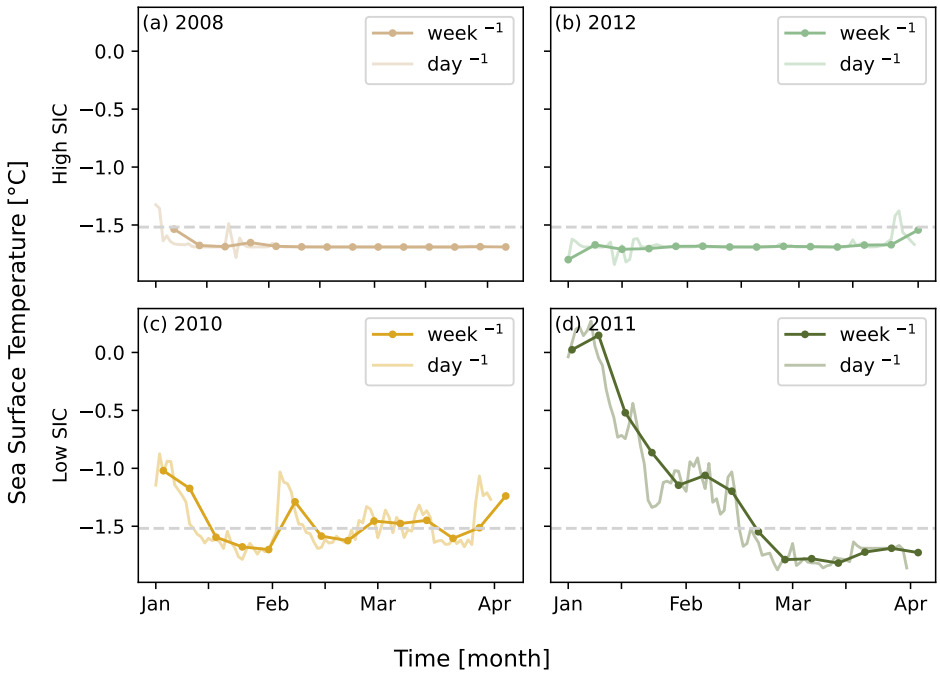

Figure C.1: *Daily and weekly SST for JFM for years with high SIC, 2008 and 2012, and years with low SIC, 2010 and 2011. The grey dashed line represents the 21-year mean for SST in JFM.*

T2M

Table C.2: *Mean, minimum and maximum T2M for January to March of the maximum(2008, 2012) and minimum (2010, 2011) years.*

Year	mean [°C]	min [°C]	max [°C]
2008	-16.51	-30.98	-2.31
2012	-15.56	-30.91	-0.68
2010	-8.55	-17.52	2.38
2011	-12.05	-22.65	1.01

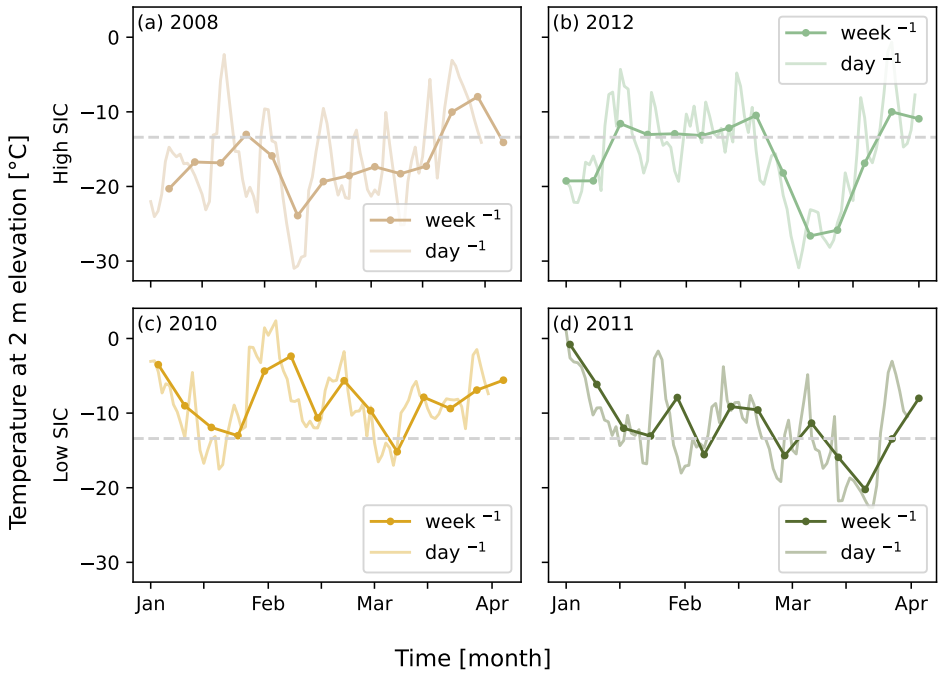

Figure C.2: *Daily and weekly T2M for JFM for years with high SIC, 2008 and 2012, and years with low SIC, 2010 and 2011. The grey dashed line represents the 21-year mean for T2M in JFM.*

SLHF

Table C.3: *Mean, minimum and maximum SLHF values for January to March of the maximum (2008, 2012) and minimum (2010, 2011) years.*

Year	mean [W m^{-2}]	min [W m^{-2}]	max [W m^{-2}]
2008	-9.50	-1.37	-36.64
2012	-12.44	-3.01	-30.43
2010	-14.13	-1.65	-36.48
2011	-22.52	-1.78	-51.32

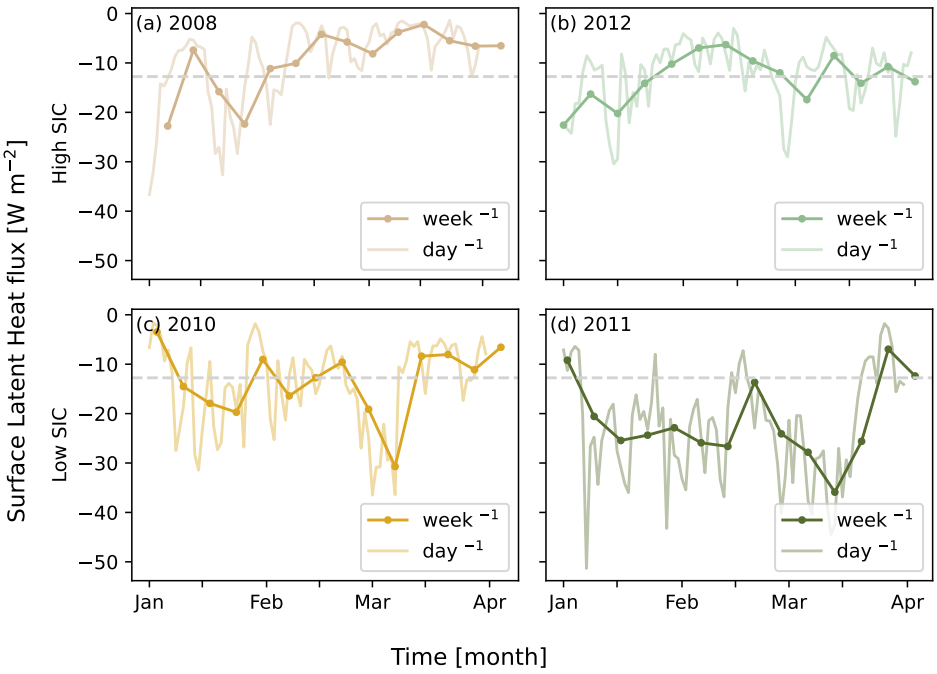

Figure C.3: *Daily and weekly SLHF for JFM for years with high SIC, 2008 and 2012, and for years with low SIC, 2010 and 2011. The grey dashed line represents the 21-year mean for SLHF in JFM.*

SSR

Table C.4: *Mean, minimum and maximum values of SSR for January to March of the maximum (2008, 2012) and minimum (2010, 2011) years.*

Year	mean [W m^{-2}]	min [W m^{-2}]	max [W m^{-2}]
2008	10.73	$8.6 \cdot 10^{-5}$	43.28
2012	12.75	0	61.28
2010	15.35	0	74.03
2011	12.93	0	51.29

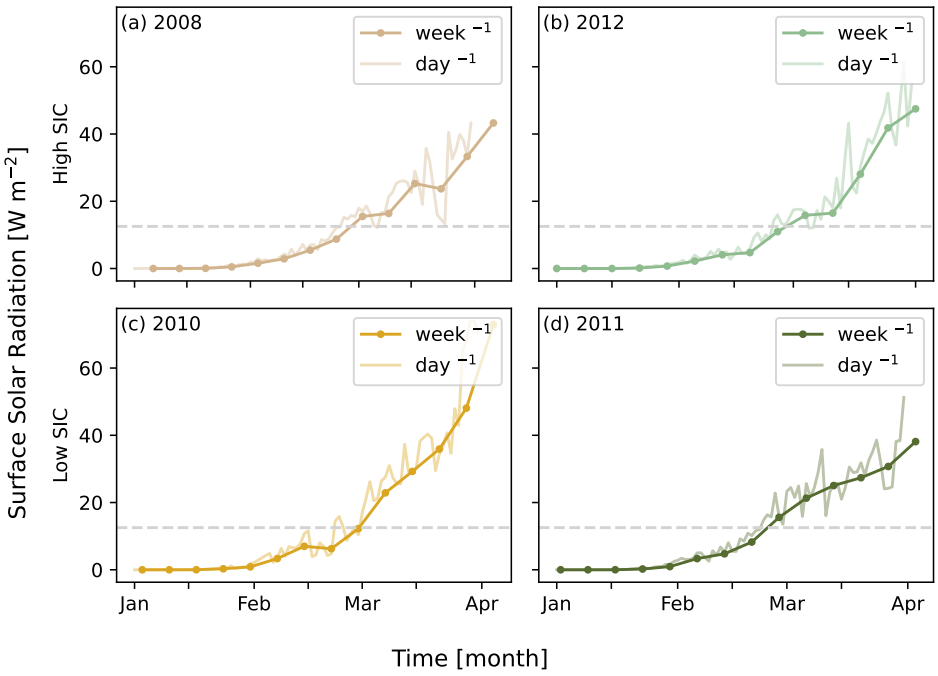

Figure C.4: *Daily and weekly SSR for JFM for years with high SIC, 2008 and 2012, and years with low SIC, 2010 and 2011. The grey dashed line represents the 21-year mean for SSR in JFM.*

Wind Speed

Table C.5: *Mean and maximum values for January to March of the high SIC (2008, 2012) and low SIC (2010, 2011) years.*

Year	mean [m s^{-1}]	max [m s^{-1}]
2008	1.4	6.0
2012	1.5	4.4
2010	1.5	5.9
2011	2.1	5.9

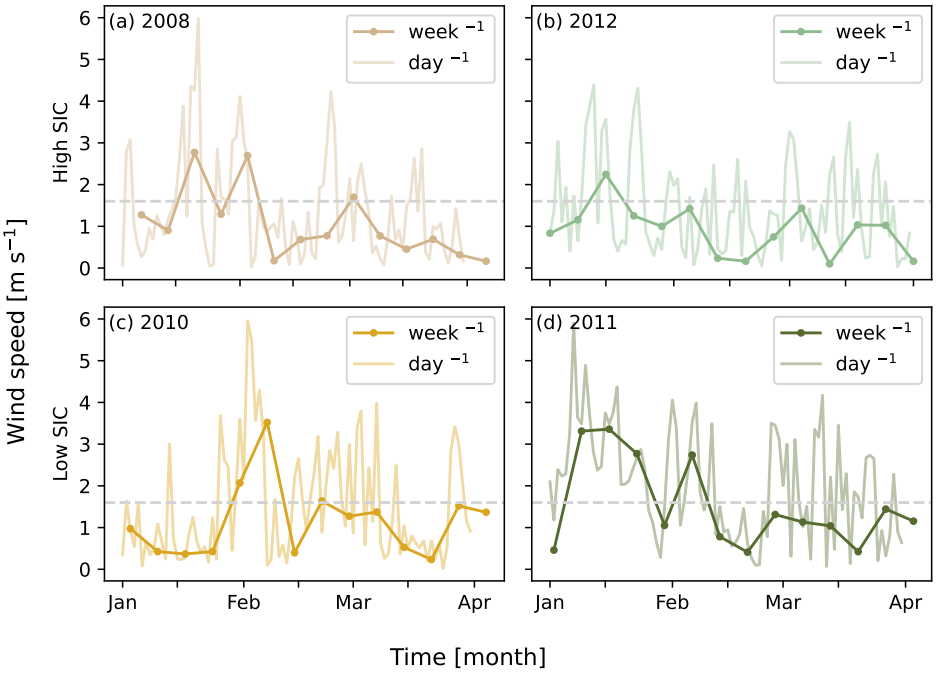

Figure C.5: *Daily and weekly wind speed for JFM for years with high SIC, 2008 and 2012, and years with low SIC, 2010 and 2011. The grey dashed line represents the 21-year mean for wind speed in JFM.*

Pre-SST

Table C.6: *Mean, minimum and maximum SST for July to September (JAS) for the summer of the previous minimum or maximum year.*

Year	mean [°C]	min [°C]	max [°C]
2007	4.96	3.47	6.67
2011	5.18	2.94	6.64
2009	5.67	2.74	7.88
2010	5.77	4.41	7.29

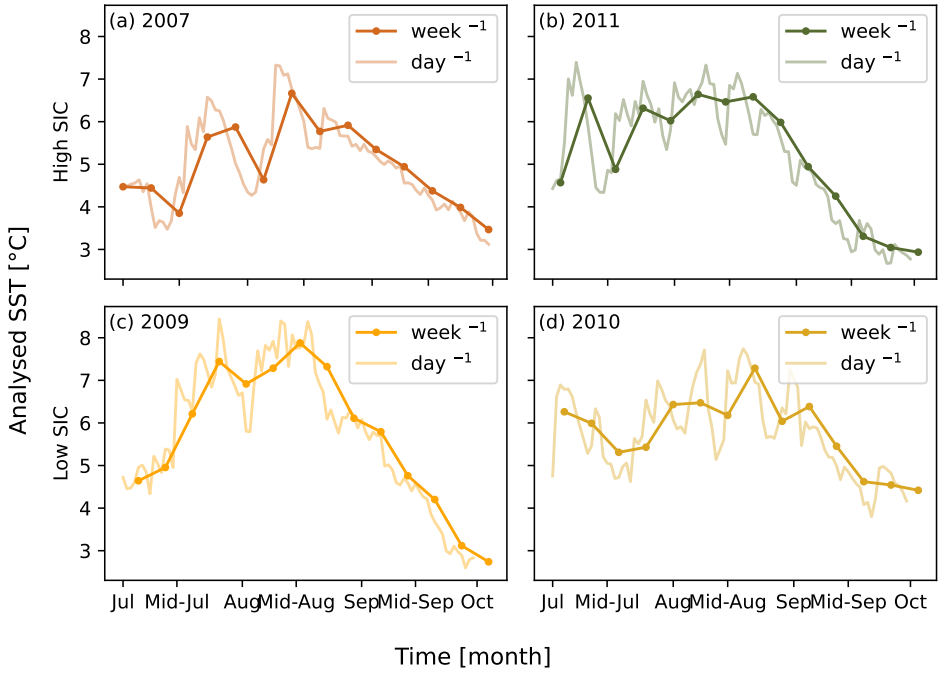

Figure C.6: *Daily and weekly SST for JAS for years with high SIC, 2008 and 2012, and years with low SIC, 2010 and 2011.*

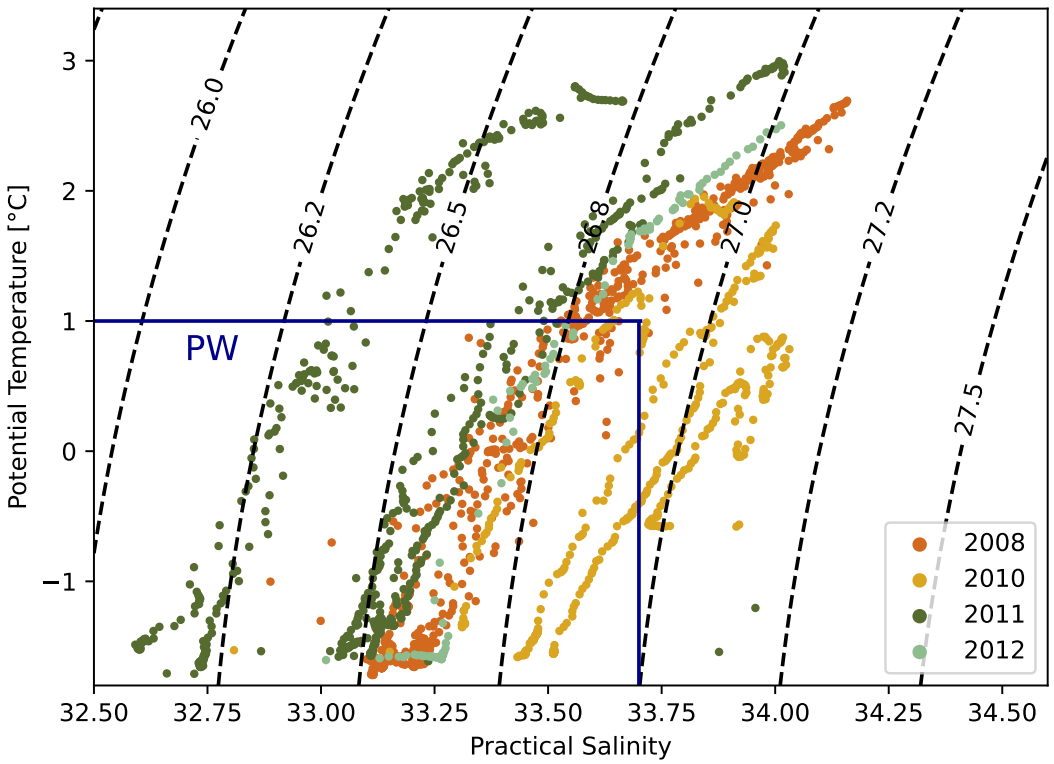

Figure C.7: *Potential temperature-practical salinity (θ-S) diagram of daily averaged hydrographic measurements for 2008, 2010, 2011, and 2012 to the common deepest depth of 136 dabr. The blue box marks the characteristics of Polar Water (PW). Dashed lines represent density contours. Water mass characteristics are defined by Tang et al. (2004).*

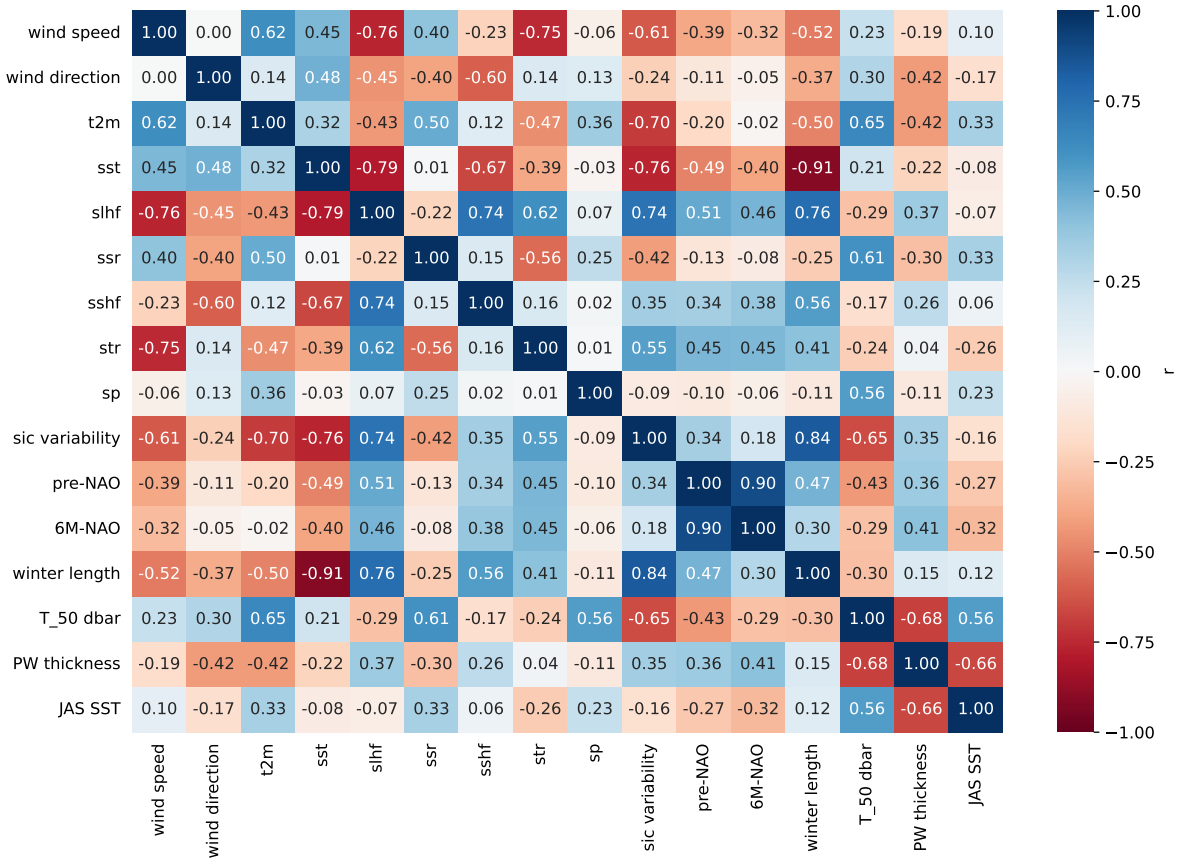

Figure C.8: *Pearson correlation coefficient represented in a heatmap*

Bibliography

Andersen, O. G. N. (1981). *The annual cycle of temperature, salinity, currents and water masses in Disko Bugt and adjacent waters, West Greenland*, volume 5. Museum Tusculanum Press.

Beaird, N., Straneo, F., & Jenkins, W. (2017). Characteristics of meltwater export from Jakobshavn Isbræ and Ilulissat Icefjord. *Annals of Glaciology*, 58(74), 107–117. https://doi.org/10.1017/aog.2017.19

Behrouz, M. S., Yazdi, M. N., & Sample, D. J. (2022). Using Random Forest, a machine learning approach to predict nitrogen, phosphorus, and sediment event mean concentrations in urban runoff. *Journal of Environmental Management*, 317, 115412. https://doi.org/10.1016/j.jenvman.2022.115412

Brakstad, A., Gebbie, G., Våge, K., Jeansson, E., & Ólafsdóttir, S. R. (2023). Formation and pathways of dense water in the Nordic Seas based on a regional inversion, journal = Progress in Oceanography. 212, 102981. https://doi.org/10.1016/j.pocean.2023.102981

Breiman, L. (2001). Random Forests,. *Machine Learning*, 45(1), 5–32. https://doi.org/10.1023/a:1010933404324

Buch, E. (1990). A monograph on the physical environment of Greenland waters. *Greenland Fisheries Research Institute Report*.

Buch, E. & Institut, M. (2002). *Present oceanographic conditions in Greenland waters*. Danish Meteorological Institute.

Buch, E., Pedersen, S. A., & Ribergaard, M. H. (2004). Ecosystem variability in West Greenland waters. *Journal of Northwest Atlantic Fishery Science*, 34. https://doi.org/10.2960/J.v34.m479

Carmack, E., Polyakov, I., Padman, L., Fer, I., Hunke, E., Hutchings, J., Jackson, J., Kelley, D., Kwok, R., Layton, C., Melling, H., Perovich, D., Persson, O., Ruddick, B., Timmermans, M.-L., Toole, J., Ross, T., Vavrus, S., & Winsor, P. (2015). Toward quantifying the increasing role of oceanic heat in sea ice loss in the new arctic. *Bulletin of the American Meteorological Society*, 96(12), 2079 – 2105. https://doi.org/10.1175/BAMS-D-13-00177.1

Chambers, J. M. (1992). *Statistical Models in S*, (Chapter Linea Models). Routledge. https://doi.org/10.1201/9780203738535

CMEMS (2023). *Global Ocean OSTIA Sea Surface Temperature and Sea Ice Analysis*. https://doi.org/10.48670/moi-00165. E.U. Copernicus Marine Service Information, (last accessed: 13.10.2023)

Curry, B., Lee, C. M., & Petrie, B. (2011). Volume, Freshwater, and Heat Fluxes through Davis Strait, 2004–05. *Journal of Physical Oceanography*, 41, 429–436. https://doi.org/10.1175/2010JPO4536.1

Dahl-Jensen, D., Bamber, J., Boggild, C., Buch, E., Christensen, J., Dethloff, K., Fahnestock, M., Marshall, S., Rosing, M., Steffen, K., et al. (2009). *The Greenland Ice Sheet in a changing climate*.

Donlon, C. J., Martin, M., Stark, J., Roberts-Jones, J., Fiedler, E., & Wimmer, W. (2012). The operational sea surface temperature and sea ice analysis (OSTIA) system. *Remote Sensing of Environment*, 116, 140–158. https://doi.org/10.1016/j.rse.2010.10.017

ECMWF (2023). *ECMWF Reanalysis v5 (ERA5), ERA5 hourly data on single levels from 1940 to present*. https://www.ecmwf.int/en/forecasts/dataset/ecmwf-reanalysis-v5. (last accessed: 13.10.2023)

Fried, N. & de Jong, M. F. (2022). The role of the Irminger Current in the Irminger Sea northward transport variability. *Journal of Geophysical Research: Oceans*, 127(3), e2021JC018188. https://doi.org/10.1029/2021JC018188

GEM (2019). *MarineBasis Disko - Water column - Disko Bay Cruise 2019, CTD measurements*. https://doi.org/10.17897/VB94-Y512. Greenland Ecosystem Monitoring

GEM (2020a). *GeoBasis Disko - Ice - AS-SeaIceCover*. https://doi.org/10.17897/SVR0-1574. Greenland Ecosystem Monitoring

GEM (2020b). *MarineBasis Disko - Water column - CTD measurements*. https://doi.org/10.17897/WH30-HT61. Greenland Ecosystem Monitoring

GEM (2020c). *MarineBasis Disko - Water column - Historic temperature and salinity, 1924 to 2010*. https://doi.org/10.17897/62VX-AX79. Greenland Ecosystem Monitoring

Gladish, C. V., Holland, D. M., & Lee, C. M. (2015a). Oceanic Boundary Conditions for Jakobshavn Glacier. Part II: Provenance and Sources of Variability of Disko Bay and Ilulissat Icefjord Waters, 1990-2011. *Journal of Physical Oceanography*, 45, 33–63. https://doi.org/10.1175/JPO-D-14

Gladish, C. V., Holland, D. M., Rosing-Asvid, A., Behrens, J. W., & Boje, J. (2015b). Oceanic Boundary Conditions for Jakobshavn Glacier. Part I: Variability and Renewal of Ilulissat Icefjord Waters, 2001–14. *Journal of Physical Oceanography*, 45, 3–32. https://doi.org/10.1175/JPO-D-14-0044.1

Good, S., Fiedler, E., Mao, C., Martin, M. J., Maycock, A., Reid, R., Roberts-Jones, J., Searle, T., Waters, J., While, J., et al. (2020). The current configuration of the OSTIA system for operational production of foundation sea surface temperature and ice concentration analyses. *Remote Sensing*, 12(4), 720. https://doi.org/10.3390/rs12040720

Hanna, E. & Cappelen, J. (2003). Recent cooling in coastal southern Greenland and relation with the North Atlantic Oscillation. *Geophysical Research Letters*, 30(3). https://doi.org/10.1029/2002GL015797

Hansen, B. U., Elberling, B., Humlum, O., & Nielsen, N. (2006). Meteorological trends (1991–2004) at Arctic Station, Central West Greenland (69° 15'N) in a 130 years perspective. *Geografisk Tidsskrift-Danish Journal of Geography*, 106(1), 45–55. https://doi.org/10.1080/00167223.2006.10649544

Hansen, M. O., Nielsen, T. G., Stedmon, C. A., & Munk, P. (2012). Oceanographic regime shift during 1997 in Disko Bay, Western Greenland. *Limnology and Oceanography*, 57, 634–644. https://doi.org/10.4319/lo.2012.57.2.0634

Hastie, T. (1990). *Generalized Additive Models*. Routledge. https://doi.org/10.1201/9780203753781

Hastie, T., Tibshirani, R., Friedman, J. H., & Friedman, J. H. (2009). *The elements of statistical learning: data mining, inference, and prediction*, volume 2. Springer. https://doi.org/10.1007/978-0-387-21606-5

Heide-Jørgensen, M., Stern, H., & Laidre, K. (2007a). Dynamics of the sea ice edge in Davis Strait. *Journal of Marine Systems*, 67(1), 170–178. https://doi.org/10.1016/j.jmarsys.2006.10.011

Heide-Jørgensen, M. P., Laidre, K., Logsdon, M. L., & Nielsen, T. G. (2007b). Springtime coupling between chlorophyll a, sea ice and sea surface temperature in Disko Bay, West Greenland. *Progress in Oceanography*, 73, 79–95. https://doi.org/10.1016/j.pocean.2007.01.006

Hersbach, H., Bell, B., Berrisford, P., Hirahara, S., Horányi, A., Muñoz-Sabater, J., Nicolas, J., Peubey, C., Radu, R., Schepers, D., et al. (2020). The ERA5 global reanalysis. *Quarterly Journal of the Royal Meteorological Society*, 146(730), 1999–2049. https://doi.org/doi.org/10.1002/qj.3803

Hersbach, H., Bell, B., Berrisford, P., Hirahara, S., Horányi, A., Muñoz-Sabater, J., Peubey, C., Radu, R., Rozum, I., Schepers, D., Simmons, A., Soci, C., Dee, D., & Thépaut, J.-N. (2023). *ERA5 hourly data on single levels from 1940 to present*. https://doi.org/10.24381/cds.adbb2d47. Accessed on 20.10.2023

Holland, D. M., Thomas, R. H., Young, B. D., Ribergaard, M. H., & Lyberth, B. (2008). Acceleration of Jakobshavn Isbr triggered by warm subsurface ocean waters. *Nature Geoscience*, 1, 659–664. https://doi.org/10.1038/ngeo316

IPCC (2022). *The Ocean and Cryosphere in a Changing Climate*. Cambridge University Press. https://doi.org/10.1017/9781009157964

Khazendar, A., Fenty, I. G., Carroll, D., Gardner, A., Lee, C. M., Fukumori, I., Wang, O., Zhang, H., Seroussi, H., Moller, D., Noël, B. P., van den Broeke, M. R., Dinardo, S., & Willis, J. (2019). Interruption of two decades of Jakobshavn Isbrae acceleration and thinning as regional ocean cools. *Nature Geoscience*, 12, 277–283. https://doi.org/10.1038/s41561-019-0329-3

Kiilerich, A. (1939). The Godthaab Expedition 1928. *A theoretical treatment of the hydrographical observation material. Medd Grenl78 (5)*.

Krawczyk, D. W., Yesson, C., Knutz, P., Arboe, N. H., Blicher, M. E., Zinglersen, K. B., & Wagnholt, J. N. (2022). Seafloor habitats across geological boundaries in Disko Bay, central West Greenland. *Estuarine, Coastal and Shelf Science*, 278. https://doi.org/10.1016/j.ecss.2022.108087

Lavergne, T., A. S., Tonboe, R., M.Kreiner, R. S., Birkedal, A., Baordo, F., Aspenes, T., & Eastwood, S. (2023). *ESA Sea Ice Climate Change Initiative ($Sea_Ice_c ci$): High(er) Resolution Sea Ice Concentration Climate Data Record Version 3 (SSM/I and SSMIS), NERC EDS Centre for Environmental Data Analysis*. https://dx.doi.org/10.5285/eade27004395466aaa006135e1b2ad1a. (last accessed: 13.09.2023)

Lavergne, T., Sørensen, A. M., Kern, S., Tonboe, R., Notz, D., Aaboe, S., Bell, L., Dybkjær, G., Eastwood, S., Gabarro, C., Heygster, G., Killie, M. A., Kreiner, M. B., Lavelle, J., Saldo, R., Sandven, S., & Pedersen, L. T. (2019). Version 2 of the EUMETSAT OSI SAF and ESA CCI sea-ice concentration climate data records. *Cryosphere*, 13, 49–78. https://doi.org/10.5194/tc-13-49-2019

Lloyd, J., Moros, M., Perner, K., Telford, R. J., Kuijpers, A., Jansen, E., & McCarthy, D. (2011). A 100 yr record of ocean temperature control on the stability of Jakobshavn Isbrae, West Greenland. *Geology*, 39(9), 867–870. https://doi.org/10.1130/G32076.1

Ludwig, V., Spreen, G., Haas, C., Istomina, L., Kauker, F., & Murashkin, D. (2019). The 2018 North Greenland polynya observed by a newly introduced merged optical and passive microwave sea-ice concentration dataset. *The Cryosphere*, 13(7), 2051–2073. https://doi.org/10.5194/tc-13-2051-2019

Ludwig, V., Spreen, G., & Pedersen, L. T. (2020). Evaluation of a New Merged Sea-Ice Concentration Dataset at 1 km Resolution from Thermal Infrared and Passive Microwave Satellite Data in the Arctic. *Remote Sensing*, 12(19). https://doi.org/10.3390/rs12193183

Madsen, S. D., Nielsen, T. G., & Hansen, B. W. (2001). Annual population development and production by Calanus finmarchicus, C. glacialis and C. hyperboreus in Disko Bay, western Greenland. *Marine Biology*, 139, 75–93. https://doi.org/10.1007/s002270100552

Masson-Delmotte, V., Swingedouw, D., Landais, A., Seidenkrantz, M.-S., Gauthier, E., Bichet, V., Massa, C., Perren, B., Jomelli, V., Adalgeirsdottir, G., Christensen, J. H., Arneborg, J., Bhatt, U., Walker, D. A., Elberling, B., Gillet-Chaulet, F., Ritz, C., Gallée, H., van den Broeke, M., Fettweis, X., de Vernal, A., & Vinther, B. (2012). Greenland climate change: from the past to the future. *WIREs Climate Change*, 3(5), 427–449. https://doi.org/10.1002/wcc.186

Met-Norway, Cyro (2023). *Sea Ice Index*. https://cryo.met.no/en/sea-ice-index. (last accessed: 19.11.2023)

Mosbech, A., Boertmann, D., & Jespersen, M. (2007). Strategic Environmental Impact Assessment of hydrocarbon activities in the Disko West area. *NERI technical report*, (618).

Motyka, R. J., Truffer, M., Fahnestock, M., Mortensen, J., Rysgaard, S., & Howat, I. (2011). Submarine melting of the 1985 Jakobshavn Isbræ floating tongue and the triggering of the current retreat. *Journal of Geophysical Research: Earth Surface*, 116(F1). https://doi.org/10.1029/2009JF001632

Myers, P. G., Kulan, N., & Ribergaard, M. H. (2007). Irminger water variability in the West Greenland Current. *Geophysical Research Letters*, 34(17). https://doi.org/10.1029/2007GL030419

Myers, P. G. & Ribergaard, M. H. (2013). Warming of the polar water layer in disko bay and potential impact on jakobshavn isbrae. *Journal of Physical Oceanography*, 43, 2629–2640. https://doi.org/10.1175/JPO-D-12-051.1

Møller, E. F., Christensen, A., Larsen, J., Mankoff, K. D., Ribergaard, M. H., Sejr, M., Wallhead, P., & Maar, M. (2023). The sensitivity of primary productivity in Disko Bay, a coastal Arctic ecosystem, to changes in freshwater discharge and sea ice cover. *Ocean Science*, 19, 403–420. https://doi.org/10.5194/os-19-403-2023

Møller, E. F. & Nielsen, T. G. (2019). Borealization of Arctic zooplankton—smaller and less fat zooplankton species in Disko Bay, Western Greenland. *Limnology and Oceanography*, 65, 1175–1188. https://doi.org/10.1002/lno.11380

Nielsen, N., Humlum, O., & Hansen, B. U. (2001). Meteorological Observations in 2000 at the Arctic Station, Qeqertarsuaq (69°15'N), Central West Greenland. *Geografisk Tidsskrift-Danish Journal of Geography*, 101(1), 155–158. https://doi.org/10.1080/00167223.2001.10649458

Nielsen, T. G. & Hansen, B. (1995). Plankton community structure and carbon cycling on the western coast of Greenland during and after the sedimentation of a diatom bloom. *Marine Ecology Progress Series*, 125, 239–257. https://doi.org/10.3354/meps125239

Nielsen, T. G. & Hansen, B. W. (1999). Plankton community structure and carbon cycling on the western coast of Greenland during the stratified summer situation. I. Hydrography, phytoplankton and bacterioplankton. *Aquatic microbial ecology*, 16(3), 205–216. https://doi.org/10.3354/ame016217

NOAA (2023). *North Atlantic Oscillation (NAO)*. https://www.ncei.noaa.gov/access/monitoring/nao/. (last accessed: 13.10.2023)

NOAA, N. C. f. E. I. (2022a). *ETOPO 2022 15 Arc-Second Global Relief Model*. https://doi.org/10.25921/fd45-gt74. (last accessed: 13.09.2023)

NOAA, N. C. f. E. I. (2022b). *ETOPO 2022 30 Arc-Second Global Relief Model*. https://doi.org/10.25921/fd45-gt74. (last accessed: 13.09.2023)

Notz, D. & Stroeve, J. (2016). Observed Arctic sea-ice loss directly follows anthropogenic CO2 emission. *Science*, 354(6313), 747–750. https://doi.org/10.1126/science.aag2345

NSDIC (2022). *Ain't no sunshine when she's gone*. https://nsidc.org/arcticseaicenews/2022/10/. (last accessed: 04.09.2023)

NSDIC (2023a). *Arctic sea ice has reached minimum extent for 2023*. https://nsidc.org/news-analyses/news-stories/arctic-sea-ice-has-reached-minimum-extent-2023. (last accessed: 02.11.2023)

NSDIC (2023b). *Arctic sea ice maximum at fifth lowest on satellite record*. https://nsidc.org/arcticseaicenews/2023/03/. (last accessed: 04.09.2023)

NSDIC (2023c). *From polar dawn to dusk*. https://nsidc.org/arcticseaicenews/2023/04/. (last accessed: 04.09.2023)

OMG (2019). *OMG AXCTD Profiles*. https://doi.org/10.5067/OMGEV-AXCT1

Onarheim, I. H., Eldevik, T., Smedsrud, L. H., & Stroeve, J. C. (2018). Seasonal and regional manifestation of Arctic sea ice loss. *Journal of Climate*, 31(12), 4917–4932. https://doi.org/10.1175/JCLI-D-17-0427.1

Parkinson, C. L. (1995). Recent sea-ice advances in Baffin Bay/Davis Strait and retreats in the Bellingshausen Sea. *Annals of Glaciology*, 21, 348–352. https://doi.org/10.3189/S0260305500016050

Pörtner, H.-O., Roberts, D. C., Masson-Delmotte, V., Zhai, P., Tignor, M., Poloczanska, E., & Weyer, N. (2019). The ocean and cryosphere in a changing climate. *IPCC special report on the ocean and cryosphere in a changing climate*, 1155. https://doi.org/org/10.1017/9781009157964.005

Rampal, P., Dansereau, V., Olason, E., Bouillon, S., Williams, T., Korosov, A., & Samaké, A. (2019). On the multi-fractal scaling properties of sea ice deformation. *The Cryosphere*, 13(9), 2457–2474. https://doi.org/10.5194/tc-13-2457-2019

Rantanen, M., Karpechko, A. Y., Lipponen, A., Nordling, K., Hyvärinen, O., Ruosteenoja, K., Vihma, T., & Laaksonen, A. (2022). The Arctic has warmed nearly four times faster than the globe since 1979. *Communications Earth & Environment*, 3(1). https://doi.org/10.1038/s43247-022-00498-3

Ribergaard, M. H. (2011). Oceanographic Investigations off West Greenland 2010. https://api.semanticscholar.org/CorpusID:133452664

Rigor, I. G., Colony, R. L., & Martin, S. (2000). Variations in surface air temperature observations in the Arctic, 1979-97. *Journal of Climate*, 13(5), 896–914. https://doi.org/10.1175/1520-0442(2000)013<0896:VISATO>2.0.CO;2

Sea & Sun Technology (2020). *CTD48M*. https://www.sea-sun-tech.com/product/multiparameter-probe-ctd-48-memory/? (last accessed: 13.10.2023)

Sea-Bird Scientific (2022). *SBE 19plus V2 SeaCAT Profiler CTD*. https://www.seabird.com/sbe-19plus-v2-seacat-profiler-ctd/product-downloads?id=60761421596. (last accessed: 13.10.2023)

Serreze, M. C., Barrett, A. P., Stroeve, J. C., Kindig, D. N., & Holland, M. M. (2009). The emergence of surface-based Arctic amplification. *The Cryosphere*, 3(1), 11–19. https://doi.org/10.5194/tc-3-11-2009

Skogseth, R., Nilsen, F., & Smedsrud, L. H. (2009). Supercooled water in an Arctic polynya: observations and modeling. *J. Glaciol.*, 55(189), 43–52. https://doi.org/10.3189/002214309788608840

Smedsrud, L. H., Muilwijk, M., Brakstad, A., Madonna, E., Lauvset, S. K., Spensberger, C., Born, A., Eldevik, T., Drange, H., Jeansson, E., Li, C., Olsen, A., Skagseth, O., Slater, D. A., Straneo, F., Våge, K., & Årthun, M. (2022). Nordic Seas Heat Loss, Atlantic Inflow, and Arctic Sea Ice Cover Over the Last Century. *Reviews of Geophysics*, 60(1). https://doi.org/10.1029/2020RG000725

Stark, J. D., Donlon, C. J., Martin, M. J., & McCulloch, M. E. (2007). OSTIA: An operational, high resolution, real time, global sea surface temperature analysis system. *Oceans 2007-europe*, 1–4. https://doi.org/10.1109/OCEANSE.2007.4302251

Stern, H. L. & Heide-Jørgensen, M. P. (2003). Trends and variability of sea ice in Baffin Bay and Davis Strait, 1953-2001. *Polar Research*, 22, 11–18. https://doi.org/10.1111/j.1751-8369.2003.tb00090.x

Straneo, F. & Cenedese, C. (2015). The Dynamics of Greenland's Glacial Fjords and Their Role in Climate, journal = Annual Review of Marine Science. 7(1), 89–112. https://doi.org/10.1146/annurev-marine-010213-135133

Stroeve, J. & Notz, D. (2018). Changing state of Arctic sea ice across all seasons. *Environmental Research Letters*, 13(10), 103001. https://doi.org/10.1088/1748-9326/aade56

Tang, C. C., Ross, C. K., Yao, T., Petrie, B., DeTracey, B. M., & Dunlap, E. (2004). The circulation, water masses and sea-ice of Baffin Bay. *Progress in Oceanography*, 63(4), 183–228. https://doi.org/10.1016/j.pocean.2004.09.005

Theodoridis, S. & Koutroumbas, K. (2006). *Pattern recognition*. Elsevier.

Thomas, D. N. (2017). *Sea ice*. John Wiley & Sons. https://doi.org/10.1002/9781118778371

Thomson, R. E. & Emery, W. J. (2014). *Data analysis methods in physical oceanography*. Newnes. https://doi.org/10.1016/C2010-0-66362-0

Wanner, H., Brönnimann, S., Casty, C., Gyalistras, D., Luterbacher, J., Schmutz, C., Stephenson, D. B., & Xoplaki, E. (2001). North Atlantic Oscillation – Concepts And Studies. *Surveys in Geophysics*, 22(4), 321–381. https://doi.org/10.1023/a:1014217317898

Weeks, W. (2010). *On sea ice*. University of Alaska Press.

Wessel, P. & Smith, W. H. (1996). A global, self-consistent, hierarchical, high-resolution shoreline database. *Journal of Geophysical Research: Solid Earth*, 101, 8741–8743. https://doi.org/10.1029/96jb00104

Wilkinson, G. N. & Rogers, C. E. (1973). Symbolic Description of Factorial Models for Analysis of Variance. *Journal of the Royal Statistical Society. Series C (Applied Statistics)*, 22(3), 392–399. https://doi.org/10.2307/2346786

Wood, M., Rignot, E., Fenty, I., An, L., Bjørk, A., van den Broeke, M., Cai, C., Kane, E., Menemenlis, D., Millan, R., et al. (2021). Ocean forcing drives glacier retreat in Greenland. *Science Advances*, 7(1), eaba7282. https://doi.org/10.1126/sciadv.aba7282

Zhang, J., Lindsay, R., Schweiger, A., & Rigor, I. (2012). Recent changes in the dynamic properties of declining Arctic sea ice: A model study. *Geophys. Res. Lett.*, 39(20). https://doi.org/doi.org/10.1029/2012GL053545

Årthun, M., Eldevik, T., Smedsrud, L. H., Skagseth, & Ingvaldsen, R. B. (2012). Quantifying the influence of atlantic heat on barents sea ice variability and retreat. *Journal of Climate*, 25, 4736–4743. https://doi.org/10.1175/JCLI-D-11-00466.1